

ARCHAEOLOGICAL INVESTIGATIONS OF GLASS FROM THE EARLY  
BYZANTINE WORKSHOP IN SIDE, ANTALYA

A THESIS SUBMITTED TO  
THE GRADUATE SCHOOL OF NATURAL AND APPLIED SCIENCES  
OF  
MIDDLE EAST TECHNICAL UNIVERSITY

BY

DENİZ GENÇ

IN PARTIAL FULFILLMENT OF THE REQUIREMENTS  
FOR  
THE DEGREE OF MASTER OF SCIENCE  
IN  
ARCHAEOLOGY

JUNE 2019



Approval of the thesis:

**ARCHAEOLOGICAL INVESTIGATIONS OF GLASS FROM THE EARLY  
BYZANTINE WORKSHOP IN SIDE, ANTALYA**

submitted by **DENİZ GENÇ** in partial fulfillment of the requirements for the degree  
of **Master of Science in Archaeometry Department, Middle East Technical  
University** by,

Prof. Dr. Halil Kalıpçılar  
Dean, Graduate School of **Natural and Applied Sciences**

\_\_\_\_\_

Prof. Dr. Musa Doğan  
Head of Department, **Archaeometry**

\_\_\_\_\_

Prof. Dr. M. Ümit Atalay  
Supervisor, **Archaeometry, METU**

\_\_\_\_\_

Assoc. Prof. Dr. Ali Akın Akyol  
Co-Supervisor, **Cons. and Rest. of Cultural Properties Dept.,  
Hacı Bayram Veli University**

\_\_\_\_\_

**Examining Committee Members:**

Prof. Dr. Musa Doğan  
Archaeometry, METU

\_\_\_\_\_

Prof. Dr. M. Ümit Atalay  
Archaeometry, METU

\_\_\_\_\_

Prof. Dr. Feriştah Soykal Alanyalı  
Archaeology, Anadolu University

\_\_\_\_\_

\_\_\_\_\_

\_\_\_\_\_

Date: 11.06.2019

**I hereby declare that all information in this document has been obtained and presented in accordance with academic rules and ethical conduct. I also declare that, as required by these rules and conduct, I have fully cited and referenced all material and results that are not original to this work.**

Name, Surname: Deniz Genç

Signature:

## ABSTRACT

### ARCHAEOMETRIC INVESTIGATIONS OF GLASS FROM THE EARLY BYZANTINE WORKSHOP IN SIDE, ANTALYA

Genç, Deniz  
Master of Science, Archaeometry  
Supervisor: Prof. Dr. M. Ümit Atalay  
Co-Supervisor: Assoc. Prof. Dr. Ali Akin Akyol

June 2019, 150 pages

Reconstructing the history of archeological artifacts leads us to examine the materials using various scientific methods. Therefore, archaeometric investigations allow us to understand the production technology, the firing temperature, provenance, the raw materials and the colorants used in the process. This thesis aims to investigate the archaeological glasses found at the Side excavation site.

Visual and optical microscope analyses were conducted to observe the physical shape, deterioration types, and the production technology of Side glass. According to the thickness measurements and their bubble shapes, Side glasses from the Late Antique period were shaped by the glass blowing technique. The color analysis has revealed that the Side glasses in various color ranges were mainly in green and blue hues. The chemical analysis of the Side glasses was conducted by Polarized Energy Dispersive-X-ray Fluorescence (PED-XRF). The results of the analysis were interpreted with respect to main, minor and trace elements. In line with these results, Side glass set was a soda-lime-silica glass fluxed with natron. The vast majority of the glasses were decolorized by the deliberate addition of manganese. The colorants are iron, copper, cobalt, manganese, vanadium, and lead. Recycling conditions were revealed using the marker elements and a comparative plot of Side and primary production glasses. In

accordance with the glass composition, glass groups were identified by hierarchical clustering and were compared with Late Antique glass from Asia Minor. Furthermore, clay-based crucibles and kiln fragments were analyzed by the thin section optical microscopy. Petrographical properties of the crucibles were demonstrated in terms of rock and mineral contents, the exposed firing temperature and their origins.

Keywords: Early Byzantine, Glass Workshop, Side Ancient City, Glass Analysis, PED-XRF

## ÖZ

### SİDE, ANTALYA ERKEN BİZANS ATÖLYESİ CAMLARININ ARKEOMETRİK İNCELEMESİ

Genç, Deniz  
Yüksek Lisans, Arkeometri  
Tez Danışmanı: Prof. Dr. M. Ümit Atalay  
Ortak Tez Danışmanı: Doç. Dr. Ali Akın Akyol

Haziran 2019, 150 sayfa

Arkeolojik buluntuların tarihini yeniden inşa edebilmek ve bilgi sahibi olabilmek için arkeolojinin yanı sıra arkeometrik araştırmalara ihtiyaç duyulmaktadır. Bu araştırmalar malzemenin üretim teknolojisini, pişirme derecesini, kökenini, üretimde kullanılan hammadde ve boyar maddelerin anlaşılmasını sağlar. Bu tez çalışması, Side Antik Kenti'nden gelen cam buluntularının arkeometrik olarak incelenmesini amaçlamaktadır.

Side cam örneklerinin fiziksel durumu, bozulma türleri ve üretim teknolojisini anlamak amacıyla görsel ve optik mikroskop analizleri uygulanmıştır. Yapılan kalınlık ölçümlerine ve habbe şekillerine göre, Geç Antik döneme ait Side camlarının üfleme tekniğiyle yapıldığı tespit edilmiştir. Renk analizleri, çeşitli renklerdeki Side camının ağırlıklı olarak yeşil ve mavi tonlarda olduğunu göstermiştir. Camların kimyasal analizleri, Polarize Enerji Dağıtımli X-ışını Floresans (PED-XRF) tekniği kullanılarak yapılmış olup, analiz sonuçları ana, az ve eser miktardaki elementlere göre yorumlanmıştır. Bu sonuçlar doğrultusunda, Side cam setinin doğal sodyum karbonat ile ergitilmiş soda-kireç-silis camı olduğu söylenebilir. Camların büyük çoğunluğu kasıtlı mangan ilavesiyle renksizleştirilmiştir ve renklendirme amacıyla demir, bakır, kobalt, mangan, vanadyum ve nadir olarak kurşun gibi boyar maddeler

kullanılmıştır. Camın geri dönüşüm durumu, belirteç elementlerin ve birincil üretim camlarıyla yapılan karşılaştırmalı çizimlerin sayesinde ortaya çıkarılmıştır. Cam kompozisyonu göre, hiyerarşik kümeleme yönetimi kullanılarak Side camları gruplarına ayrılmış ve Anadolu'daki Geç Antik döneme ait diğer camlarla karşılaştırılmıştır. Ayrıca kil bazlı pota ve fırın parçaları, ince kesit optik mikroskopisi ile analiz edilmiş, bu örneklerin petrografik özellikleri, kaya ve mineral içeriği, maruz kalınan pişirim sıcaklığı ve kayaç kökeni bakımından incelenmiştir.

Anahtar Kelimeler: Geç Antik Dönem, Cam işliđi, Side Antik Kenti, PED-XRF, Arkeometri

Aileme,

## ACKNOWLEDGEMENTS

I would like to express my gratitude to Prof. Dr. Ümit Atalay, supervisor of the thesis, and Assoc. Prof. Dr. Ali Akın Akyol, co-supervisor of the thesis, for his mental and physical support in every step of this study.

I am very grateful to Prof. Dr. Feriştah Alanyalı and Prof. Dr. Hüseyin Sabri Alanyalı, the head of the Side excavation, for sharing their samples.

I am extremely grateful to Prof. Dr. Yusuf Kağan Kadioğlu at the Department of Geological Engineering at Ankara University for chemical and petrographical analyses. Also, I am thankful to Gülşen Albuz Geren and Dr. Murat Eroğlu for their continuous help.

Further, I want to thank my friends, Emre Özsever, Ezgi Ünçe and Elşen Aydın for tirelessly answering my questions.

Finally, special thanks to my amazing parents, Sema Genç and Şükrü Genç, my friends and Erdem Bayram for their endless support and tolerance for my painful process.

## TABLE OF CONTENTS

ABSTRACT .....	v
ÖZ .....	vii
ACKNOWLEDGMENTS.....	x
TABLE OF CONTENTS.....	xi
LIST OF TABLES.....	xiv
LIST OF FIGURES .....	xv
CHAPTERS	
1. INTRODUCTION .....	1
1.1 Aim of the Study .....	2
2. GENERAL ASPECTS OF GLASS AND ITS HISTORY .....	5
2.1. Definition of Glass .....	5
2.2. Chemical Structure and Composition.....	6
2.2.1. Network Formers .....	7
2.2.2. Network Modifiers.....	9
2.2.3. Colorants, Opacifiers And Decolorants.....	13
2.3. Brief History of Glass from the Beginning to the Late Byzantine period..	19
2.3.1 The Origins of Glass and its Chemical Composition until the Roman Period .....	19

2.3.2 Roman and Early Byzantine Glass and its Chemical Composition.....	23
2.4. Glass Production Models.....	31
2.5. Recycling.....	32
3. SIDE ARCHAEOLOGICAL AREA.....	35
3.1. Ancient Side.....	35
3.2. Evidence of Glass Production in Side .....	40
4. MATERIALS AND METHODS.....	45
4.1. Materials .....	45
4.2. Methods .....	50
4.2.1. X-Ray Fluorescence (XRF) Spectroscopy.....	51
4.2.2. Thin Section Optical Microscopy.....	56
5. RESULTS AND DISCUSSION.....	57
5.1. Visual and Binocular Microscope Analyses .....	57
5.2. Color Analysis.....	58
5.3. Chemical Analysis Results.....	59
5.3.1. Sand.....	67
5.3.2. Colorant.....	70

5.3.3. Recycling.....	77
5.3.4. Identification of Compositional Groups .....	81
5.4. Petrographic Thin-Section Optical Microscopy Analysis.....	95
6. CONCLUSION .....	97
REFERENCES.....	101
APPENDICES	
A. Figures.....	115
B. Tabela.....	127

## LIST OF TABLES

### TABLES

Table 1.1. Glass coloring ions in different furnace environments .....	14
Table 2.1. Average elemental compositions of Side glass groups.....	83
Table 4.1. The table showing the porosity, endured temperature, rock and mineral types and the origin of the rocks of the clay samples.....	95

## LIST OF FIGURES

### FIGURES

Figure 1.1. The tetrahedral molecular form of silica.....	7
Figure 1.2. Schematic representation of compound $A_2O_3$ : (a) $A_2O_3$ in the crystalline state, (b) $A_2O_3$ in the vitreous state.....	8
Figure 1.3. Two-dimensional schema of glass.....	10
Figure 2.1. Location of Side archaeological site in Asia Minor.....	36
Figure 2.2. Drills of Dionysus Temple in 2009- 2012 excavation season.....	39
Figure 2.3. Moil sample from Side excavation.....	41
Figure 2.4. Glass lump adhered to porous clay.....	41
Figure 2.5. Profile of the spilled glass adhered to clay fragments from the complete Side set, showing the layers of material.....	42
Figure 2.6. Dionysus Temple and the glass kiln.....	43
Figure 3.1. Spots for the traces of glass production in Side Theater.....	45
Figure 3.2. Chunks samples from the complete Side sample set .....	47
Figure 3.3. Product and vessel fragments from the complete Side set .....	47
Figure 3.4. Window panes from the complete Side sample set .....	48
Figure 3.5. Droplet samples from the complete Side sample set.....	48
Figure 3.6. Spilt glass adhered to clay fragments from the complete Side set.....	49

Figure 3.7. <<Loss/ Use Ratio of Coins Per Annum>>according to the "1000/ total x", "amount per period/ total excavated from the site" formulae of the 161 samples with exact dates identified among the 230 coins collected from Side, Dionysus Temple 2009-2012 excavation.....	49
Figure 3.8. Generation of characteristic X-ray radiation.....	52
Figure 3.9. WD-XRF setup.....	54
Figure 3.10. ED-XRF setup.....	55
Figure 4.1. The Scatter plot of potassium oxide vs. magnesium oxide for Side sample set.....	60
Figure 4. 2. Triangular plot (SiO <sub>2</sub> - Na <sub>2</sub> O- CaO) of the Side glass set .....	61
Figure 4. 3. Triangular plot (SiO <sub>2</sub> - Na <sub>2</sub> O- CaO) of Side chunk group.....	62
Figure 4. 4. Triangular plot (SiO <sub>2</sub> - Na <sub>2</sub> O- CaO) of Side product group .....	63
Figure 4. 5. Triangular plot (SiO <sub>2</sub> - Na <sub>2</sub> O- CaO) of Side window-pane group.....	64
Figure 4. 6. Triangular plot (SiO <sub>2</sub> - Na <sub>2</sub> O- CaO) of Side droplet group .....	65
Figure 4.7. Spider diagram showing the trace elements of 4 different Side glass groups (values are normalized to the average continental crust) .....	66
Figure 4.8. Cluster column chart showing the differences of the regions according to the selected elements.....	66
Figure 4.9. Scatter plot of MnO vs. Ba of Side glasses.....	67
Figure 4.10. Strontium graph of Side glass samples.....	69
Figure 4.11. Zirconium graph of Side glass samples.....	69
Figure 4.12. Scatter graph demonstrating Fe <sub>2</sub> O <sub>3</sub> vs MnO for Side glass set.....	71

Figure 4.13. Spider diagram of high manganese purple-colored glasses, normalized to the average continental crust.....	72
Figure 4.14. Scatter plot of copper and tin for the samples that contain >100ppm of Cu.....	75
Figure 4.15. Scatter plot of arsenic and cobalt for samples that contain cobalt.....	76
Figure 4.16. Scatter plot of iron oxide and cobalt and cobalt for samples that contain cobalt.....	76
Figure 4.17. Scatter plot of cobalt vs. nickel for cobalt-bearing samples.....	77
Figure 4.18. K <sub>2</sub> O to P <sub>2</sub> O <sub>5</sub> for the samples Sb=20-800ppm.....	78
Figure 4.19. CaO to P <sub>2</sub> O <sub>5</sub> for the samples Sb=20-800ppm.....	79
Figure 4.20. The scatter plot of CaO and K <sub>2</sub> O for the 8 recycled colorless/naturally colored glass.....	80
Figure 4.21. The scatter plot of K <sub>2</sub> O and P <sub>2</sub> O <sub>5</sub> for the 8 recycled colorless/naturally colored glass.....	80
Figure 4. 22. Cluster dendrogram of Side assemblage performed on MgO, K <sub>2</sub> O, CaO, TiO <sub>2</sub> , MnO, and Fe <sub>2</sub> O <sub>3</sub> .....	82
Figure 4. 23. (a) Scatter graph of Zr vs. TiO <sub>2</sub> for Side assemblage; (b) Scatter graph of Fe <sub>2</sub> O <sub>3</sub> vs. TiO <sub>2</sub> for Side assemblage.....	86
Figure 4. 24. Scatter graph showing Fe <sub>2</sub> O <sub>3</sub> vs TiO <sub>2</sub> concentrations for Side HIMT(?) glasses.....	87
Figure 4. 25. Scatter graph showing Zr vs. TiO <sub>2</sub> concentrations for Side HIMT(?) glasses.....	87
Figure 4. 26. Scatter graph showing Fe <sub>2</sub> O <sub>3</sub> vs MnO concentrations for Side HIMT(?) glasses.....	88

Figure 4. 27. Scatter graph showing $\text{Fe}_2\text{O}_3/\text{TiO}_2$ vs. $\text{Fe}_2\text{O}_3/\text{Al}_2\text{O}_3$ concentration for Side HIMT(?) glasses with HLIMT glass samples of Ceglia et al, 2015; CaO-rich HIMT and CaO-rich/NaO-poor HIMT glass samples from Gliozzo et al, 2015.....	88
Figure 4.28. Spider diagram showing the trace elements of High CaO HIMT glass samples from Side, Pergamon, and Herdonia.....	89
Figure 4.29. The scatter diagram of variant HIMT glass group samples from Anatolia, Europe, and Egypt showing $\text{TiO}_2/\text{Al}_2\text{O}_3$ vs. $\text{Al}_2\text{O}_3/\text{SiO}_2$ .....	90
Figure 4.30. The scatter diagram of Levantine glass group samples from various Anatolian sites showing $\text{TiO}_2/\text{Al}_2\text{O}_3$ vs. $\text{Al}_2\text{O}_3/\text{SiO}_2$ .....	92
Figure 4.31. The spider diagram showing the trace elements of Levantine glass from Side, Pergamon, Apollonia and Bet Eli'ezer.....	92
Figure 4.32. (a) Scatter graph showing $\text{TiO}_2$ vs. $\text{Fe}_2\text{O}_3$ for Side glass (b) Scatter graph showing $\text{TiO}_2$ vs. Zr for Side glass.....	93
Figure 4.33. Spider diagram showing the trace elements of seven glass groups from Side .....	94
Figure 4.34. Thin section optical microscope photographs of the clay samples.....	96

## CHAPTER 1

### INTRODUCTION

Archaeological finds have great value not only by being a part of cultural heritage but mainly for numerous information that can be obtained from them. A tiny piece of an archaeological object may provide information on cultural structures, trade links, social, religious, economic and political relations, industry consumption habits, traditions, industry, rituals, fabrication techniques, *chaine opératoire*, production materials, provenance studies, dating and so on. In obtaining this information, archaeometric investigation plays a critical role.

Glass, first as a tool and a luxury material, later as a household object, becomes indispensable for human life starting with the use of natural glass-obsidian and manmade glass. To fully comprehend glass with its history, condition and production technology, several scientific research should be conducted via instrumental methods. These methods can be gathered under four categories; (i) electron beam methods, e.g. Scanning Electron Microscopy (SEM)- Energy Dispersive X-Ray Spectroscopy (EDX), Electron Probe Micro Analysis (EPMA), Raman Spectroscopy etc. (ii) X-ray methods e.g. X-ray Fluorescence (XRF), X-Ray Diffraction (XRD), X-ray Photoelectron Spectrometry (XPS) etc., optical spectrometric methods e.g. Inductively Coupled Plasma-Optical Emission Spectrometry (ICP-OES), Atomic Absorption Spectrometry (AAS), (iii) mass spectrometric methods e.g. ICP-MS (Inductively Coupled Plasma Mass Spectrometry, Isotope Ratio Analysis etc., and (iv) oxidation state methods such as Electron spin resonance (ESR) and Ultraviolet and Visible Spectroscopy (UV-VIS) (Davison, 2003).

In this study, Side glasses were examined by using physical, chemical and petrographic techniques. Glass samples were documented by using optical microscopy, thickness meter and chromameter. Chemical analyses were conducted using PED-XRF. Finally, glass pots and furnace samples were petrographically examined by thin-section analyses.

The analyses of Side glass have been presented in six chapters. The first chapter mentions the scientific glass examination techniques and the aim of the study. The general aspects of glass in terms of its components and its history from the beginning until the late Byzantine period were given in the second chapter. While the third chapter gives information about Side archeological site, the fourth chapter introduces the materials and the methods used for the investigation of the Side samples. The results and the discussion were presented in the fifth chapter. Finally, the sixth chapter includes the summary and conclusion.

### **1.1. Aim of the Study**

Interestingly, and regardless of its economic and political significance and its proximity to primary glass production centers, the investigation of Anatolian glass and glass workshops in Late antique period is rather an untouched field of study.

Ömür Dünya Çakmaklı (2014) briefly mentions the existence of Roman and Byzantine glass workshops in Caria region. In her paper, Çakmaklı gathers the evidence regarding glass working in Aphrodisias, Nysa, Tralleis, and Kaunos. Emre Taştemür (2017) compiled the ancient Anatolian glass production centers in his article “Antik Cam Fırınları ve Anadolu Örnekleri”. Taştemür’s synoptic article gives information about Anatolian glass history, used techniques, main glass finds, production types, furnace forms, and historical sites that acquire in-situ glass furnace or glass production evidence.

When it comes to archaeometry, investigations on Anatolian Late Antique glass are scarce. The limited archaeometric studies regarding Late Antique Anatolian glass

come from Ephesos (Uhlir et al. 2006), Sagalassos (Degryse et al., 2005 and Degryse 2015), Boğazköy (Nakai et al., 2014), Elaiussa Sebaste (Akyol et al., 2008), Pergamon (Rehren et al. 2015) and Brill's (1999) studies about Sardis and Aphrodisias. Unfortunately, complete research on the glass ateliers from the Late Antique period in Asia Minor is not available in an archaeometric perspective. Hence, this study can be regarded as a touchstone for Late Antique glass workshops in Anatolia.

Side, currently excavated by Hüseyin Sabri Alanyalı and Feriştah Soykal-Alanyalı, has been the subject of many researches. However, among various detailed research topics, glass studies in Side consist of several short reports of Ahmet Tolga Tek in the Conference of Excavation Results dated between 2009 to 2012 which solely refers dating, location, typology, and decoration. Unfortunately, no further published research has been conducted on Side glass finds. The aim of the study is to present an analytical perspective to Side glasses and the glass workshop with the hope of contributing to the studies on Anatolian Late Antique glass.

This study aims to elucidate glass production processes in Side by conducting a chemical and petrographic analysis of various finds from the glass workshop. These analyses enable us to find out the raw material preferences, added colorants and opacifiers, heating temperatures, glass quality, weathering conditions, and glass-working techniques. The analysis of the trace elements will enable us to figure out whether the glass was recycled or not. Additionally, the chemical data helps us identify the compositional glass groups which, as a result, contributes to the formulation of an opinion about the trade links with the primary glass production centers of the period such as Levant and Egypt. Further, the study presents a comparison between different compositional groups of Side and Late Roman-Early Byzantine Anatolian glass.



## CHAPTER 2

### GENERAL ASPECTS OF GLASS AND ITS HISTORY

#### 2.1. Definition of Glass

Glass is basically a state of matter with a disordered chemical structure, a non-crystalline material. Glass, a translucent amorphous material, initially appears as obsidian before the man-made glass. Natural glass, obsidian, originates in subterranean by exposing high temperatures. When the molten silica, magma, reaches the surface it cools rapidly, which inhibits the arrangement of atoms and molecules into crystalline order. Obsidian, which can occur in black, green and brown colors, was generally used as a sharp-edged tool (Davison, 2003).

In antiquity, manmade glass is composed of three necessary ingredients which are silica, lime, and an alkali. These glasses are entitled as soda lime glasses; in batch, silica appears around 60-70 percent, sodium oxide stands at 10-20 percent and calcium oxide is about 5 to 10 percent. Totally these elements can form more than 90 percent of the glass composition. Adding certain oxides to silica is crucial since they act as stabilizers, network formers, flux, and colorants. These ingredients form glass when heated between 1300-1500°C. Silica, having the highest amount in the batch, is the main constituent of sand, crushed quartz or crushed flint. Because the ancient glassmakers supply sand from the seashore or riverbeds, it contains the fragments of shells, which provides lime (Wight 2011). Lime, calcined limestone, provides durability to the glass. An alkali comes from the ashes of plants, which is known as potash or soda ash. It serves to reduce the melting point of glass as flux.

In this dissertation, the term 'glass' will be used for historic and ancient silicate glasses.

## 2.2. Chemical Structure and Composition

Glass falls outside the concepts of classical states of matter; it is solid in terms of being rigid and having a proper shape, but it is rather liquid in terms of its random and disordered structure. Its structure is more likely to plastics which is called polymerized state (Shortland, 2012). However, glass can be separated from other polymerized-structured matters with its rigidity and stable form in normal temperatures because of its intense cross-linking between chains (Newton & Davison 1989; Shortland 2012).

The crystalline structure of silica transforms after it melts at 1710°C. When the molten silica cools the randomly scattered molecules form a less random arrangement because of the high viscosity of the glass, and the presence of the network modifiers. When the temperature of the molten glass becomes 1050°C, glass takes a solid form. However, because the structure of the solid glass is not like crystalline but more spaced and scattered, the density of glass is lower than silica (Davison, 2003).

Main glass composing oxides are the network formers (mainly SiO<sub>2</sub>, also B<sub>2</sub>O<sub>3</sub>, P<sub>2</sub>O<sub>5</sub>, GeO<sub>2</sub> As<sub>2</sub>O and so on) and the network modifiers, namely fluxes (alkali metal oxides like Na<sub>2</sub>O, K<sub>2</sub>O) and stabilizers (alkaline earth oxides like CaO, MgO). Producing a pure soda-lime-silica glass is inconceivable, minor and trace elements occur in small quantities. The elements arise in the glass either deliberately as an impurity of raw material or accidentally as contamination from the environment or the crucibles and so on. Although these impurities are present in small amounts, they can have a great effect on the batch, such as coloring, decoloring and opacifying.

### 2.2.1. Network Formers

Network former is the main component of glass. For ancient glass, silica ( $\text{SiO}_2$ ) is the chief network former; for later or modern glass, other oxides such as boron, lead, phosphorus, arsenic, and germanium can be used as network forms. Crystalline silica has a tetrahedral molecular form; silicon atom in the center attached to four oxygen atoms at the corners. Every tetrahedral unit shares two oxygen atoms in the crystalline structure (Figure 1.1). However, if it is heated and cooled rapidly, silica cannot form a crystalline structure. Instead, the atoms rearrange randomly and form a non-crystalline structure. Figure 2 shows an imaginary slice of a three-dimensional network of silica. If we consider the dots as atom A and the circles as atom O, the composition represented in Figure 1.2 is shown as  $\text{A}_2\text{O}_3$ . While Figure 1.2a shows the regular, crystalline structure of  $\text{A}_2\text{O}_3$ , Figure 1.2b reveals the non-crystalline, vitreous form of  $\text{A}_2\text{O}_3$ , which is the scheme occurred after melting and rapidly cooling the former structure (Davison, 2003). As a result, the spaces occurred in the glassy state cause an increase in the volume and consequently a decrease in the density compared to the crystalline state.

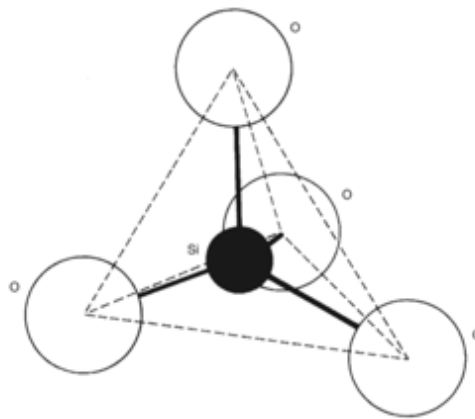


Figure 1.1. The tetrahedral molecular form of silica (Pollard and Heron, 2008)

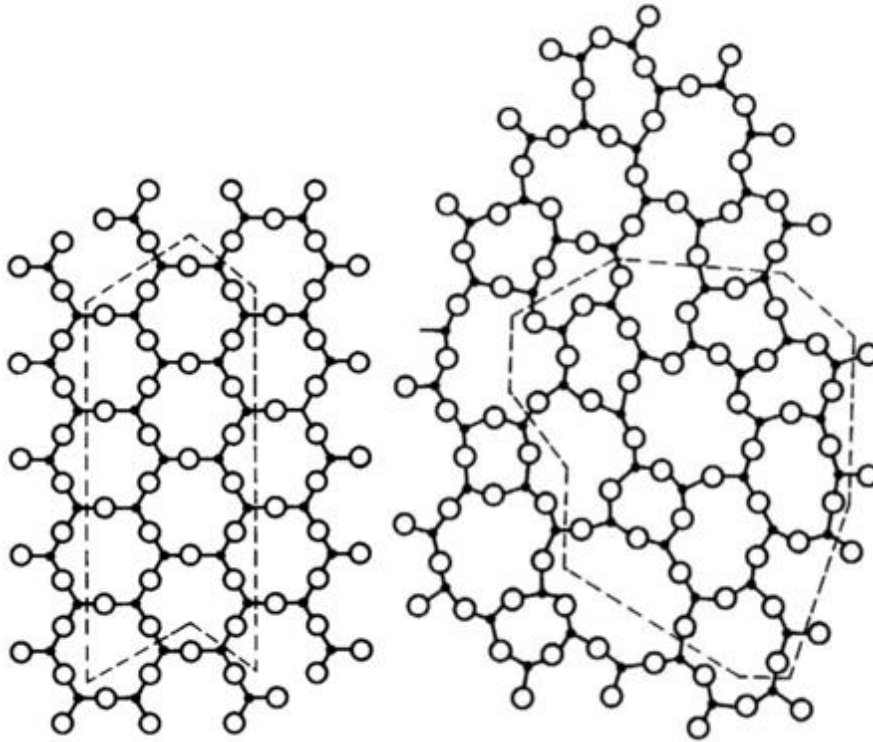


Figure 1.2. Schematic representation of compound A<sub>2</sub>O<sub>3</sub>: (a) A<sub>2</sub>O<sub>3</sub> in the crystalline state, (b) A<sub>2</sub>O<sub>3</sub> in the vitreous state. (Davison, 2003)

Silica was either obtained from beach sand and desert sand or from white quartzite pebbles of the river beds (Turner, 1956). The former source contains more impurities, such as aluminum, iron, calcium, titanium etc., than the latter (Brill, 1999 in Shortland, 2012). The indicative of the latter is the angular grains detected under the microscope. The grain size, which changes the melting performance, can be altered by the environment where sand formation occurs (Henderson, 2013). To purify and prepare the silica source, sand and pebbles may need crushing and sieving, however, the preparation of sand is easier compared to pebbles (Shortland, 2012). Additionally, from 14<sup>th</sup> to the 17<sup>th</sup> century, Venetian glassmakers used chert as a silica source (Zecchin, 1987 in Henderson, 2013).

The rock types, from which sands are derived, affects the purity of the source; for instance, crystalline rocks contain more feldspar and heavy minerals compared to

rocks composed of sand (Henderson, 2013). The selection of sand source may be problematic due to the impurities, since miniscule inclusion may affect the quality of glass such as iron-bearing minerals result in the greenish hues in glass color. These impurities can be summarized: feldspar, which is one of the most common minerals in sand, is responsible for the formation of aluminum, sodium, potassium, and calcium; titanite or sphene introduces chromium, titanium, and calcium to the glass composition; chromite brings out chromium and iron; epidote introduces alumina, iron, and calcium to the glass composition (Henderson, 2007). These impurities may allow us to trace the origin and type of glass.

Boron, which is added to the glass with the ashes of a boric oxide containing plants, is a key opponent in distinguishing glass compositions. Western Anatolia is rich in colemanite (hydrated calcium borate). Therefore, some Byzantine glasses may contain high boron (0.25%) compared to other ancient glasses with 0.01-0.02% (Davison, 2003).

### **2.2.2 Network Modifiers**

Network modifiers are composed of fluxing agents which are alkali metal oxides such as  $\text{Na}_2\text{O}$  and  $\text{K}_2\text{O}$  and stabilizers which are alkaline earth oxides such as  $\text{CaO}$  and  $\text{MgO}$ . Two ingredients are adequate for glass manufacture, sand, and soda or sand and potash. Soda (composed of sodium oxide) and potash (composed of potassium oxide) are the two main fluxing agents which provide a decline in the melting temperature of the network former, silica. These agents are highly soluble in water, which cause instability of glass in water. The silica tetrahedron ( $\text{SiO}_4$ ) can melt at the temperature of  $1710^\circ\text{C}$ , with the addition of a fluxing agent, such as soda ( $\text{Na}_2\text{CO}_3$ ), the melting temperature drops under  $1000^\circ\text{C}$ , which becomes reachable by ancient furnaces. Figure 1.3 shows an imaginary two-dimensional section of a glass network with the addition of modifiers. One or more positively charged network-modifying ions (cations) cause the formation of spaces in the silica network. Positively charged

(cations) modifying ions form an ionic bond with negatively charged (anions) non-bridging oxygen ions. By means of this ionic bond, the bridging atoms within this tetrahedral network were disrupted and the weakened bond within the silica network induces the temperature drop. These cations are generally alkali metal ions, sodium (Na+) or potassium (K+). Because they have only one positive charge, they can easily move within the network, therefore, if glass interacts with water, cations shift towards the water (Davison, 2003).

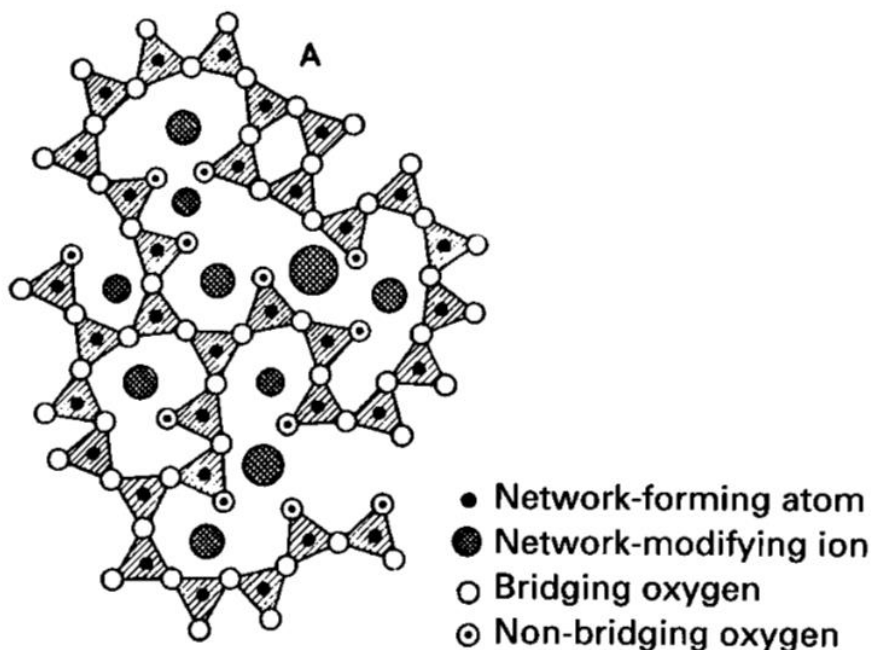


*Figure 1.3. Two-dimensional schema of glass*

Soda, also known as sodium carbonate ( $\text{Na}_2\text{CO}_3$ ), decomposes under high temperatures by releasing carbon dioxide and forms sodium oxide ( $\text{Na}_2\text{O}$ ). It is the second most common substance in the ancient glass and when the glass is not weathered the soda content is around 15-23 percent (Shortland, 2012). Fluxing agents come from mineral or plant sources. Rehren and Freestone (2015) categorize ancient glass in four compositional groups; plant-ash glass, mineral-natron glass, lead & lead-barium glass, and wood ash glass.

Till the 9<sup>th</sup> ct. BC by Mesopotamians and Egyptians, later by the Romans and Sasanians at intervals, glass -was made by using the ashes of halophytic plants, which live under salty environment, as fluxing agents due to their high sodium carbonate-containing structure as they turn to ash. Halophytic plant ashes, which can be found in the coastal margins, dunes and around desert edges, contain various salts that interact with silica like carbonates, bicarbonates, sulfides, sulfites and hydroxides (Henderson, 2013). Halophytic plants with genus like *Salsola kali* and *Salicornia* contain high impurities like potash and magnesia accompanying soda (Henderson, 2000). There are two other kinds of plants to be used as a flux; one type is a tree-like beech that has potash-rich ash and the other type have a high level of soda and also potash (Shortland, 2012). Natron ( $\text{Na}_2\text{CO}_3 \cdot 10\text{H}_2\text{O}$ ) or trona ( $\text{Na}_2\text{CO}_3 \cdot \text{NaHCO}_3 \cdot 2\text{H}_2\text{O}$ ) and other soda-rich minerals that contain carbonates and chlorides, which are partially reactive, were collected from large evaporitic lakes and were used for glass production in antiquity. According to Pliny, Romans widely used natron 'preferably Egyptian soda' during the 1<sup>st</sup> millennium BC and AD. Within this period, natron was acquired from Wadi Natrun, the most significant source in Near East (Shortland, 2004). According to the researches conducted with natron from el-Barnugi, it can be used without pre-treatment (Jackson et al., 2016). Although the natron composition can be varying even in the same area, they are mainly composed of sodium compounds including carbonates, bicarbonates, sulfates and, chlorides (Jackson et al., 2016). When compared to plant ash, natron is a purer source of alkali and has a more condensed alkali structure, the magnesia, and potash percent of natron glass is below 1.5 wt% (Henderson, 2013). However, by the 9<sup>th</sup> century, Egyptian glassmakers started to use plant ash instead of natron back again (Rehren et al., 2015). Also, there are several other alkali-rich mineral sources like *reh* (combination of sodium carbonate, sodium chloride, sodium sulfate, calcium, and magnesium), *oos* and *nepheline*, which are mainly used in India (Wadia, 1975; Brill 2001; Henderson, 2013). Nepheline syenite – a sodium, potassium, and aluminum silicates, together with quartz and feldspar, was used in Sagalassos, Antalya, Turkey in the production of a

frit as a network modifier (Degryse and Poblome, 2002; Henderson, 2013).

Another type of network modifier is the stabilizers which are crucial for glass considering their unstable and soluble structure. The addition of stabilizers such as calcium, magnesium, and aluminum provide stabilization to the glass. The addition of alumina increases the working properties of glass during shaping and forming (Goffer, 2007). The alkaline earth cations such as calcium ( $\text{Ca}^{++}$ ) and magnesium ( $\text{Mg}^{++}$ ) take double positive charge, which makes them tightly bound to adjacent non-bridging oxygen atoms unlike single positively charged, loosely bounded network-modifying ions (Davison, 2003). Therefore, alkaline earth cations make glass stronger, durable and relatively insoluble.

In ancient times, calcium was added unintentionally to glass, either by the impurities in silica source as the small shell fragments in sand or by the inclusions of the soda source as calcium-containing plants derived from limestone (Whitehouse, 2012). Another calcium source is bone and dolomitic limestone, which was intentionally used between 16<sup>th</sup> to 19<sup>th</sup> centuries in Europe. However, the addition of the latter gives a positive correlation between magnesia and calcium (Henderson, 2013). Moreover, glass can be accidentally contaminated from calcium-bearing crucibles and calcium-bearing minerals in the sand. While some states that magnesia derives from dolomite or dolomitic sandstones, the weak correlations disproves this relation. On the other hand, the positive correlation between potassium oxide and magnesia indicates that magnesium enters the batch through potash (Henderson, 2007).

Lime and alumina are generally used for separating glass groups because they reflect the glassmaking sand (Schibille et al., 2017). For instance, Roman natron glasses contain alumina between 1.7- 3.5% due to feldspar that is found in sand. Likewise, while bronze age and Islamic glasses contain relatively low calcium due to the usage of Halophytic plant ash, 1<sup>st</sup> millennium AD glass has 6.5-9% calcium inclusion (Henderson, 2013).

### 2.2.3 Colorants, Opacifiers And Decolorants

In antiquity, glass was first emerged as colored and it was used to imitate precious and semi-precious stones.

Network formers, stabilizers, and modifiers specify the main properties of glass. However, minor and trace elements, forming a maximum 5 percent of the total mass, can change the properties of glass, like the color of the glass (Goffer, 2007). The colorless glass generated only by pure silica, soda and lime can be colored with the addition of metal oxides. There are several metals that change the color of the glass; iron, copper, cobalt, tin, manganese, lead, antimony etc. However, apart from the metal oxides, many other factors affect the color of the glass.

Preparing the batch with fine particles of colorants and heating the batch in high temperatures provides a homogenous color. (Stoch et al., 1978; Henderson, 2000) Further, during solidification, unlike glass, some components in the glass may crystallize. These crystalline impurities, some of which are deliberately added to the batch or occurred during different heat treatments, lead to opacification. Due to their insolubility in glass and their deflective property, light scatters and does not pass through the glass (Biek and Bayley, 1979; Goffer, 2007). Besides, the masses of tiny bubbles generate opacification in ancient glasses (Davison, 2003). Calcium antimonate, tin oxide, and calcium fluorophosphates are the main substances to create white opal glass; and lead antimonate together with lead-tin oxide were the opacifying agents to create yellow opal glass.

As Biek and Bayley (1979) noted the atmosphere of the furnace can change the color of the glass; for instance, iron can generate blue or red color regarding the oxidizing or reducing atmosphere in the furnace. An oxidizing atmosphere is an environment where oxygen prevails while reducing atmosphere is where carbon dioxide and carbon monoxide prevails. While the conditions are oxidizing, the iron that is in the 3<sup>rd</sup> state can give blue/green hues to the glass, the iron reduces to Fe<sup>2+</sup> ion in a reducing

atmosphere and creates black/brown hues (Shortland, 2012). The coloration can also be affected by the heating cycle; how long the melt stays in specific heats and the maximum temperatures achieved (Henderson, 2000). The type of fuel and its particle size are also important since they affect the reached temperature.

Table 1.1 shows the coloring effects of the ions in reducing and oxidizing furnace environments.

*Table 1-1 Glass coloring ions in different furnace environments*

Glass color	Coloring metal		Glass furnace environment
	Metal	Ionic form	
Black	Manganese	$Mn^{2+}$	Reducing
	Copper	$Cu^+$	Reducing
Red	Copper	$Cu^+$	Reducing
	Gold	–	Reducing
Pink	Manganese	$Mn^{4+}$	Oxidizing
Yellow	Uranium	$U^{4+}$	Oxidizing
	Silver	–	Reducing
Green	Copper	$Cu^{2+}$	Oxidizing
	Iron	$Fe^{2+}$	Reducing
	Chromium	$Cr^{3+}$	Oxidizing
Blue	Copper	$Cu^{2+}$	Oxidizing
	Cobalt	$Co^{2+}$	Reducing
Violet	Manganese	$Mn^{3+}$	Reducing

The main coloring elements are given below.

### Copper

Copper is one of the oldest colorants in the glass world, which dates back to 4000 BC in the Near East and Egypt (Tite, 1987). The common feature of minerals that are mainly used to color glass such as malachite, azurite and turquoise is copper, which gives glass various colors like blue, green, red and black. While highly oxidized copper -the cupric ions  $Cu^{+2}$ - can color the glass to blue, lightly oxidized copper-cuprous ions  $Cu^+$  - provides red color (Goffer, 2007). Small amounts, approximately

0.5 % w copper oxide is enough to color the glass. However, smaller amounts around 0.1 % w of copper may result from contamination, not a deliberate addition, and it is present in all colored glasses (Shortland 2012). From Classical times to the Roman period, copper sulfide -ferretto- was roasted to obtain metallic copper (Henderson, 1985).

Since oxygen dissolves the opacifying agents, the reducing atmosphere of the kiln may cause the formation of dendritic cuprite particles in suspension, which results in opacification when copper is added in high amounts. Although the red color was mainly generated from copper, it can be formed by several variations of colorants such as just copper, copper-antimony; copper-tin-antimony, copper-tin-lead-zinc; solely antimony (Shortland, 2012). While some Egyptian glasses contain small amounts of tin and lead, Near Eastern glasses from LBA do not contain tin, which shows Near Eastern glassmakers used a pure source of copper instead of bronze (Shortland 2012). There are some assumptions that the use of lead may result in the occurrence of green tint instead of blue color. Further, copper impurities found in cobalt glass is evidence of using cobalt-rich copper ore as a colorant source (Henderson, 1985).

## Cobalt

The first use of cobalt is seen in the Bronze age to imitate lapis lazuli, a highly valuable precious stone. It is confirmed that Egyptians deliberately added cobalt to the batch in the 2<sup>nd</sup> millennium (Farnsworth and Ritchie 1938; Shortland 2012). It was continued to be used in the Iron age and later in the Chinese porcelains. In the 2<sup>nd</sup> century BC, the manganese-rich sources started to be chosen over antimony-rich sources as the source of cobalt (Henderson 1991). Cobalt is found in ancient rock mineralization, which contains other minerals such as copper, nickel, manganese, iron, zinc, and arsenic regarding the type of the mineral. These ores are Erythrite ( $\text{Co}_3(\text{AsO}_4)_2 \cdot 8\text{H}_2\text{O}$ ), Trianite ( $2\text{Co}_2\text{O} \cdot \text{CuO} \cdot 6\text{H}_2\text{O}$ ), Cobaltite ( $\text{CoAsS}$ ), Skutterudite ( $(\text{Co}, \text{Ni}, \text{Fe})\text{As}_3$ ), Bieberite ( $\text{CoSO}_4 \cdot 7\text{H}_2\text{O}$ ) and Absolane ( $\text{CoOOH}$ ) and they contain trace elements such as bismuth, vanadium, lead and antimony (Henderson 2013).

Compared to other colorants, cobalt is the most powerful one, even the smallest additions such as 0.02% ( $\text{Co}^{2+}$ ) can change the color of the glass to deep blue (Henderson 2013). On the other hand, when it is in the +2 state it gives a pink color.

## Iron

Iron oxide is one of the most common colorizers in ancient and modern glass production. The characteristic greenish tint of the ancient colorless glass comes from the iron (II) which appears as an impurity in the sand (Davison, 2003). In the glass, iron impurities appear as ferrous and ferric ions which supply the formation of various colors from blue to black. Iron creates very dark colors as added to the batch in (+2) state, but in (+3) state, it creates a yellow tint. However, if reduced ferrous ( $\text{Fe}^{2+}$ ) and the oxidized ferric ( $\text{Fe}^{3+}$ ) irons are mixed, glass gets the green color. Less than 1 percent of iron oxides is adequate for the classical green tint (Goffer, 2007). During melting, redox reactions give rise to alteration of these ions. While reducing conditions cause the formation of brown/black colors, oxidizing conditions cause blue-green tint. According to Henderson (1985), black color derives from the deliberate addition of iron. Also, the addition of other colorants gives rise to a change in the color of the glass. For instance, in the addition of manganese, because they gradually reduce and oxidize each other, various hues emerge (Biek and Bayley, 1979). When Fe(III) and sulfides, which occurs with the reduction of sulfur, combine, yellow-amber color appears (Lambert, 1997).

## Manganese

Manganese gives violet color when it is in the (+3) state Mn(III) and pink color in (+4) state Mn(IV), also when it is charged in (+2) state it is less colored (Lambert, 1997). Pyrolusite ( $\text{MnO}_2$ ), a common manganese mineral, was used by the Romans to offset the green tint and also to produce a violet color (Goffer, 2007). Psilomelane, dialogite, rhodochrosite, and wad are some of the other less pure manganese containing minerals, which first needs to be prepared before using (Jackson, 2005). While

pyrolusite is a purer mineral, psilomelane contains a significant amount of barium, which is an indicator of psilomelane addition as a source of manganese. On the other hand, pyrolusite cannot be detected since it is purer (Shortland, 2012). Manganese sources generally include several trace elements, and one of the most common is iron. Manganese is not just a colorant but also a decolorant, which is discussed below.

## Silver

During the Roman period, the silver mineral was added to the batch to give the glass a yellow tint. Additionally, it was used to shade the glass. As Goffer (2007) states, the procedure has three stages. First, the powdered silver minerals together with a clay binder and water are applied to the glass surface by a brush, then the glass is heated in 600°C in a reducing atmosphere to fix the coating and finally it is left to cool. Silver ions oxidize to silver oxide when glass starts to melt at >600°C and under reducing atmosphere, silver ions reduced to metallic silver which shades the glass. The thickness of the coating can change the level of shading.

## Opacifying elements

From at least 2000 BC, antimony was found in glass, probably as an impurity and since then it has continued to be used as an opacifier till the late Roman period (Davison, 2003 and Rooksby, 1976). Stibnite and bindheimite are among the antimony-containing minerals. Stibnite, antimony sulfide, reacts with other components to form metal antimonites. Antimony is added to glass to obtain calcium antimonate caused by the reaction of antimony with calcium, which induces crystals that reflect the light (Henderson, 2007). Regarding the metal in the batch, melt transforms to opal glass with different colors. For instance, the presence of calcium leads to the formation of white opal glass because of the crystallization of calcium antimonite. Likewise, the presence of lead gives rise to a yellow variety of opal glass (Wainwright et al., 1986).

Lead antimonate was a colorant and an opacifier used before 2<sup>nd</sup> ct. BC and the main ore is Bindheimite ( $\text{Pb}_2(\text{Sb,Bi})_2\text{O}_6$ ). The presence of bismuth in the glass batch might be indicative of the use of this mineral in the production of glass (Henderson, 2007). The combination of lead and antimony, as in the calcium and antimony reaction, leads to the formation of undissolved pyroantimonate crystals, that generates yellow opaque color.

Cassiterite, tin oxide mineral, was used as an opacifying agent since the sixth century BC in Mesopotamia till it was replaced by antimony. However, after the Roman Empire, with 4<sup>th</sup> century AD, tin was started to be preferred instead of antimony throughout Europe and the Middle East. Cassiterite can produce white opacity. According to Biek and Bayley (1979) the opaque blue glasses after the Roman period started to contain tin oxide and yellow opaque glasses contain lead-tin oxide. Lead stannate ( $\text{O}_3\text{PbSn}$ ) can generate paler yellow color compared to lead antimonate (Henderson, 2007).

#### Decolorants

Normally glass colorants appear in reduced conditions in the furnace, however, antimony oxide, manganese oxide, and arsenic are added to the batch to oxidize the iron (Davison, 2003; Arletti et al., 2013).

If manganese appears around 0.1% to 1.6%, the reduction of manganese and oxidation of iron gives glass transparency because both metals transform from highly colored to lightly colored models (Lambert, 1997). Pyrolusite, also known as glassmaker's soap, was used both as a decolorizer and a colorant which gives violet color (Goffer, 2007). When manganese oxidizes iron, ferrous ions alter to less colorant ferric ions, which give rise to translucence. Due to the decrease in highly colorant ferrous ions, four colors compensate each other which lead to the formation of gray color (Brill, 1988). If manganese exceeds 1 w% in the composition, glass is apt to be colorless regarding low levels of iron (Jackson and Paynter, 2016; Freestone, 2015).

Although manganese is used as a decolorizer, antimony is more effective. It also performs as a fining agent in glass by removing dissolved gases which makes glass more brilliant (Silvestri, 2008). According to the research of Jackson and Paynter, high manganese (more than 1wt%) glass with the iron of 0.6 wt% can end up with a blue-green hue. However, the addition of higher amounts of iron (0.8 wt%) to the antimony decolorized glass results in colorless glass. According to Silvestri (2008), manganese does not decolorize effectively unless the ratio of MnO to Fe<sub>2</sub>O<sub>3</sub> is bigger than 2. According to the experiments of Brill (1988), even the correct ratio of MnO to Fe<sub>2</sub>O<sub>3</sub> is achieved to make glass decolorized, if the furnace atmosphere is highly reducing, manganese does not affect properly as an oxidant which restrains decolorization.

### **2.3. Brief History of Glass from the beginning to the late Byzantine period**

In this section, the emergence of glass, its development, production techniques and its chemical compositions up to the late Byzantine period are mentioned.

#### **2.3.1 The Origins of Glass and its Chemical Composition until The Roman period**

Pliny the Elder, the Roman author and commander, mentions the origins of glass in his book Natural History. According to Pliny, the natron traders docked to the mouth of the River Belus and prepared their meal. However, there were not any stones to support their cauldrons, therefore, instead of stones, they used the natron –an alkali- in their ships. Once they are heated, the natron that mixed with the sand, turned into translucent liquid (Wight, 2011). However, it is known that the Mesopotamians discovered vitreous materials long before those traders. The earliest written source for glassmaking, a clay tablet, rises to the surface from Tell Umar, Mesopotamia dating between 1400-1200 BC This cuneiform tablet gives a recipe for red glass production (Wight, 2011).

Although the exact dates and the origin are unknown, it is thought that glass was emerged either as an accidental side-product of metal production or as a consequence

of glazed pottery production. As E. J. Peltenburg states that metal seems the real antecessor of glass for the need of reaching to the molten state, Robert H. Brill claims glazed pottery is the antecessor of glass because of using similar compositions (Lambert, 1998). On the process of metal production, metal ores are refined from impurities such as silica. After this refinement, the decomposed silica solidifies and acquires a glassy form. Theodore A. Wertime accepts these slaggy lumps from Eshnunna as the earliest known glasses (Lambert, 1998). The Archaeological evidence that comes from Northern Mesopotamian sites shows that glass production started before 25<sup>th</sup> century BC (Davison, 2003). However, according to another belief, the vitreous glazes, which have been used for coloring beads, tiles, pottery and making them impermeable and enduring, were accepted as the first steps of glass (Wight, 2011).

Early glazes and glasses have common compounds, in both, alkali is added to silica as a network modifier (Lambert, 1998). The vitreous glazes, the modified silica, were used for imitating precious, and semi-precious stones (Davison, 2003). This surface glaze is generally called Egyptian faience, tin-glazed quartz was discovered from various Predynastic sites in Egypt between 5500-3050 BC and they are also found in Mesopotamia from 4300 BC onwards (Davison, 2003). Faience contains glassy materials, blue crystals of cuprorivaite,  $(Ca,Cu)Si_4O_{10}$  and especially, crystalline material because it does not expose to high temperatures as glass does, therefore the crystals cannot dissolve in the composition (Henderson, 2013b). While faience can be produced in small kilns, glass need furnaces to reach high heat. Moreover, a single firing procedure is adequate for producing faience where glass needs reheating and working (Henderson, 2013). According to Hodges (1992), the real glass might have been initially observed by incidental overheating of faience. The chemical difference of Egyptian blue compared to glass is its high silica and low alkali composition.

The earliest glass objects, which dates to 2500 BC, were produced by molding and cold-working. The ancient glassworkers could not reach the high temperatures that are

enough to drain the liquid glass into molds, therefore they used casting. This technique was achieved by putting a variety of heated glass chunks into a mold. After the annealing process, the glass is finalized by cutting or polishing (Wight, 2011). With 15<sup>th</sup> century BC, glass was relatively common, however, before the 16<sup>th</sup> century BC, glass finds were highly rare and more prestigious (Shortland, 2012). The small number of glass finds from this period are mainly beads, glass lumps, inlays, and pendants.

During the late Bronze age, Mesopotamians and Egyptians mainly produced small vessels, pendants, and beads out of glass. However, glass ingots were among the merchandise goods. These ingots were economically preferable because they can melt and fuse at lower temperatures, about 750°C (Wight, 2011). For the same reason, broken and old glass was used as recycled glass. Difficulties in melting glass led glassworkers to deal with various techniques. Core-forming was revolutionary for glassmaking to become an industry. First glass vessels were produced by this method. To shape the glass, they first created a core from terracotta and roll the glass threads around it and span the rolled glass threads on a surface. After the object was fired, the core of the terracotta was removed by carving. This technique was used in the making of long thin glass vessels, scent bottles and jewelry (Özgümüş, 2000). The core-formed glass was first used to resemble precious or semi-precious stones, they were opaque and mainly blue. To achieve this resemblance, glass was exposed to heat treatments which provokes the calcium antimonite crystals that causes opacity (Henderson, 1989).

In the 15<sup>th</sup> century BC, right after core-formed glass vessels, Mesopotamians produced small and cylindrical zig-zag-patterned, polychrome vessels by using a mosaic technique, which was developed in the Hellenistic and Roman periods (Wight, 2011). Glassworkers united various single-colored glass rods to create multi-colored glass rods. These rods were elongated and cut into small pieces, then the small pieces were placed between two molds before firing. In order to smoothen the rim, a spiral rod was used, and the vessel was finally lustered by fire or by a wheel (Özgümüş, 2000). As

another casting technique, molding appears contemporary with the aforementioned techniques to create pendants, furniture inlays, figurines, and jewelry. In molding, one person spills the molten glass into a mold, and the other person pushes the piston to make the glass penetrate elaborately into the mold. However, in this period, whether the glass was poured into molds or whether molds were pressed down on a surface is not known (Davison, 2003). Later on, the casting was applied by using the lost-wax technique. In this technique, the wax-filled molds are heated and the wax leaks with the heat; the glass pieces that are thrown in the mold melt and shape the mold (Özgümüş, 2000).

In LBA, glass manufacturing developed quickly in northern Mesopotamia and spread to other places like Near East, Cyprus, Mycenaean Greece and so on. Despite the ambiguity of the origin of the glass, most scholars think that the birthplace was Mesopotamia but the place where the glass was improved was Egypt. Their composition of silica-lime glass remained quite similar to the present. Moreover, the Levant region was a significant glassmaking area where raw glass and finished products were traded. As Pusch and Rehren (2007) suggest, LBA glass manufacturing was generated in elite-attached workshops as glass ingots -with one or limited range of colors-, which are later sent to elite-attached studios for output. In this period, glass vessels resemble faience vessels. (Peltenburg, 1987) The earliest glass vessel representatives are from Alalakh, Turkey.

Unfortunately, the 13<sup>th</sup> century was the start of a decline for the glass industry, later on, glass even disappears for a while, which is accepted as a dark age for glass. The few finds from this period did not resemble earlier periods with their muddy colors, highly corroded layers, inclusions and bubbles (Shortland, 2012). Probably the collapse of the great empires of the Bronze age, endless wars, invasions, and severance of trade affected the glass industry for hundreds of years. Glass vessels reappear in the 8<sup>th</sup> and 9<sup>th</sup> centuries from Egypt and Mesopotamia (Freestone, 2006).

It is known that the first glasses are made with two ingredients; silica and plant ash. The tradition of plant ash glasses lasted from 2500 BC to 800 BC (Henderson 2013). LBA Egyptian and Near Eastern glassmakers use quartzite pebbles, which is rather a pure silica source. Therefore, alumina inclusion is lower at 0.7-0.8% levels than latter sand-used glasses (Shortland, 2012). Soda amounts are below 20%. LBA glassworkers use plant ash as flux, therefore magnesia and potash levels are high compared to later periods where natron was used. Magnesia levels vary between 3-7% and potash levels vary between 0.5 to 3.5%. However, potash values range according to color; while blue cobalt samples have lower potash values, other colors have concentrations around 2 to 2.5% (Kaczmarczyk, 1986 in Shortland 2012). Sayre and Smith (1961) classify these plant ash glasses as High Magnesia Glass (HMG). This type is seen around Mesopotamia, Egypt, and Greece during the late Bronze Age. Between 1100 and 750 BC, a different type of glass emerged in Europe which is characterized by mixed alkalis, low calcium oxide, and low magnesium oxide. This type is called low magnesium, high potassium -LMHK-, while magnesium levels are below 1%, total alkalis are around 14-16% (Henderson 1988). This type is the most common glass found in Europe with 8-13% K<sub>2</sub>O and 1-2% MgO (Shortland, 2012). After 800 BC, natron glass, with high magnesia high potash, was used during Middle Eastern Iron Age, and later used by Etruscans and Phoenicians in Iron Age Europe, by the Hellenistic Greeks, Romans, Byzantines and so on (Henderson, 2013).

### **2.3.2 Roman to Late Byzantine Glass and its composition**

Romans produced their glass objects with mold-pressed casting technique. However, the end of the 1<sup>st</sup> millennium BC was a milestone for glass production. The blowing technique, which was probably invented around the Syro-Palestinian area, has opened a new age in glassmaking by terms of mass production and new forms. By means of glassblowing, production process shortened, therefore glass began to be used at households and it became no longer a luxury item as it was before. Glassmakers create new shapes and types of glasses when they get freed from the burden of the thick glass.

For instance, the first thin and flat window panes are seen in this period. Furthermore, by the last quarter of the 1<sup>st</sup> century, the trend of intensely colored glass has mostly shifted to a colorless or unintentionally colored glass with blue-green hues, with an increasing demand for tableware (Silvestri, 2008).

The basic of the glassblowing is shaping the glass by turning and inflating the glass which is on the tip of a metal blowpipe. There are mainly three types of glassblowing. First one is tube blowing which needs glass tubes instead of blowpipes. One end of the tube is sealed up and the glass is blown from the other side of the tube. The open side is broken when the glass is shaped. The second method is free-blowing. In this method, Glassworkers heats up one end of the blowpipe till it gets red and warms it down by water. The process requires getting a glob of glass to the end of a blowpipe and spinning it in the air before rolling and shaping the glass on a marver while blowing to the pipe. The last method is mold-blowing. The molds can be made of soil, metal or wood (Özgümüş, 2000). During blowing, the end of the pipe is placed into the mold and the glass is inflated until the whole mold is filled. It reaches up to 1000°C.

Syro-Palestinian region is the place that Roman glass was evolved during the 3<sup>rd</sup> century BC, with the conquest of Syria and Egypt in the first century BC, the glassmakers of the area were introduced to Rome (Lambert, 1997). Millefiori (thousand flowers) or mosaic glass technique was advanced in this period especially in the capital. In this period, glassblowing helped the development of cased glass, where multiple layers of different compositional glass are applied on an object. Cameo glass is a variation of this technique, where dark-colored glass is covered with white opaque glass, which is later removed by etching the unwanted parts to create a white-colored figure on a dark surface. When the empire started to lose its power by the end of the 5<sup>th</sup> century, glass flourishing came to an end.

In consequence of the discovery of a new technique in 50 BC, glassblowing, the use of glass increased rapidly. Therefore, to supply the increased demand the structure of

the furnaces has changed. The new reverberatory furnaces have low-roofed rectangular tanks, a combustion chamber and a vent (Whitehouse, 2012). Unlike the small-sized furnaces, the new Roman furnaces have the capacity to produce tons of glass at a time. The mass-produced glass was divided into ingots and chunks, which are later shipped and cargoes to the secondary production sites where they are re-melted and shaped. Thus, the emergence of blowpipes and tank furnaces was a milestone for the glass world.

The style and the form of the Roman glass were progressive across the empire, however, as researchers like Turner and Sayre and Smith explained, the composition of the glass was rather homogeneous for almost six hundred years which made the provenance and technology researches problematic (Lemke, 1998) and strictly controlling the production technology aroused this homogeneity throughout the empire. Also, large-scale manufacturing with standard techniques in discrete locations could be the reason for this consistent composition for the 4<sup>th</sup> century and later (Jackson et al., 2003). Or else the recycling of the chunks that come from the primary production sites could be the reason of this homogeneity.

According to work of Sayre and Smith (1961), there are 2 types of early soda-lime-silica glass composition; one of them is high potash high magnesia both being higher than 2%, the other one is low potash low magnesia. Generally, because the Romans mainly used natron as a soda, the main composition is the latter. If the chosen source of soda is plant-ash, the composition is the former. The potassium content of the Roman glass is generally lower than 1%. Although plant-ash glass was replaced by natron after 800 BC, few examples of plant ash glass continued to be seen around the Middle East and Europe such as emerald green glass in England and black colored glass from Austria during 3<sup>rd</sup> c. BC-1<sup>st</sup> c. AD; black unguentaria in Egypt between 2<sup>nd</sup> to 4<sup>th</sup> c.; several samples from northern Italy from 4<sup>th</sup> c. AD, red opaque enamel or mosaic glass from Roman and Byzantine sites and so on (Cosyns et al., 2006; Mirti et al., 1993; Freestone et al., 1990; Henderson, 1996; Brun et al., 1991; Shugar, 2000;

Santagostino Barbone et al., 2008 as cited in Henderson, 2013). In the Roman period, sand was preferred instead of pebbles as a source of silica (Turner, 1956). Feldspar, a common mineral inclusion found in sand, involves a serious amount of alumina in its content. Therefore, alumina appears more than one percent in Roman glass composition (Brill, 1999; Shortland, 2012). Later in the Byzantine period, the glass may include boron in their structure (0.25%) more than typical ancient glasses (0.01-0.02%) due to mineral colemanite that is found in western Turkey (Davison, 2003).

During the Roman period, especially from the late 1<sup>st</sup> century AD and into the 2<sup>nd</sup> century AD, the popularity of colorless glass increased compared to previous ages (Jackson, 2005). Different from its antecessors, manganese was used as a decolorant alternative to antimony. However, from the 2<sup>nd</sup> century BC to 5<sup>th</sup> century AD antimony was revived in the compositions (Lambert, 1997). Especially in the non-Roman Middle East, it was prolifically used from first to third centuries AD, until the increase in manganese (Lambert, 1997 and Jackson, 2005). By the 5<sup>th</sup> century, the use of antimony was completely finished, and tin oxide took its place as an opacifier. (Lambert, 1997) As studies show, the soda content in the manganese-decolorized Roman glass is higher than antimony-decolorized natron glass (Jackson and Panthyr, 2016). In the Roman and pre-Roman periods, calcium antimonate was used as an opacifier for white opal glass, however, from 5<sup>th</sup> to 18<sup>th</sup> centuries, mainly tin oxide and occasionally calcium fluorophosphate were used, which was later replaced by calcium fluoride and lead arsenate. Likewise, while glassmakers chose lead antimonate in the earlier periods, they turned to lead-tin oxide in the later times (Davison, 2003).

Glass production in the first millennium AD was dominated by a few primary production sites with high manufacturing capacities. Unlike the small workshops of the previous periods, in the new millennia, glass was produced in the large workshops of significant regions with distinctive glass compositions and distributed to the secondary production sites for working. Therefore, Mediterranean region housed

several main glass groups during the late antique period; Roman blue-green, Roman antimony-decolorized, Roman manganese-decolorized, HIMT, Levantine I, Levantine II, Wadi Natrun (Egypt I), Egypt II, and Magby. Identification of glass groups is significant for detecting the inter-communal trade links and the chronological shifts in the goods of primary production centers (Rehren and Cholakova, 2010).

The most widespread glass type of the Roman period, between the first and the third centuries CE, was the Roman blue-green glass. The color of the glass generates from the iron impurities of the raw materials (Silvestri, 2008). The compositional characteristics show that iron content is around 0.75%, manganese oxide levels are approximately 0.55% and alumina content is ~2.5%. Relatively lower contents of magnesia (0.6%), titanium oxide (0.08%), potash (0.8%) were detected. Antimony levels (~0.2%) show signs of recycling due to its inadequate amount for a deliberate addition (Foster and Jackson 2009). There have been arguments that Roman blue-green glass was made both with Egyptian natron and Palestinian sand from the mouth of River Belus, however it has been objected due to the incoherent lime to alumina ratios and different oxygen and neodymium isotopes (Foy et al., 2000; Nenna et al., 1997, Freestone et al., 2000; Degryse and Schneider, 2008 in Foster and Jackson, 2009).

Roman antimony-decolorized glasses (Rom-Sb) have Sb levels varying between 0.3-0.8% and manganese levels are below 0.05%. The Rom-Sb glasses from Yasmina Necropolis, Carthage show a strong correlation between MgO and FeO and a weaker correlation between FeO and Al<sub>2</sub>O<sub>3</sub> and TiO (Schibille et al., 2007). The British Isles present comprehensive examples of Rom-Sb, which contain low alumina (1.90%), low magnesia (0.49%), low lime (5.74%), fairly low potash (0.39%) and low barium (148 ppm) compared to Roman blue-green glass (Foster and Jackson 2010). Another decolorized group widely circulated from 1st to 4th centuries is Rom-Mn that is characterized by manganese above background levels (MnO>0.025%). The antimony

level of this type is below the detection limits (0.03%). When compared with roman antimony-decolorized it contains lower soda, higher lime, alumina potash and magnesia levels (Schibille et al 2007). Foster and Jackson (2010) demonstrates two subgroups for Rom-Mn; first one is Colourless 2a with low alumina (~1.81%), higher magnesia than the other colorless glass groups (~0.67%), low lime (5.77%), very low potash (0.29%), rather low barium (~199 ppm) and the second group is Colourless 2b samples with higher alumina (2.37%), slightly lower mean magnesia (0.41%), high lime (8.02%) and higher potash (0.61%).

Probably due to the large-scale economic and political alterations in the 4<sup>th</sup> century, HIMT glass replaced Roman blue-green glass and became widespread all-around Europe and Mediterranean region (Freestone et al., 2002). The transparent HIMT glass has a yellowish green or olive-green tint unlike the classical blue-green glass of the Roman period (Freestone, 1994). This type is termed by Freestone as HIMT due to its **H**igh **I**ron, **M**anganese and **T**itanium concentration. It is thought to be originated from Egypt regarding its high titanium content as in the Egyptian sands (Foy et al., 2003). Iron level is above 0.7%, titanium level is above 0.1% and manganese levels are around 1-2%. While lime is relatively low at 5-6.5%, soda is higher between the range of 17-20% and magnesia is usually higher (>0.8%) compared to previous glass types (Freestone et al., 2005; Foster and Jackson, 2009). However, not every glass with high concentrations of iron, manganese, titanium can be designated as HIMT glass, there should be a strong correlation between titanium, magnesium, manganese, iron and additionally aluminum oxide (Freestone et al., 2005). Furthermore, zirconium and barium are elevated and variable (Mirti et al., 1993; Freestone et al., 2005; Foy et al., 2003). Aosta, Italy (Mirti et al., 1993), Carthage (Freestone, 1994), North Sinai (Freestone et al., 2002), France, Tunisia, Egypt (Foy et al., 2003) and numerous Mediterranean sites show the characteristics of HIMT glass.

HIMT glasses are divided into two groups by Foy and his co-workers; Série 1 and Série 2. Série 1 from the 5<sup>th</sup> century contain higher Fe, Ti, and Mn and lower lime

(6%) concentration compared to Série 2 of the 6<sup>th</sup> and 7<sup>th</sup> centuries with higher lime (7.7%) (Foy et al. 2003). Foster and Jackson (2009) define these two subgroups as HIMT 1 (strong HIMT) and HIMT 2 (weak HIMT). Iron (1.36%), manganese (1.71%), titanium (0.33%) levels of HIMT 1 group double the iron (0.72%), manganese (0.98%) and titanium (0.12%) concentration of HIMT 2 group. Both subgroups show correlations between the aforementioned elements, although HIMT 1 glass demonstrates stronger correlations (Foster and Jackson 2009). Magnesia (0.98%), barium (600 ppm), chromium (30 ppm), zirconium (117 ppm), strontium (501 ppm), vanadium (33 ppm) concentrations of HIMT1 glass is higher than HIMT 2 glass (0.76%, 290 ppm, 8 ppm, 31 ppm, 446 ppm, 17 ppm respectively). Both HIMT1 and HIMT2 groups from Romano-British assemblage contain low levels of lime and high levels of soda. Another subgroup is defined by Rehren and Cholakova (2010) as HIT (High Iron Titanium) for the glasses with low manganese from late 5<sup>th</sup> century Dichin, Bulgaria. Ceglia and his coworkers (2015) introduce the term HLIMIT (High Lime Iron Manganese Titanium) to the literature for the glass of the 6<sup>th</sup> and 7<sup>th</sup> centuries with high lime (7-9%). Although HLIMIT glass, which refers to Foy's Serie 2, from Cyprus contain high iron, it is still relatively low compared to HIMT glasses. HLIMIT glass, which is widely found in Europe in Frankish/ Merovingian/Anglo-Saxon contexts, resembles weak HIMT with its similar titanium concentration (Freestone et al 2018).

Levantine I group, a contemporary example of HIMT glass, originates from Palestinian region and prevails during the late Roman / Early Byzantine period between 4<sup>th</sup> and 7<sup>th</sup> centuries AD. In this category, Jalame presents examples from the 4<sup>th</sup> century and Dor, Bet Shean, Apollonia offer samples from 6<sup>th</sup> to 7<sup>th</sup> centuries; even Romano-British sites show similar homogenous compositions from the late antique period. This type corresponds to Foy's (2003) Group 3 and when we compare Levantine I with Foy-2, magnesium, boron, and lithium concentrations are lower (Schibille et al., 2016). While the soda (~15%), iron oxide (~0.4%) and alumina (2.5-3%) contents are lower, lime (8-9%) content is higher compared to other predominant

glasses of the period (Foster and Jackson, 2009). The soda to lime ratio is approximately 2:1. Jackson and Foster presents two subgroups to this category; Levantine 1a with a significant amount of magnesia, approximately at 1-2% and Levantine 1b with trace amounts of magnesia at 0.1%. According to Freestone et al. (2000), Levantine glass during late antiquity involves low levels of zirconium and high levels of strontium. Considering strontium is obtained from the shell pieces, it has been accepted that coastal sand involves high strontium (>150 ppm) and low zirconium (<160 ppm). Otherwise, we can mention the use of inland sand compared to coastal sand. It has been thought that Levantine glass has been made from the sands of the Syro-Palestinian region (Foster and Jackson, 2009).

From the beginning of the 4<sup>th</sup> century HIMT glass and Levantine I glass were manufactured in the Eastern Mediterranean in close regions. These two glass types dominate the Mediterranean region; however, when compared, HIMT producers were more accomplished in distributing their glass. They have shipped off their goods even to the north-west provinces of the empire (Foster and Jackson, 2009).

Levantine II glass of the 7<sup>th</sup>-8<sup>th</sup> centuries contain lower lime (6-8%), lower sodium (10-13%) with higher alumina (3-4%) and silica (73-76%) contents compared to Levantine I, which suggests a different sand origin in the Palestinian coast (Freestone et al., 2002). Bet Eli'ezer near Hadera, Israel shows comprehensive examples for Levantine II type dating Late Byzantine-Ummayyad period. Manganese (<0.1%) was not preferred in the Byzantine period Bet Eli-ezer glasses compared to 4<sup>th</sup> century Levantine I glasses from Jalame, until the 9<sup>th</sup>-10<sup>th</sup> centuries (Freestone et al., 2000).

Gratuze and Brandon (1990) analyzed two Egyptian origin glass from Wadi Natrun; Egypt I and Egypt II. While Egypt I type, dating to 7<sup>th</sup> century, has low lime (2-4%) and high alumina (3.5-4.5%) content (Freestone, 2003), the other relatively later composition from Wadi Natrun dating 8<sup>th</sup> and 9<sup>th</sup> centuries, Egypt II glass type, was characterized with low alumina (1.5-2.5%) and high lime (9%) (Freestone et al., 2000). Egypt II is also known from the glass studies of Sayre and Smith (1974), Tal

and his colleagues (2008), and Nenna and colleagues (1997). Egypt I group is characterized by high magnesia (0.9-1.3%) and low lime (2.6-4.5%) (Ceglia et al., 2015). Additionally, low strontium content of Wadi Natrun types proves that inland sand was used (Freestone et al., 2000).

Magby (Magnesium Byzantine) glasses dating to the late 6<sup>th</sup> early 7<sup>th</sup> century, use plant-ash as a flux, instead of natron (Schibille et al., 2016). Magnesium and potassium oxide concentrations are above 1.5 wt%. Magby glasses from Schibille and her colleagues' work (2016) show a strong correlation between MgO, K<sub>2</sub>O with elevated phosphorus concentrations. Titanium, zirconium, hafnium, and iron are similar to the weak HIMT glass.

#### **2.4. Glass Production Models**

In order to talk about glass production, it is necessary to grasp the difference between the terms of *glass making* and *glass working*. If the glass is obtained from its raw materials like sand and alkali, it is called *glass making*; however, if the glass is taken as a raw material itself -such as glass ingots or glass rods- and transformed into an end-product in the same or another workshop, it is called *glass working* (Dardeniz, 2016).

Throughout the years, two main models of glass production –local and centralized- have developed (Degryse et al., 2014). Until the 1990s it is believed that glass was produced *locally* like ceramics; every workshop makes their own glass from nearby sources and creates their own composition and typology (Freestone, 2005). However, according to the *centralized* model, unlike Medieval Europe, in the Roman era, glass production occurs both in primary and secondary production sites. Primary production sites are the centers where glass making has occurred in large-scales by melting the main ingredients in great furnaces that appears close to the source of raw materials. During the 4<sup>th</sup> to 8<sup>th</sup> centuries, a small number of primary production centers, mainly located in Egypt and Syro-Palestine, have the capacity to produce 8-9 tons of glass at

once in the tank furnaces with a size of up to 6 meters (Freestone, 2005, Freestone et al., 2000). The tons of glass slab were cut into chunks and shipped into small sized but numerous secondary workshops. These secondary production centers are the sites where the raw glass supplied from primary production centers is worked by coloring and shaping the unformed glass into objects. Moreover, these workshops are highly common compared to primary production sites. In order to provide the standardization in these workshops, Syrian skilled glassworkers were slaved and shipped to Rome (Fleming and Swann, 1999). Therefore, in this centralized model, few major glass compositions can be detected throughout the empire, which solely formed in the main glass production centers. These major glass compositions may subject to slight changes in the secondary production centers due to coloring procedures. Additionally, there is a third model in which glass is produced both in large primary centers together with some exceptional local primary centers (Degryse et al., 2014).

## **2.5. Recycling**

Glass production is an industry which always needs a lot of energy and source. Therefore, people have started to recycle glass. Considering how hard it was to reach such high degrees in ancient times together with the scantiness of primary production sites, the need for recycling can be understood more clearly. Since the pacification of the Mediterranean in the Augustus period along with the evolution of blowpipes, glass became a frequently used product (West, 1932; Degryse et al., 2014). During the Roman period, cullets were traded for re-melting and reproducing. The long distance and seaborne transport have been revealed with the discovery of the shipwrecks of *Iulia Felix* and *Embiez*. These shipwrecks together with the ones in the coast of Israel have carried raw chunks, glass cullets and scrap glass to the secondary production sites for recycling (Silvestri, 2008; Gorin-Rosen, 2000).

As Jackson and Foster (2014) state, detection of recycling is rather problematic since the ‘markers’ of recycling is similar to the components of colorants or decolorants. These markers are highly small quantities of antimony, cobalt, lead, copper and tin

(Henderson, 1995 and Jackson, 1996, as cited in Jackson and Foster, 2014). In the recycled glass, unlike the raw batch, some contaminations appear due to the mixing of highly colored glass with the colorless or naturally colored glass or due to long and continuous exposures to heat and furnace atmosphere (Paynter, 2008; Jackson and Foster, 2014). The level of the impurities found in the colorless recycled glass is neither as high as the components in the colored glass nor as low as in the raw glass. On the other hand, diagnosing recycling is hard for highly colored glasses because those impurities may already derive from the colorant minerals. However high concentrations of antimony for colored glass is also a sign for recycling. As a result of Foy's (2003) study, the impurities of naturally colored raw glass are as follows:  $\text{Cu} \leq 89 \text{ ppm}$ ,  $\text{Pb} \leq 0.01\%$ , and  $\text{Sb} \leq 0.01\%$ . However, to be more certain, highest impurity levels of raw should be evaluated, if the colorless/naturally colored glass sample have concentrations such as  $\text{Cu} \geq 100 \text{ ppm}$ ,  $\text{Pb} \geq 0.1\%$ ,  $\text{Sb} \geq 0.1\%$ , the sample is considered as recycled (Foster and Jackson, 2009). While Rehren and Brüggler (2015) specify the maximum limits of raw HIMT glass as 100 ppm Cu; 75 ppm Pb; 25 ppm Sn and 20 ppm Sb, recycling is indicated via higher concentrations. Moreover, according to scholars, glassworkers either use manganese or antimony as a decolorizer, therefore detection of manganese and antimony together in one composition is a clear sign of recycling. As Cholakova and Rehren (2018) 20-800 ppm of antimony, which is considered low for deliberate addition of a decolorizer, represents the contamination from the pre-existing antimony-rich glass.

The experiments of Paynter (2008) which were conducted on pots, furnaces, and glass prove that continuous heating resulted in numerous changes in glass over time. The alkali-rich gases occurred by wood firing in the furnace cause an increase in the alkali, potash and phosphate concentrations in the glass composition. According to results, lime-rich ash, which is another by-product formed as a result of heating, does not significantly affect the composition of glass, unlike potash. In recycled glass, while potassium and calcium tend to strongly correlate with phosphorus, chlorine may represent a weak inverse correlation with  $\text{K}_2\text{O}$  due to its volatile structure which

results in depletion of chlorine (Al-bashaireh et al., 2016; Tal et al., 2008). Glass composition can also be affected by the absorption of iron from the working materials such as pontil and from the pot surface and furnace materials (Freestone, 2015).

Also, the more the glass melts, the more the composition becomes homogenous and fewer imperfections are detected according to Paynter's experiments. With prolonged heating of glass, the grains of quartz, feldspar, zircon, potassium and spinel have gradually dissolved, and bubbles have become less visible, also alkali fluxes start to diminish as a result of continuous reheating. (Freestone, 2015; Paynter, 2008). Additionally, some glass became dull especially when they are overheated because of the sulfur and zinc-containing atmosphere. Change in color and increase in viscosity are among the effects of recycling (Jackson and Paynter, 2016; Freestone, 2015).

## CHAPTER 3

### SIDE ARCHAEOLOGICAL AREA

#### 3.1. Ancient Site Side

Side, the prominent city of the Pamphylia region, is an ancient Greek site in Antalya province, on the southern Mediterranean coast of Turkey (Figure 2.1). Pamphylia, located in the shores of southern Anatolia, is the region that is surrounded by the Taurus mountains in the north, the Mediterranean Sea on the south, Lykia in the west and Kilikia Trakheia in the east (Bosch, 1957). The region, due to its location, becomes an important part of the trade network among Egypt, Syria, Phoenicia, Aegean islands, and the Greek mainland. The history of Pamphylia dates back to prehistoric periods, however, there were no prehistoric ruins found in and around Side. Though the name was mentioned in the Hittite Period, a column of the late Hittite period, which was unearthed during the excavations, is still on display at the Side Museum.



Figure 2.1. Location of Side archaeological site in Asia Minor

According to Strabo (1917) and Arrian (1999), Side was established in the 7<sup>th</sup> century BC by the colonists that came from Cyme in Aeolis Region, an area of western Anatolia. However, according to Arif Müfid Mansel, the first official archaeologist of Side, the settlers forgot the Greek language and started to speak the language of Side, which is the local language that was used in the Pamphylia Region. The roots of the word “Side”, which means “pomegranate”, comes from Luwian language, not Greek. Therefore, one may think that the city of Side could have been established long before the Greeks and it was not a Greek colony, instead, it became a city where Greek communities settled since the 7<sup>th</sup> century BC considering the inscriptions from the 2<sup>nd</sup> and 3<sup>rd</sup> centuries BC written mainly in the language of Side (Mansel,1967; 1978).

It can be said in general that Side did not play an important role in the history of Anatolia and it mostly shared the fate of Pamphylia (Mansel, 1967). In the 6<sup>th</sup> ct BC, Side, together with Pamphylia, first came under the domination of the Lydian kingdom. From the collapse of the Lydians in 547 BC until the besiege of Alexander

the Great in 334 BC, Side remained under the domination of Persians. Right after the death of Alexander the Great, Side became a fighting issue among the Hellenistic Kingdoms. For a short time in the 4<sup>th</sup> century, the city was controlled by Antigonos, later in the 3<sup>rd</sup> century, Ptolemaic Kingdom took the charge. However, in the 2<sup>nd</sup> century BC Antiochus the Great seized the power until he got defeated by the fleet of Rhodes that was on the side of the Romans. Thus, Side was given to the Pergamum Kingdom, the ally of the Romans. Thanks to the grand mercantile fleet and its protecting war fleet, Side improved its trade with Eastern Mediterranean countries, therefore it reached prosperity (Mansel, 1967). The city also became a center of science and culture until the spread of the pirates from Kilikia and the conquer of Mithridates VI of Pontus.

After the Romans saved Pamphylia, Side was under the government of Romans while having a certain autonomy. However, during the reign of Augustus, Pamphylia was bounded to the Galatia Kingdom and in 25 BC became a state by itself. Hereafter, Side was dependent on Roma in foreign policy but independent in domestic affairs. The 2<sup>nd</sup> and 3<sup>rd</sup> centuries were the second golden era of Side thanks to maritime commerce and the slave trade. In this era, Side became a central metropolis of the regional governor and administrative staff and great boulevards and monumental structures were erected.

In the second half of the third century, Pamphylia was attacked by the Scythian pirates (Mansel, 1978) and by the Isaurian tribes from the Taurus mountains, which were later defeated by the Roman troops (Alanyalı, 2016). During the attacks, the city was damaged, with the 4<sup>th</sup> century, the city got poorer and took a Christian outlook (Mansel, 1967).

By the year 395, the Empire was divided, while the Western Roman Empire began to be ruled from Rome, the Eastern Roman Empire was ruled from Constantinople. Therefore, Pamphylia remained in the Eastern Empire. As the traditional rivalry continued, Side was chosen as the prime Bishop of Pamphylia and Perge was chosen

as the second Bishop. Although the empire and Pamphylia's situation were not bright during the 5<sup>th</sup> and the 6<sup>th</sup> centuries, Side as the spiritual metropolis of Pamphylia, gradually slipped away from poverty and lived its third golden era (Mansel, 1978). The settlement reached its original limits and even surpassed the Hellenistic period walls.

However, in the 7<sup>th</sup> century, the city was weakened both by Arab and pirate raids. As the Arab historian Idrisi mentions, with the fire in the 10th century, the city was completely abandoned, and the inhabitants moved to Antalya (Mansel, 1967).

The Side was first explored by the European travelers in the 19<sup>th</sup> century and the first comprehensive scientific investigations were made by the Austrians. Arif Müfid Mansel conducted the first excavation in 1947 and it continued for 20 years. After Mansel, respectively, Jale Inan, Ülkü İzmirligil and Prof. Dr. Mehmet Karanlı continued the excavations. Since 2009, the excavations have been carried out by Prof. Dr. Hüseyin Sabri Alanyalı and Prof. Dr. Feriştah Alanyalı, the Head of Archeology Department of Anadolu University's Faculty of Letter.

The great majority of the glass finds comes from the Theater (115 finds) and the Dionysus Temple (68 finds) and the small majority is from the Museum Zone (8 finds), APS-Attius Philippus Wall (3 finds), N2 (8 finds) and TT (3 finds).

Dionysus temple, with an entrance from the southern front, was built in the second half of the 1<sup>st</sup> century BC before the construction of the theatre. The temple was named by the Mansel because of its close proximity to the theater and also because of the numerous epigraphic, archaeological and numismatic documents belonging to the Dionysus cult in the city (Mansel, 1963). However, many votive inscriptions of Nemesis from the theatre and surrounding areas, documents regarding the Emperor cult around the temple from 1<sup>st</sup> century BC, the portraiture of Augustus that is found in the walls of the theatre and also the known presence of the Dea Roma cult from 188 BC in Side arouse suspicions that the temple belonged to Dionysus (Alanyalı, 2016).

The excavations were conducted from 2009 to 2012 with 17 drillings to understand the development of the structure in the historical process (Figure 2.2).



*Figure 2.2. Drills of Dionysus Temple in 2009- 2012 excavation season*

In the light of the areal survey and excavations, the construction is handled in four construction phases. As Feriřtah Alanyalı (2016) asserts, the first phase represents the time between the construction of the temple and the erection of the theatre in the first half of the 2<sup>nd</sup> century AD. When the temple partly remained under the Roman theatre, the plan of the temple changed (Phase II). In the last quarter of the 4<sup>th</sup> century, as the temple lost its religious significance, the area was leveled by removing the stair steps from the first phase of the structure and the area continued to be used without interfering the inside (Phase III). The temple turned into a podium in the second half

of the 6<sup>th</sup> century and afterward (Phase IV). In place of the dismantled blocks, a simple wall was built to reinforce the building and a water basin was placed in front of this wall. This wall and the basin are part of a workshop. The available data indicate that the building and its surroundings were used as workshops until the middle of the 7<sup>th</sup> century (Alanyalı, 2016).

The theatre, which is in the center of the city, was constructed in the 2<sup>nd</sup> century AD on the ruins of the Hellenistic period. The theatre has a unique plan among the Anatolian theatres with its cavea supported by vaults, unlike its counterparts which stand upon a hillside (Bean, 1999). The infrastructure that carries the upper cavea is composed of vaulted galleries, which are mostly damaged. The galleries on the first floor have reached the present day in good condition. One of the galleries must have been transformed into a chapel with an addition of a wall with an apse. The chapel was supposed to have been built with the repair of the theater in the 5<sup>th</sup> century AD and then turned into a glass workshop in the 7<sup>th</sup> century AD (Yıldırım, 2013).

### **3.2. Evidence of glass production in Side**

During the processes of glass making and working, various traces can be found in the area to detect glass production. Furnace and crucible fragments, clay containers, fuel deposits, forming and shaping tools as blowpipes, pontils, jacks, molds, by-products of manufacturing like drops, pulls and dribbles of glass, vessel fragments and raw glass cullet are some of the evidence for production (Henderson, 2013).

Side provides comprehensive evidence regarding glassmaking such as furnace and crucible pieces, vitrified clay materials, chunks, drops and pulls of glass, spilled glass adhered to ground or furnace pieces, scrap glass, and vessel fragments. Side sample set contains one cylindrical in a greenish shade (Figure 2.3). Moils are waste products that occur at the end of the blowing pipe after cracking the vessel off (Price, 1988; Amrein, 2001). These moils are the direct proofs of glassblowing.



*Figure 2.3. Soil sample from Side excavation*

Moreover, glass rods, trails, pulls of glass, drops, droplets and blobs that are found in the area are the by-products of glass manufacturing. These wastes are formed during gathering, blowing and working. The large spills are lime-rich glassy wastes some of which have porous and dull surface due to long exposure to high temperature (Jackson, 2008). Complete Side glass set contains tens of lumps in various sizes (Figure 2.4 and Figure 2.5) which have a layer of glass and highly porous limy and ashy debris beneath it. These lumps either occur as a waste product or by spilling the raw glass while mixing it in the furnace.



*Figure 2.4. Glass lump adhered to porous clay*



*Figure 2.5 Profile of the spilled glass adhered to clay fragments from the complete Side set, showing the layers of material*

The spots of the kiln and the workshop, located in the Dionysus Temple, are shown in Figure 2.6.

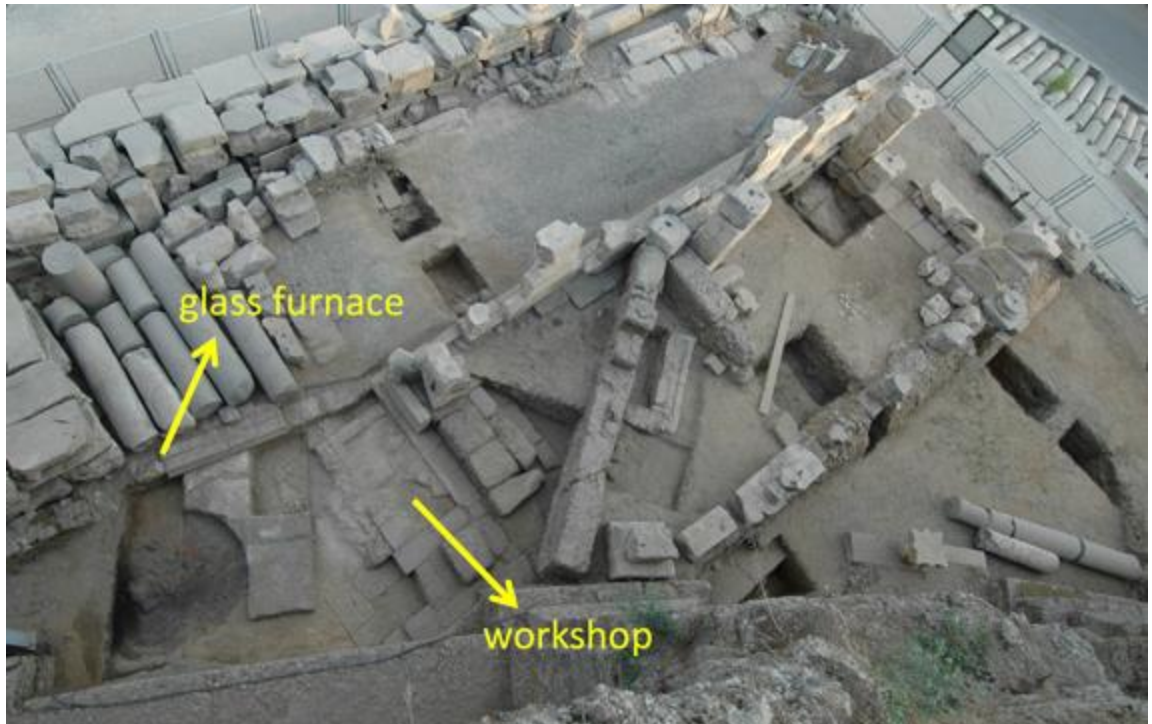


*Figure 2. 6.* Dionysus Temple and the glass kiln



## CHAPTER 4

### MATERIALS AND METHODS

#### 4.1. Materials

Within the archaeometric analysis of the Side excavation, 207 glass samples that were found from Theatre, Atius Philipus Wall, Temple of Tyche, Museum Area and N2 area were investigated. The archaeological context of the glass samples is listed in Table B.1. Most of the samples come from the theatre building and its surrounding (the galleries and the Dionysus Temple) since this area has been used by glass workshops. Figure 3.1. marks the areas with traces of glass production around the Theatre and Dionysus Temple.



*Figure 3.1.* Spots for the traces of glass production in Side Theater (Tek, 2014)

207 samples were classified into categories; chunks, products, drops-threads, window panes, crucible or kiln fragments, tesserae, waste glass, and slaggy lumps. For the visual examination, the coded samples were documented photographically. The samples were measured and photographed under a binocular microscope. The visual examination was completed by color analysis. Once the documentation and visual examination were finished, samples were selected for further chemical and petrographic analysis. Of 207 samples, 78 glass samples and 9 clay samples were chosen for this study. During the selection, representation of different categories, color diversity, adequate sample weight, and physical condition were taken into consideration. The samples were selected from five different categories; chunks (Figure 3.2, Figure A.1.), products -vessel fragments- (Figure 3.3, Figure A.2), window panes (Figure 3.4, Figure A.3.), droplets-threads (Figure 3.5, Figure A.4.), and crucible-kiln fragments (Figure 2.5, Figure 3.6, Figure A.5.).

Within the complete Side glass set, 15 raw chunks (ranging between 5 x 2.7 cm to 2.1 x 1.3 cm) of dark navy, black and green shades were found, which were probably broken from larger chunks or primary glass chunks to make artifacts. However, it is more likely that they are parts of larger chunks considering their edgy forms. 32 products (comprises of vessel fragments, goblet pieces, broken handles, glass bases, and rims), 21 window panes and 10 droplets-threads were chemically investigated by PED-XRF. The products have a wide variety of colors; cobalt blue, blue, blue-green, dark green, green, yellow, olive-green, amber. Five samples (ASK-G62d, ASK-G73, ASK-G75b, ASK-80a, ASK-G81) from the products are colorless glass. While the droplets and threads are mainly in blue-green, blue and green hues, the color range of the window panes varies between colorless to blue and green.



*Figure 3.2.* Chunks samples from the complete Side sample set



*Figure 3.3.* Product and vessel fragments from the complete Side set



*Figure 3.4.* Window panes from the complete Side sample set



*Figure 3.5.* Droplet samples from the complete Side sample set

Side sample set contains spilled glass adhered to crucible and furnace fragments (Figure 3.6, Figure 2.5.). Eight crucible and furnace fragments were analyzed chemically and petrographically. Their glassy layers were detached from the clay pieces and separately analyzed. Additionally, one slaggy lump (ASK-G4) was examined to understand the composition of its clayish porous structure.



Figure 3.6. Spilt glass adhered to clay fragments from the complete Side set

Figure 3.7. shows a graph about the chronology of the glass finds that were found between 2009 and 2012 according to the coin assemblage.

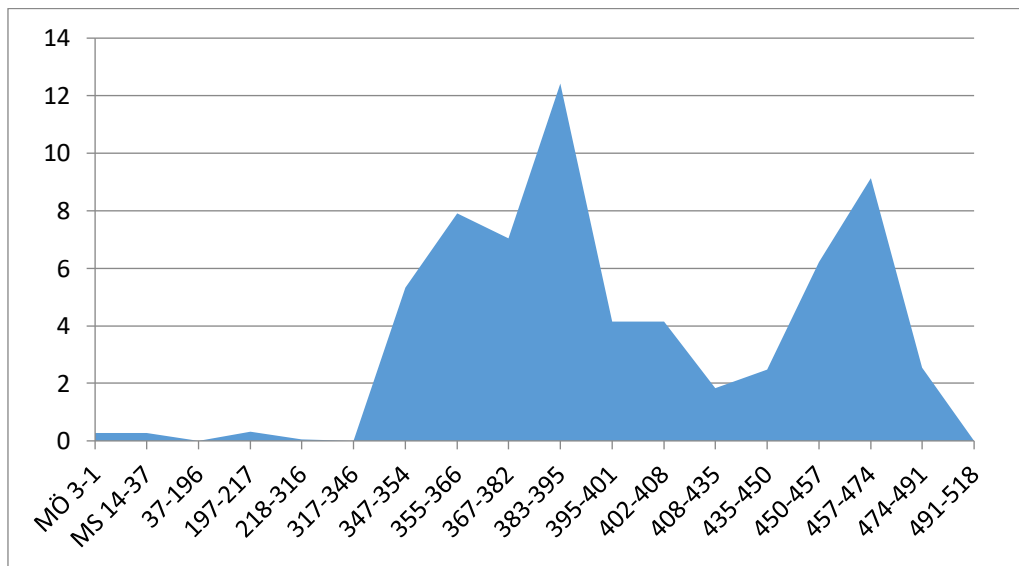


Figure 3.7. <<Loss/ Use Ratio of Coins Per Annum>>according to the "1000/ total x", "amount per period/ total excavated from the site" formulae of the 161 samples with exact dates identified among the 230 coins collected from Side, Dionysus Temple 2009-2012 excavation (Tek, 2014).

## 4.2. Methods

Archaeometric studies of Side samples include visual, chemical and petrographic analysis. The complete Side glass sample set was documented before the various archaeometric analysis on selected samples. The sample set was coded and classified as chunk, window panes, waste glass, crucible, slag, end-product, threads, and drops. In the coding, “ASK” symbolizes the initials of the city and the name of the excavation area (Antalya, Side Excavation / Antalya, Side Kazısı) and “G” symbolizes the type of the sample material, glass. Accordingly, ASK-G1 refers to glass sample #1.

The Nikon D5100 (16.2 Mp) digital camera was used for photographic documentation. The sample photographs of 78 glass samples are given in Figure A.1 – Figure A.5. In order to have an idea about the production technique of the window panes, the thicknesses of the walls of the glasses were measured with digital thickness meter. Glass sample measurements and the excavation data are listed in Table B.1 and Table B.2. Their photographs were taken under a binocular microscope (Figure A.6.) to examine the physical condition, the shape of the bubbles and its quality.

Chromametric analysis was carried out to document the colors of the glass samples. ColorQA PocketSPEC with Pro System III software was used. Color analyses were made using the standard CIE L\*a\*b\* (Commission Internationale de L’Eclairage) color system. (L) value stands for the lightness value of the color, where (a+) is the intensity of red in the color; (-a) is the intensity of green in the color; (+b) is intensity of yellow in the color and (-b) stands for the intensity of blue color (Ohno, 2007). The color codes and the color schema are listed in Table B.2 and Table B.3.

The main, minor and the trace elemental composition of the glasses were identified by the Polarized Energy Dispersive X-Ray Fluorescence Spectroscopy (PED-XRF) method (Table B4-B9). SPECTRO XLAB 2000 Model PED-XRF device with a liquid nitrogen-cooled Si(Li) detector was used. The analysis applies the USGS (United States Geological Survey) standards and referred to GEOL, GBW-7109, and GBW-

7309. The resolution values were  $<150$  eV Mn K $\alpha$ , 5000 cps. For the preparation, the sample impurities were removed initially, and the samples were crushed in an agate mortar as a fine powder, which was later pressed into thick pellets of 32 mm diameter using wax as a binder. The precision limit of the device is 0.5 ppm for heavy elements and 10 ppm for light elements. For this work, 48 elements were identified, and the elements were evaluated for 87 samples (Table B.4 – Table B.9).

#### **4.2.1. X-ray Fluorescence (XRF) Spectroscopy**

X-ray fluorescence (XRF) is a technique used to analyze the chemical composition of a material in solid, powdered or liquid forms. XRF, a nondestructive technique in principle, can detect any element from beryllium to uranium ( $Z = 4$  to 92). XRF can detect major, minor and trace elements qualitatively and also quantitatively. While the measurement of the energy of the photons permits qualitative analysis, the detection of the number of photons permits quantitative analysis (Streli et al., 1999). Application field of XRF is highly extensive; geology, metallurgy, mining, soil survey, oil analysis, medicine, cement production, environmental studies, fine arts, and archaeology are some of the areas. In terms of glass, XRF is used for investigating raw materials, characterizing the glass types, testing quality, detecting trace elements and for supporting other inspection methods. (Bach & Krause, 2010)

In simple terms, high-intensity x-ray, obtained from an x-ray tube, irradiates the specimen by bombarding it with accelerated electrons as the origin of primary radiation. This high intensity (high enough to extract electrons from the orbit K) x-ray beam activates the inner electrons of the atoms since the energy of the sent photons or ions exceeds the binding energy of the bound inner electrons (Kramar, 1999 and Uhlig, 1999). When the inner electron is ejected, the atom gets unstable, and one of the elements in the outer shell transfers to the inner shell for stabilization causing an energy difference between the initial and the final energy state which is released as a photon of the energy (Figure 3.8) (Kramar 1999). The emission of the electromagnetic radiation, secondary spectrum, reveals the elemental composition since every element

has its own distinct X-ray fluorescence radiation generating from the unique energy differences between the higher and lower states of the atom. The characteristic line spectrum comprises of various possible electron transitions. Such as, when a K-shell electron is replaced by an L-shell electron  $K\alpha$  radiation occurs and when a K-shell electron is replaced by an M-shell electron,  $K\beta$  radiation occurs (Valentin 2010). This analysis is conducted under vacuum to prevent the loss of intensity. The intensity is assessed by flow or sealed proportional and scintillation counter, which is later compared with known standard intensities to quantify (Uhlig, 1999). Regarding the measured raw intensities, elemental percentages are calculated according to the analytical software programs.

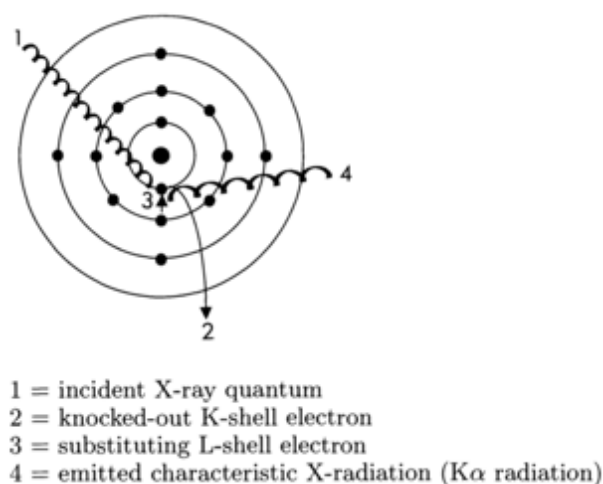


Figure 3.8. Generation of characteristic X-ray radiation (Valentin, 2010)

XRF analyzes the characteristic  $K\alpha$ -lines or L-lines (for the ones with higher atomic numbers) of the elements (Kramar, 1999). These specific X-ray lines can be detected with two types of X-ray spectrometer; by wavelength-dispersive spectrometers (WD-XRF or WDS) which use wave phenomena of X-rays, or by energy-dispersive spectrometers (ED-XRF or EDS) using their energy characteristic. While ED-XRF generates a broad spectrum of wavelengths or energies at the same time, WD-XRF counts solely the X-rays of a single wavelength at a time. Simultaneous measurement

has its merits such as detecting many elements in a short span of time, yet the count rate of EDS is restricted to 50-70 kcps (Streli et al., 1999).

Mainly, WD-XRF counts the X-rays beams of the distinct wavelengths that are emitted by a crystal. The characteristic radiation of the sample is diffracted in various wavelengths according to Bragg's law, which later scatters into distinctive spectral lines when reflected from analyzer crystal. The emerging radiation is recorded by detectors that separate the distinctive energies. To briefly describe, the logarithmically curved analyzer crystal selects the wavelength radiation that comes to the detector, a scintillation counter or a proportional counter. In the analyzer, the beams are dispersed from different atomic layers and as to Bragg's law, the wavelength of the radiation constitutes constructive interference at a certain angle. In WD-XRF, scanning a wide spectral range and identifying the wavelength characteristic X-ray radiation of the specimen is achieved by shifting the angle thanks to the movable crystal and the detector. Therefore, this setup limits the wide and overlapping peaks. Compared to ED-XRF, this setup has higher resolution, high sensitivity for trace elements and low atomic number elements, however, the major challenge for WD-XRF is longer run times, complex design and higher cost. Figure 3.9 shows the WD-XRF setup which includes an X-ray tube, the sample chamber, analyzer crystal and the detector unit with an amplifier, window discriminator, lower level and registration unit (Kramar, 1999).

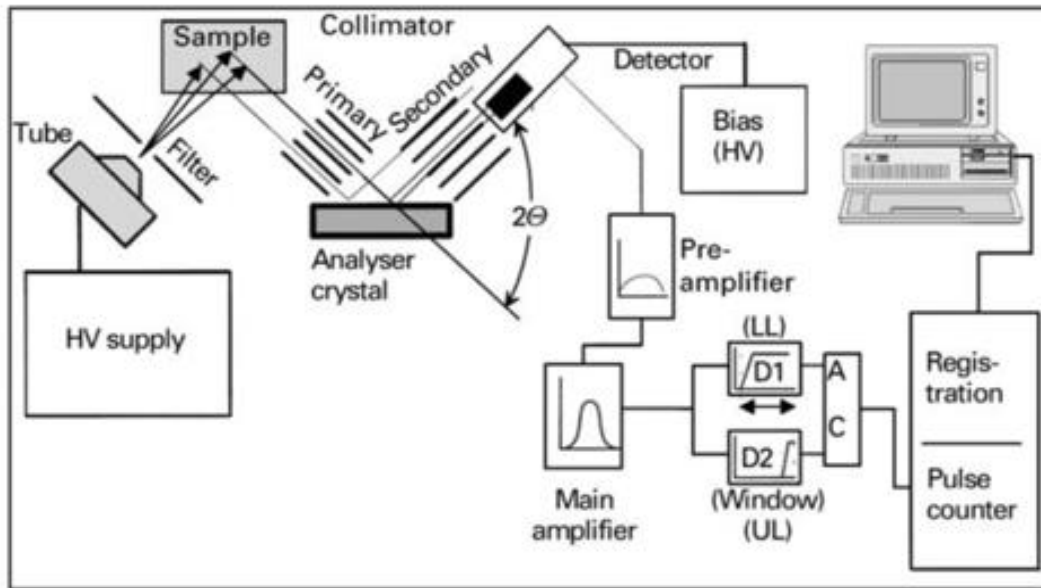


Figure 3.9. WD-XRF setup (Kramar, 1999)

The energy-dispersive analysis uses a detector to classify the energies of photons. X-ray tube provides polychromatic radiation which scatters according to the Rayleigh or Compton effect towards the detector, generating a high bremsstrahlung background and line interferences originating from the characteristic lines of the anode material and the emerging Compton peak. Typically, EDS composes of an X-ray tube, sample support, pre- and main amplifier, pile-up rejecter, analog-to-digital converter and multichannel analyzer (Figure 3.10) (Kramar, 1999). While the low costs, the simple design and the fast run times make EDS favorable, its poor resolution, poor accuracy at low concentrations, poor sensitivity for low atomic number elements and broad overlapping peaks are the undesirable facts of the energy-dispersive spectrometers.

On the other hand, the accuracy and the sensitivity of the polarized X-ray fluorescence (PXRF) are superior to WDS and the detection limits are better than normal ED-XRF. The polarized beam is used to diminish the scattering from the specimen. Unlike nonpolarized radiation, the spectral background is highly low. In this technique, the

primary X-rays are polarized regarding Bragg's law or Barkla scattering to energize the atom and the secondary x-rays are calculated by the orthogonal geometry to the polarization plane (Kramar, 1999). While the Barkla polarizer scatters the complete spectrum of the stimulating radiation, the Bragg polarizer also conducts like a monochromator (Streli et al., 1999).

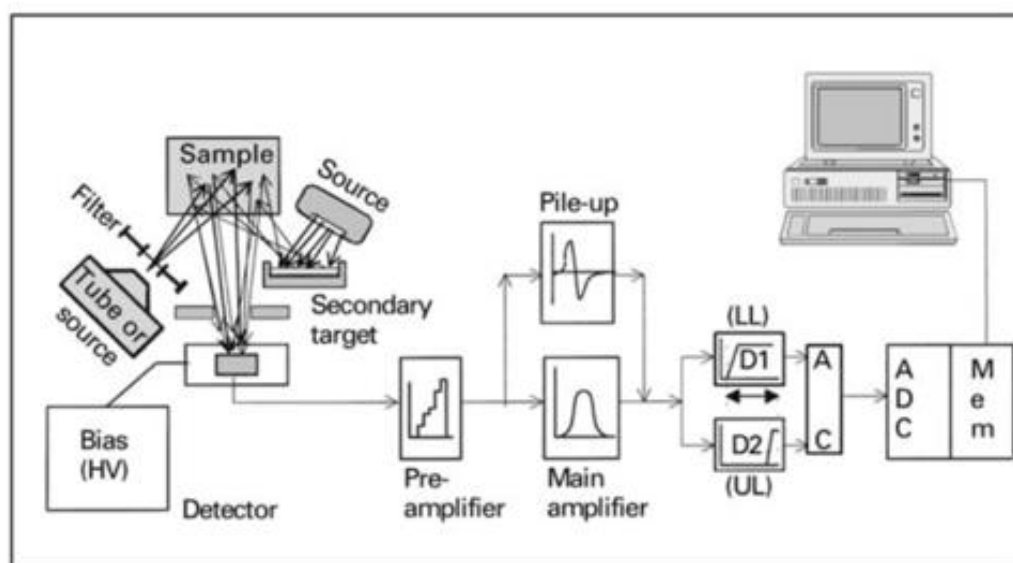


Figure 3.10. ED-XRF setup (Kramar, 1999)

In general, the major advantage of XRF is its low costs compared to other devices. Being a non-destructive method makes XRF a desirable technique in archaeology and art history. Portable XRF is a non-destructive device with zero preparation procedure (if the sample is not weathered). However, since the penetration depth is relatively low in XRF spectroscopy, the sample should be homogenous for an accurate evaluation and representing the entire volume. Thus, to make the sample homogenous for the heterogeneous material, it should be destructed. On the other hand, ED-XRF and WD-XRF are also preferable with its relatively rapid and simple preparation possibilities. Solid and heterogeneous samples are crushed or ground and turned into pellets by pressing. Additionally, the homogenous solid samples can solely be

prepared by milling and polishing the surface. For the liquid ones, cups or filter preparations are adequate (Uhlig, 1999).

XRF spectrometry is a frequently used method for determining the chemical composition of glasses since it is simple, quick and cheap. However, XRF analysis also has some major disadvantages such as the poor detection limits for the low atomic numbered elements (between  $Z=5$  and 11), especially at small concentrations. For instance, lithium ( $Z=3$ ) cannot be detected due to its low fluorescence radiation and the measurement of boron ( $Z=5$ ) is only possible with special equipment (Bach & Krause, 2010). Since boron is a characteristic of the Byzantine glasses from Asia Minor (Davison, 2003) low detection limits become problematic for some samples. Another negative part of this method is its insufficiency to analyze low mass samples. Moreover, it is dependent on the signal from the matrix composition, which necessitates a set of calibration standards for high precision analysis (Meckel et al. 1999).

#### **4.2.2. Thin Section Optical Microscopy**

Thin sections of kiln or crucible pieces or clay fragments were prepared and examined under the optical microscope (Figure 4.34). In the examinations, the optical microscope LEICA Research Polarizing Microscope DMLP Model was used. Photographs were taken by the digital camera Leica DFC280, connected to the microscope and assessments were made by using the Leica Qwin Digital Imaging Program (Kerr, 1977; Rapp, 2002).

## CHAPTER 5

### RESULTS AND DISCUSSIONS

#### 5.1. Visual and Binocular Microscope Analyses

According to visual analysis, samples are either highly or moderately weathered apart from some exceptions. The humid and salty environment of Side makes weathering inevitable. Dulling, iridescence, black discoloration, and milky surfaces were observed in most of the samples. To briefly explain, dulling is the loss of transparency; iridescence is the occurrence of shiny, rainbow colors on the surface; milky, enamel-like surfaces are generally opaque white corruptions; black discoloration is the opaque blackened layer on the surface caused by the oxidation of iron and manganese ions (Davison, 2003).

In the assemblage, chunks were the less corroded group. On the other hand, window panes were highly corroded. Black discoloration appears in ASK-G6, ASK-G22c, ASK-G36a, ASK-G40a, ASK-G62a, ASK-G75a, and ASK-G93a. ASK-G47 shows milky surfaces and all the rest of the window panes show either a thin or thick layer of iridescence. ASK-G93a and ASK-G93b detach layer by layer. Droplets and threads are moderately weathered. ASK-G72c and ASK-G58e display small black discoloration layers. Iridescence is observed in ASK-G51e, ASK-G55b, ASK-G60b and, ASK-G60c in small quantities. Dulling is detected in almost all of the drops. Products show a high amount of corrosion. In ASK-G42 the corroded surface is started to flake away. Most of the products (ASK-G31c, ASK-G37, ASK-G50c, ASK-G55a, ASK-G62c, ASK-G62e, ASK-G69a, ASK-G69c, G71a, and G84) show black discoloration. These samples have high manganese (>1.2%) amounts which can result in oxidation. ASK-G82b is marked by milky enamels. Dulling and iridescence are

visible for the rest of the products. Dulling may have been caused also as a result of recycling due to the sulfur and zinc-containing atmosphere.

The thickness measurement was only applied on the window panes. The thickness of the Side window pane samples varied between 1.3 – 4.6 mm. Even thicknesses and elongated bubbles are among the features of cylinder-blown glasses (Davison, 2003). Considering their thin structure (<3 mm) with almost even thickness and elongated bubbles, 18 out of 21 window panes were made with cylinder-blown technique. The three glass samples (ASK-G47, ASK-G52b, and ASK-G75a) draw attention with their relatively thick structure and normal bubbles. Elongated bubbles of the window panes are visible in the optical microscope photographs. Figure A.6 shows the optical microscope photographs of the samples. However, highly weathered samples cannot be photographed due to the corrosion layers. The black photographs show the weathered samples.

The optical microscope photographs demonstrate that the majority of the Side glass have seedy complex, only a few samples have fine, bubble-free structure. Although antimony acts as a fining agent to dispose of the seeds (Brill, 1988), the bubble-free samples of Side do not include antimony in their composition. The dulling can be detected from the microscopic photographs of ASK-G51e, ASK-G62d, ASK-G75a and, ASK-G80a.

## **5.2. Chromametric Analysis**

According to the color analysis, Side samples show a wide color range from dark green to light blue, cobalt blue, blue-green, light green, purple, aqua and decolored glass. The color codes and the shade card are available in Table B.2 and Table B.3.

Most of the chunks (11 out of 15 samples) are in green tones. The largest chunks (ASK-G39a, ASK-G52c, ASK-G62b and, ASK-G88a) have the darkest green hues. The colors of ASK-G39a and ASK-G52c are almost black. The small chunks ASK-

G67c and ASK-G74c are cobalt blue. The only amber-colored sample in chunks is ASK-G66d. ASK-G2 has the lightest green and ASK-G49 is the only olive-green chunk.

The window panes range between blue, green and colorless. The colorless glass of window panes (ASK-G41, G45, G52b, G93a, G93b) are not completely colorless, the blue or green tint cannot be avoided due to high iron inclusion.

The color of the droplets and threads vary in blue and green hues. Two samples (ASK-G51e, G60c) are olive green or yellowish green, three samples are green (ASK-G58e, 72c, 72d) and four samples are blue-green or blue.

The most colorfully varied group is products. Brown, amber, dark-green, green, blue-green, yellowish green, yellow, blue, cobalt blue, blue-tinted colorless, colorless are among the color varieties.

It is stated that while Levantine glass typically has blue-green color, Egyptian glass shows a wide color range from yellow-green to pale tint (Freestone et al. 2018). The origin of these glasses either with blue-green or yellow-green tones will be illuminated in the chemical results section.

### **5.3. Chemical Analysis Results**

The PED-XRF results reveal that silica is the chief network former, soda is the main fluxing agent and lime is the main stabilizer for Side glasses. According to the main glass components, the silica content of the sample is in the range of 48.08% -75.16% with an average of 63.33% ( $\pm 5.53$ ), the lime content is in the range of 1.00-21.93% with an average of 8.12% ( $\pm 2.58$ ) and the soda, the fluxing agent, content is between 0.09-16.39%. and the average is 11.80% ( $\pm 2.87$ ). Although the average  $\text{SiO}_2$  and  $\text{Na}_2\text{O}$  contents are lower than its contemporaries, PED-XRF data reveals that Side glasses are soda-lime-silica glass, compatible with the period. The low results ( $\text{SiO}_2 < 60\%$ ,

$\text{Na}_2\text{O} < 15\%$ ) can be associated with the weathering of glass. Additionally, the low soda content indicates the preference of the blowing method instead of casting. Since blowing does not necessitate high fluidity as casting, small amounts of soda are adequate for the glass paste (Schibille et al, 2008).

The glasses contain less than 1.5% magnesium oxide (MgO) and potassium oxide ( $\text{K}_2\text{O}$ ) which is an indication of natron usage as a source of a fluxing agent instead of plant ash (Sayre and Smith, 1961). Side samples are natron glasses that show low magnesia and potash content with three exceptions (ASK-G74a -window pane-, ASK-G39a, ASK-G88a -chunks-) (Figure 4.1). While exceeding the limits of 1.5wt% for  $\text{K}_2\text{O}$  (1.7%, 2.3%; 1.9% respectively), these three samples -highlighted with red in the graph- have low MgO levels (<1%).

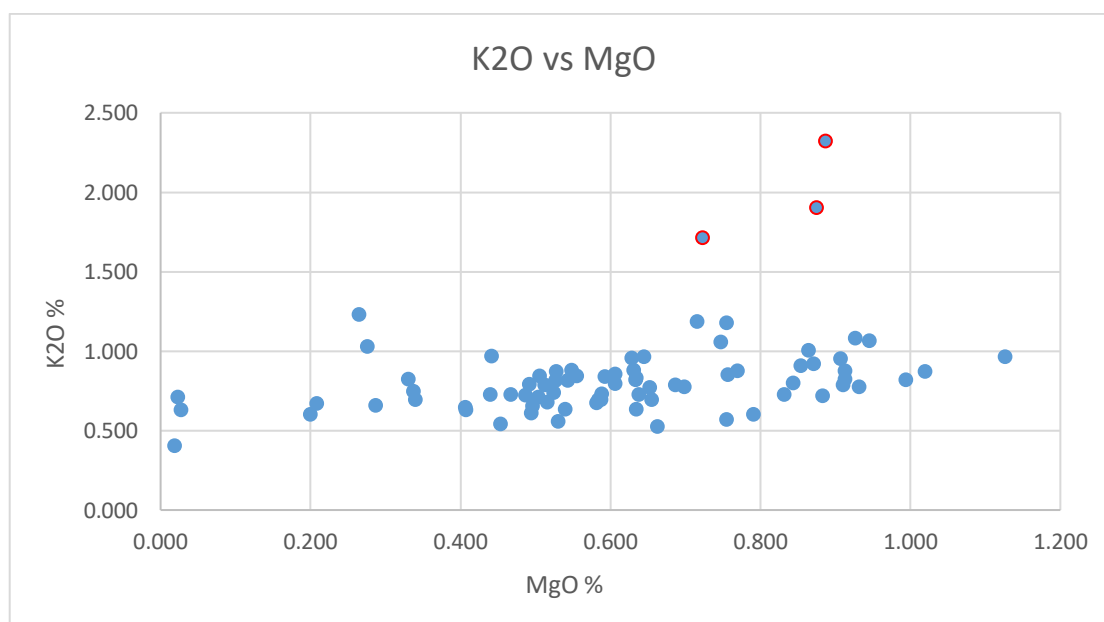


Figure 4.1. The Scatter plot of potassium oxide vs. magnesium oxide for Side sample set

The triangular plot (Figure 4.2) drawn according to the main components of glass (silica-soda-lime) shows that the Side glass set is more or less homogeneous. The triangular plotting was also applied on separate glass groups.

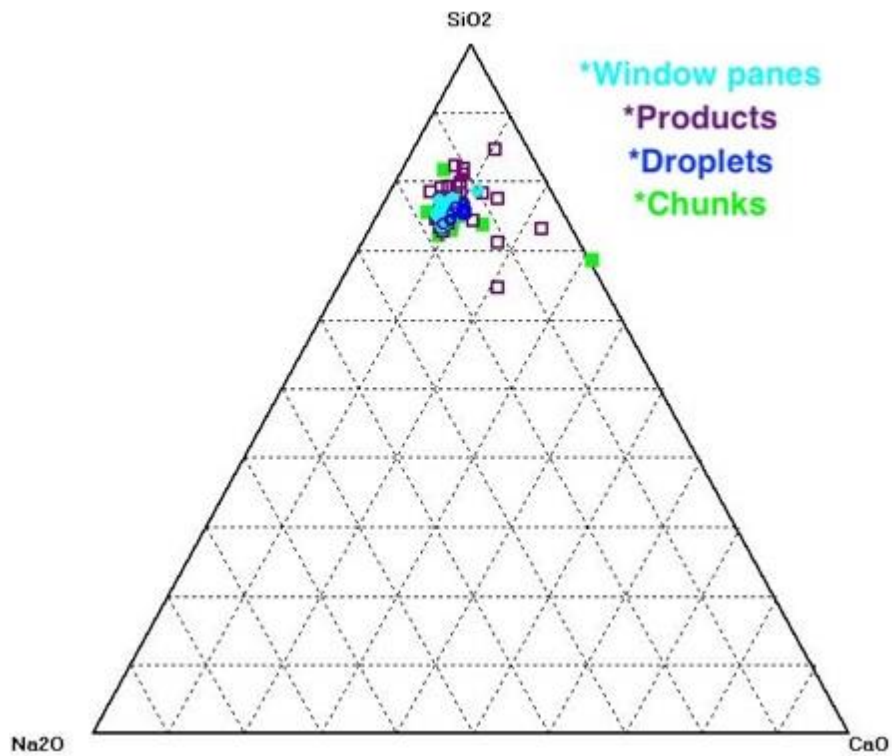


Figure 4.2. Triangular plot (SiO<sub>2</sub>- Na<sub>2</sub>O- CaO) of the Side glass set

According to the plot (Figure 4.3), chunks are also homogenous with two exceptions. The average silica, soda, and lime concentration of the chunks are 61.24% ( $\pm 6.17$ ), 11.73% ( $\pm 3.81$ ), and 8.78% ( $\pm 4.00$ ) respectively. Sample ASK-G52c is an outlier, which has the highest lime (21.93%), lowest soda (0.089%) and silica (48.08%) concentration and also, ASK-G71b has the highest silica (75.16%) concentration compared to chunk group.

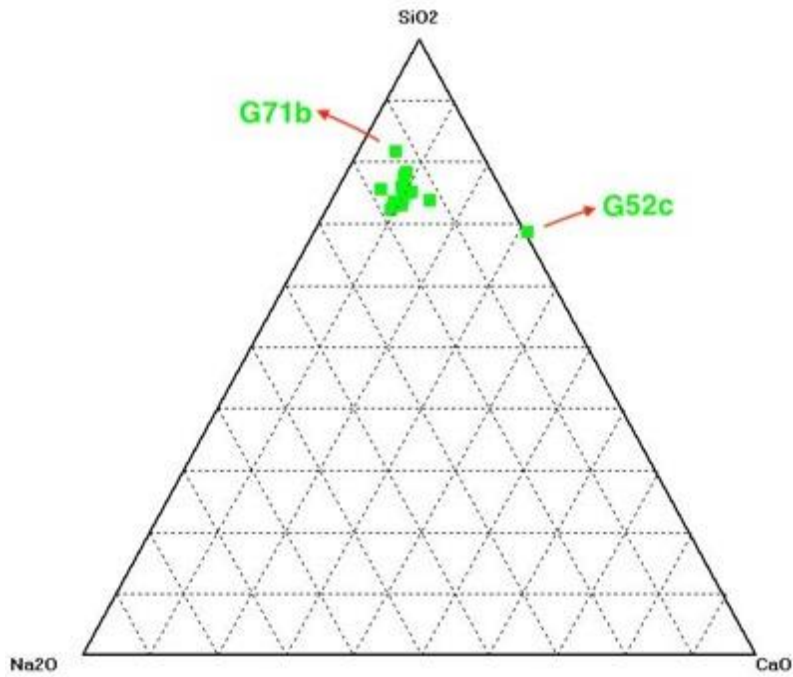


Figure 4.3. Triangular plot (SiO<sub>2</sub>- Na<sub>2</sub>O- CaO) of Side chunk group

The silica, soda and lime averages of the product group are 64.47% ( $\pm 6.42$ ), 11.03% ( $\pm 3.15$ ), and 8.19% ( $\pm 2.85$ ) respectively. Although quite homogenous, the triangular plot of the products (Figure 4.4) is slightly dispersed compared to the other glass groups of Side. Out of 32 product, 7 samples outstand from the group. ASK-G62e is the most detached sample with the highest lime (16.30%) and the lowest silica (50.29%) content. Two samples (ASK-G44a and ASK-G69b) outstand with their drastically low soda (3.07 and 3.03%) concentration. G69b has rather low silica (51.66%) and high lime (15.85%) contents. ASK-G51f has rather low soda (9.4%) and rather high lime (14.91%). ASK-G77 has slightly low soda (10.89%) and rather high lime (11.03%) content. The last distinguished sample is ASK-G54a with its rather low soda concentration (7.6%).

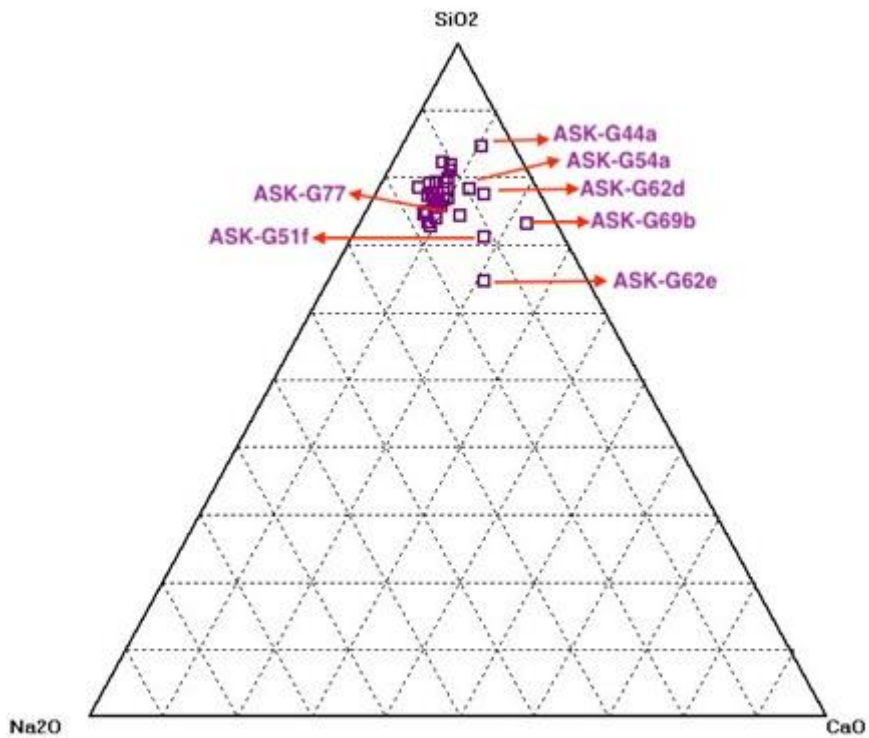


Figure 4.4. Triangular plot (SiO<sub>2</sub>- Na<sub>2</sub>O- CaO) of Side product group

The average silica, soda, and lime concentration of the window panes are 64.23% ( $\pm 3.13$ ), 12.93% ( $\pm 1.82$ ), and 7.43% ( $\pm 0.77$ ) respectively. The triangular plot seen in Figure 4.5 demonstrates the window panes, which is highly homogenous with one exception. ASK-G52b outstands with the lowest Na<sub>2</sub>O value (7.73%).

The silica, soda and lime averages of the droplets and threads are 60.91% ( $\pm 4.31$ ), 11.41% ( $\pm 1.43$ ), and 8.35% ( $\pm 0.93$ ) respectively. The triangular plot seen in Figure 4.6 demonstrates the droplets. This group is the most homogenous one compared to other groups.

When the glass groups of Side were compared, the highest SiO<sub>2</sub> was observed at the products and the lowest SiO<sub>2</sub> was identified at droplets. The highest Na<sub>2</sub>O value was

seen in window panes and the lowest  $\text{Na}_2\text{O}$  value was seen in products. While the highest  $\text{CaO}$  concentration was detected in chunks, the lowest  $\text{CaO}$  was spotted on window panes.

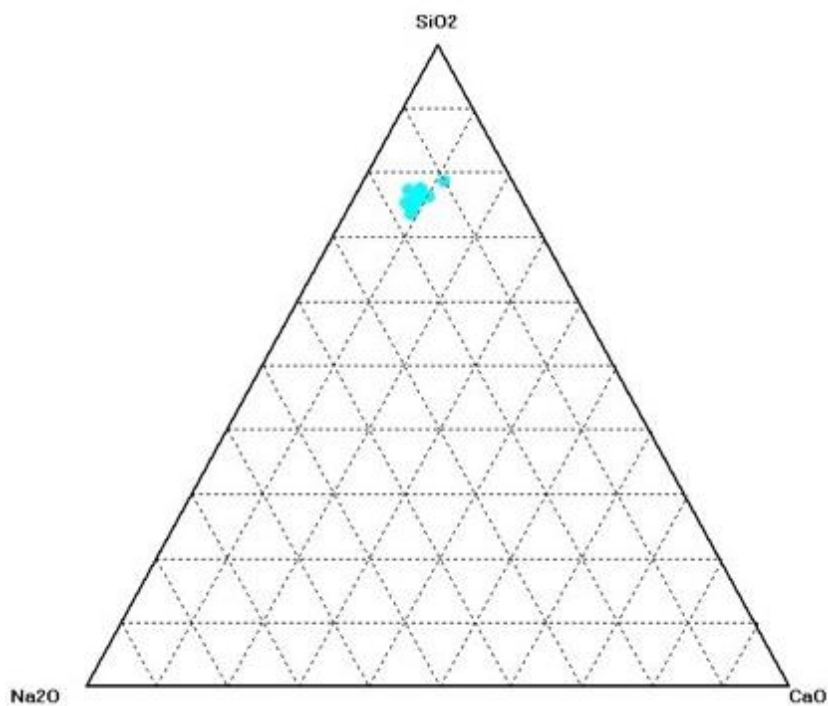


Figure 4. 5. Triangular plot ( $\text{SiO}_2\text{-Na}_2\text{O-CaO}$ ) of Side window-pane group

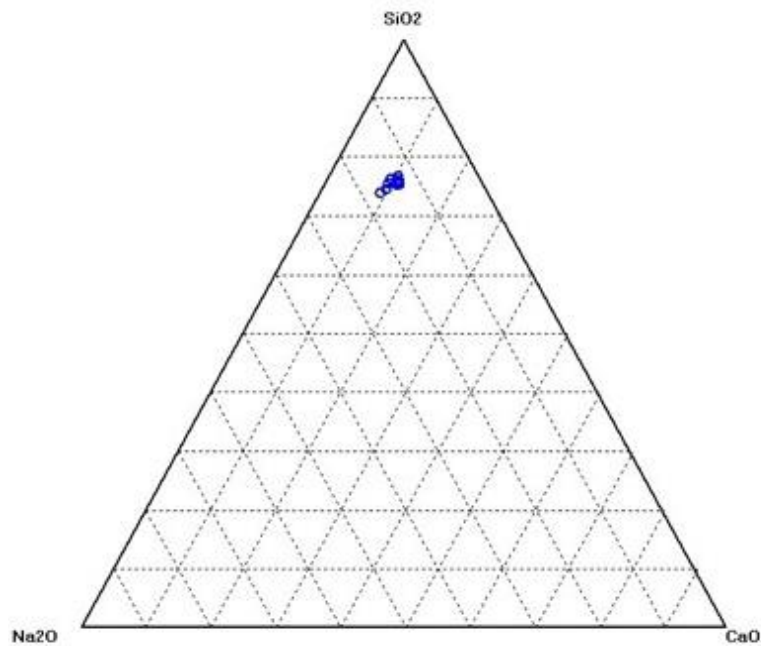


Figure 4.6. Triangular plot (SiO<sub>2</sub>- Na<sub>2</sub>O- CaO) of Side droplet group

Trace elements can help to distinct groups and verify the associations between the groups (Freestone, 2004). The traces are normalized to the continental crust in Figure 4.7. According to the diagram, while Side vessels and window panes follow a similar path, chunks and vessels dissociate from each other. Therefore, vessels and window panes of Side glass are associated with each other regarding the raw material source.

When Side assemblage was examined according to the location, such as Dionysus Temple, Theatre, MZ, N2, TT and APS, no meaningful difference is detected. The comparison of the selected main elements (Figure 4.8) does not provide a distinct glass variation. We can say that the artisanal quarter of Side produces a more or less similar glass type. Thus, no need for further investigation of the regional differences was seen.

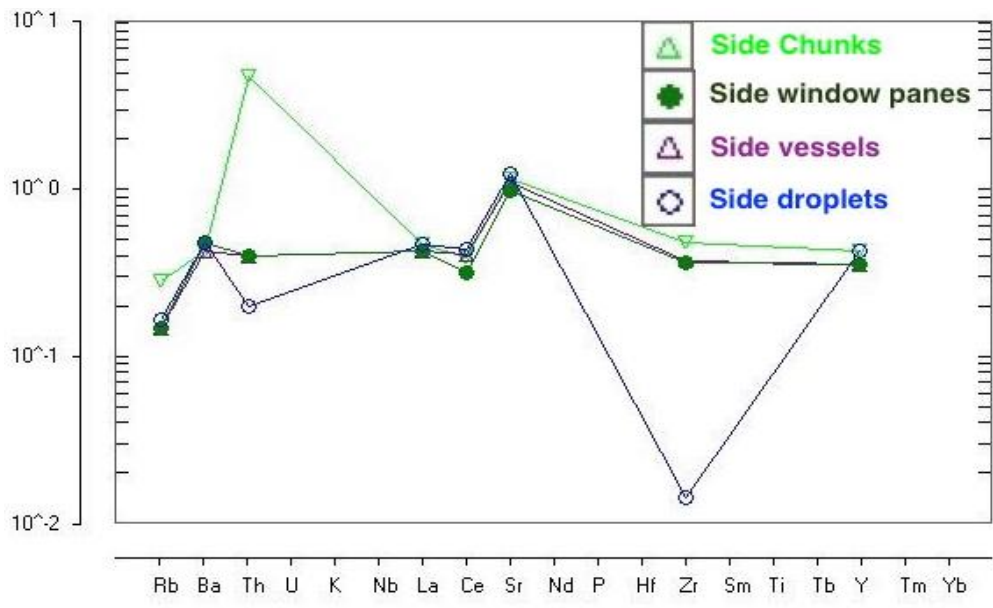


Figure 4.7. Spider diagram showing the trace elements of 4 different Side glass groups (values are normalised to the average continental crust)

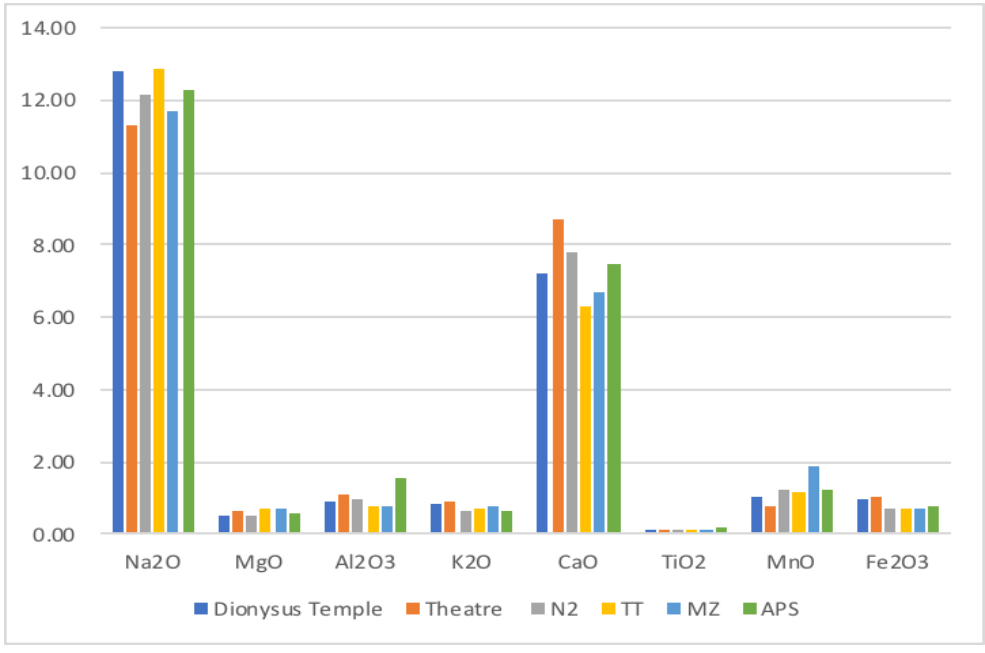


Figure 4.8. Cluster column chart showing the differences of the regions according to the selected elements

### 5.3.1. Sand

Strontium, zirconium, and barium are associated with the sand used for glass production. Ba is linked to the content of alkali feldspars in the sand (Silvestri et al., 2008). The barium content of Side glass varies from 102 ppm to 672 ppm with an average of 318 ppm ( $\pm 103$ ). No significant difference is detected between Side glass groups. However, the barium content is differing among samples; the small amount of the samples has low barium content at  $\sim 100$  ppm, which is related with sand that is poor in alkali feldspar and more than half of the samples contain  $>300$  ppm, which is linked to sand, rich in alkali feldspar.

A positive correlation between barium and manganese (Figure 4.9) may show that manganese and barium come from the same source. In addition to pyrolusite ( $\text{MnO}_2$ ), psilomelane  $[(\text{Ba},\text{H}_2\text{O})_2\text{Mn}_5\text{O}_{10}]$  may also be used as a source of manganese, due to its barium-bearing structure (Silvestri et al., 2008).

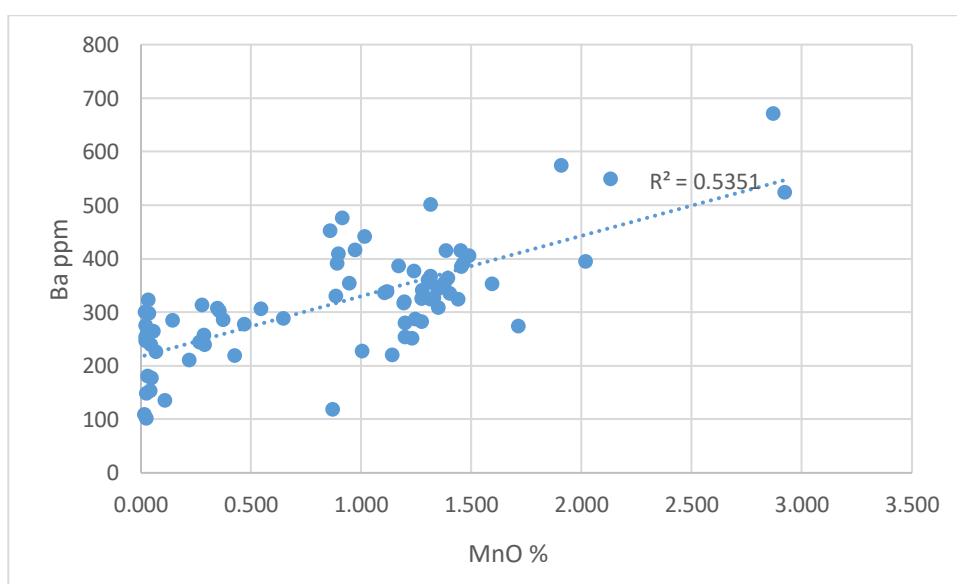


Figure 4.9. Scatter plot of MnO vs. Ba of Side glasses

Strontium (Sr) and zirconium (Zr) contents provide some implications about material sources. Sr is geochemically similar to Ca and contains lime-containing substances (such as sea shell, limestone, and plant ash). Sr levels, which are higher than 400 ppm, suggests that the sand used in the production of the glass is nautical (Freestone et al., 2003). Whereas, Zr is expected to be higher than 160 ppm, in glasses produced with terrestrial sand. Sr content of the Side chunks varies between 358-698 ppm with an average of 585 ppm. Zr is between 28-139 and the average is 103.84 ppm. The Sr levels of the threads are between 465-834 ppm and have an average of 628 ppm. Zr is between 47-117 ppm and has an average of 81.95 ppm. The Sr level of the products is between 455 and 691 ppm, with a mean of 542 ppm. Zr is between 68.7 and 143 and has a mean of 94 ppm. Sr levels of ASK-G52c, ASK-G69b, ASK-G2, and ASK-G80a are lower than 400ppm, which is 218, 333, 358, and 379 ppm respectively. However, only ASK-G52c has high levels of zirconium at 256 ppm. Since ASK-G69b, ASK-G2, and ASK-G80a have zirconium levels below the terrestrial limits of 160 ppm and their strontium levels are slightly lower than 400 ppm, they are presumably of nautical origin. To sum up, the results show that all the samples except ASK-G52c are made with marine sands. Figure 4.10 and 4.11 show the graphs demonstrating Sr and Zr concentration of Side glass set.

According to Henderson (2013), the positive correlation between calcium and magnesium is an indicator of the use of dolomite as a source of lime. However, there was no positive correlation between calcium and magnesium in Side glasses, which suggests that lime derives from shell fragments within the sand. Moreover, the aluminum levels of Side glasses are extremely low with an average of 1.04% ( $\pm 0.71$ ). This is accepted as an indication for the use of pure high silica sand.

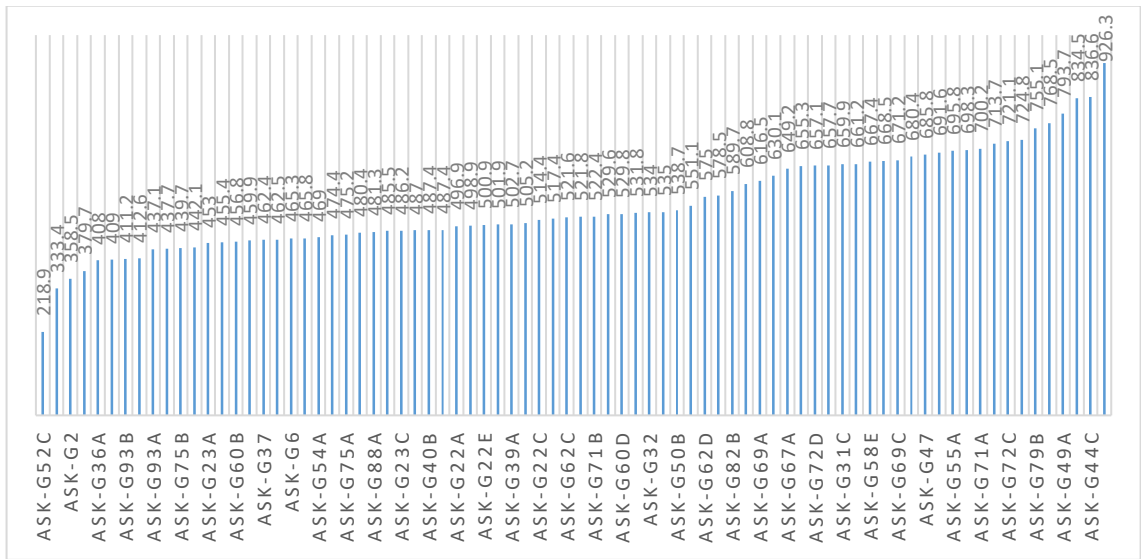


Figure 4.10. Strontium graph of Side glass samples

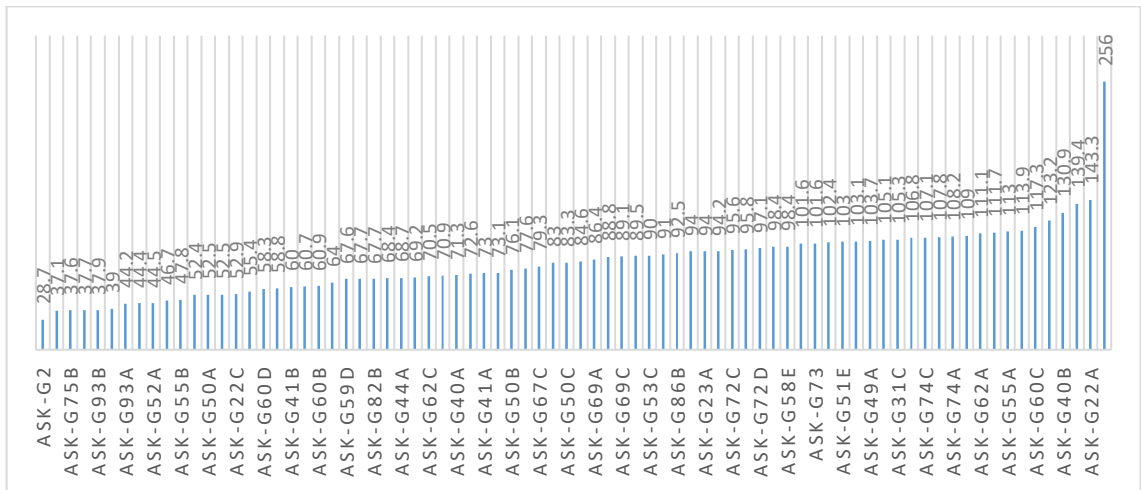


Figure 4.11. Zirconium graph of Side glass samples

### 5.3.2. Colorants

Side glasses have a wide variety of colors. The samples are mostly green and blue, but also have purple, yellow, black and cobalt blue colors. The elements for coloring the Side samples are detected as iron, manganese, copper, and cobalt. Furthermore, the main decolorant is manganese, however, antimony is detected in four samples.

There are different opinions about the deliberate addition of manganese in Late Antique glass. While according to Wedepohl and his coworkers (2011), the levels above 0.1-0.2 percent is considered deliberately added; this level reaches to 0.2 percent in Sayre's work (1963), 0.4 in Brill's study (1988), 0.5 in Jackson's article (2005) and up to 1% in Henderson's (1985) and Mirti's (2001) studies. According to Brems and Degryse (2014), the glass, which is appropriate for production, contains manganese between 0.004 and 0.078%. Thus, the natural background impurity is lower than 0.1 percent. Moreover, Brill notes that the values between 0.1 and 0.4% imply mixing of different cullets, some of which include more manganese than others. According to these statements, it can be said that 15 samples out of 78 have manganese lower than 0.1%, 8 samples have manganese inclusion between 0.1 and 0.4% and the rest of the Side samples (55 samples) have greater values than 0.4%. Therefore, we can conclude that manganese is intentionally added to more than half of the samples.

Additionally, manganese presence can either occur as an impurity associated with iron or deliberate addition, to testify it manganese and iron correlation can be investigated (Nakai et al. 2014). Figure 4.12 shows that there is no correlation between iron and manganese. This scatter graph can verify our statement about manganese. Moreover, as asserted by Freestone and his coworkers, 250 ppm of manganese appears in glass naturally, higher levels are the indicators of pyrolusite ( $MnO_2$ ) inclusion. According to this statement, Side samples with 6 exceptions (ASK-G50a, ASK-G52a, ASK-G54a, ASK-G69b, ASK-G75b, ASK-G80a and ASK-G55b) were decolorized by the mineral pyrolusite.

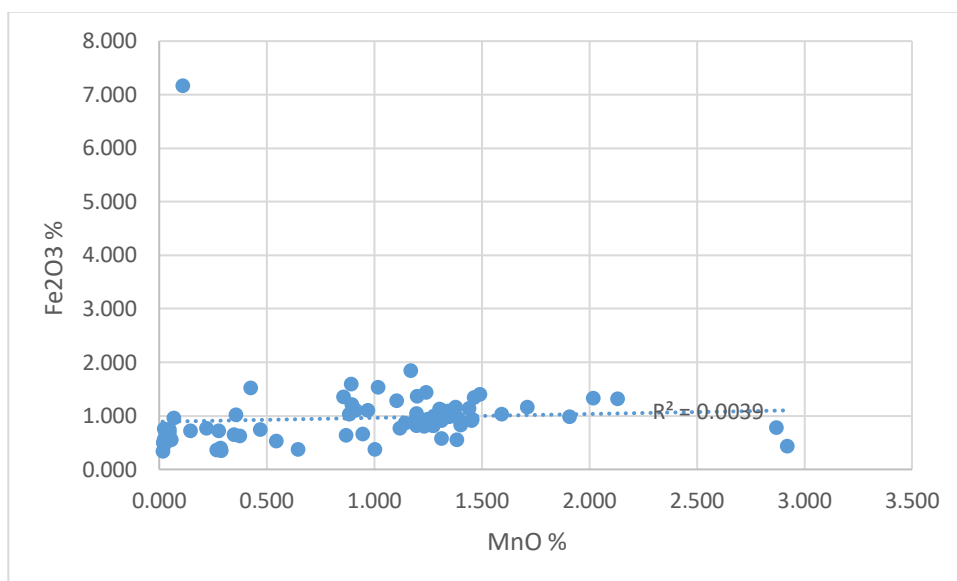


Figure 4.12. Scatter graph demonstrating Fe<sub>2</sub>O<sub>3</sub> vs MnO for Side glass set

Manganese was also used as a colorant that gives brown, purple tones. There are 3 brown/purple-colored samples in the Side glass set; 1 chunk (ASK-G66d), 2 vessels (ASK-G79c and ASK-G83a). These 3 samples have the highest manganese levels (2.13, 2.92 and 2.89% respectively) compared to the Side assemblage with an average of 0.89% ( $\pm 0.67$ ). These three samples were graphed according to their trace elements which were normalized to average continental crust. This spider diagram (Figure 4.13) reveals the similarities of the samples to understand whether these glasses can be attributed to the same source. According to the spider diagram, all three samples follow quite a similar pattern, the sand used to produce these samples might be from the same region.

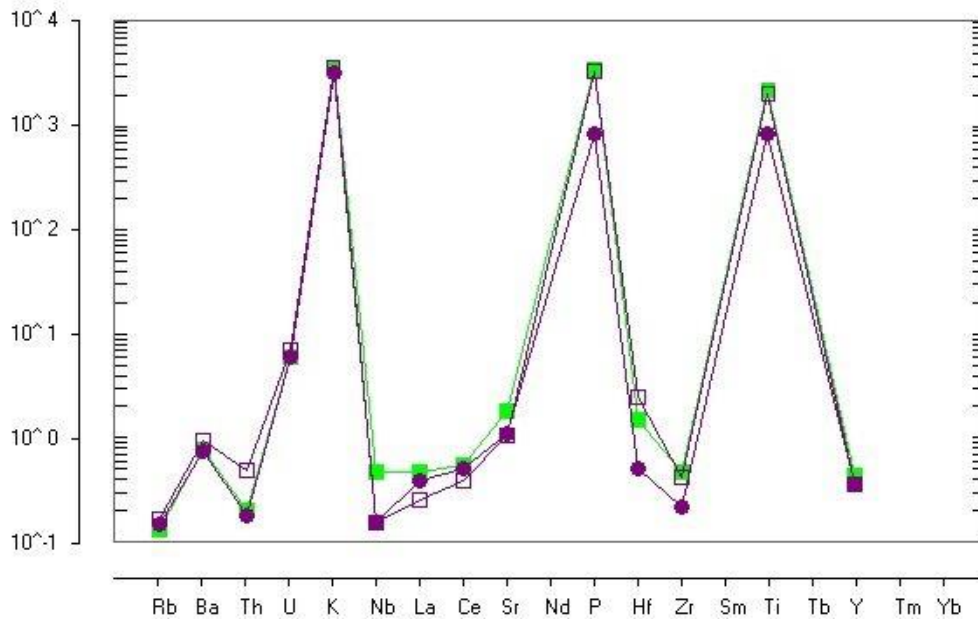


Figure 4.13. Spider diagram of high manganese purple-colored glasses, normalized to the average continental crust

Antimony is the strongest decolorant in the ancient glass world, and the less tinted glasses of Side is decolorized with antimony. Only 4 samples (ASK-G75b, ASK-80b, ASK-G81, ASK-G82b) include a significant amount of antimony as 3381, 7395, 4451 and 8918 ppm. ASK-G75b is completely colorless, which does not contain greenish or bluish tints. However, although highly colorless, ASK-G80a and ASK-G81 involve remarkably pale-yellow tint due to their iron inclusion at 0.7 and 0.6%. Even with the highest antimony content, ASK-G82b is a dark-colored glass. In this situation, antimony did not act as a decolorizer but as a reducer depending on the red-ox conditions of the furnace environment (Schibille et al., 2016).

Copper, iron, and cobalt elements are the most used colorants in the ancient glass world. The iron (III) oxide concentration of the Side assemblage is 0.95% ( $\pm 0.78$ ), when the outlier (ASK-G52c with 7.16%  $\text{Fe}_2\text{O}_3$ ) is excluded,  $\text{Fe}_2\text{O}_3$  concentration is

in the range of 1.83-0.33%. When the outlier (ASK-G52c with 26710 ppm) is excluded, the average copper content is 118 ( $\pm$ 236) ppm and ranges from 2 ppm to 1386 ppm. Also, the average cobalt content is 28 ( $\pm$ 51) ppm and ranges from 4 ppm to 405 ppm in the absence of the outlier (ASK-G52c with 1570 ppm).

Chunks contain two black-colored (ASK-G52c, ASK-G39a) opacified samples. While ASK-G52c include the highest levels of cobalt (1570 ppm), copper (26710 ppm) and iron (7.16%), ASK-G39a do not contain a high amount of cobalt (16 ppm), copper (63 ppm) and iron (0.7%). The dark color of ASK-G39a can be explained by the remarkably low manganese content (0.27%). These two black samples are opacified with lead (Pb=916 and 84270ppm). 8.4% of lead is the highest lead concentrations by far, compared to Side glass. Other dark green chunks (ASK-G8b, ASK-G22e, ASK-G62b, and ASK-G88a) have iron content above 1% and copper concentrations are 94, 116, 66 and 114 ppm, respectively. Likewise, the iron content of ASK-G86b and ASK-G53c is above 1%, but due to their high manganese concentration (1.3 and 1.4%), they are not as dark as the other 4 high-iron samples. The highest copper (Cu= 1386, 912, 438 ppm) and cobalt (Co= 405, 173, 71 ppm) values occur in the two cobalt blue (ASK-G67c, ASK-G74c) and one blue (ASK-G71b) chunks.

The cobalt blue sample ASK-G51f has the highest copper (1269 ppm), cobalt (179 ppm) and lead (4511 ppm) content among the products. The highest lead levels are detected in the two cobalt chunks (ASK-G67c, ASK-G74c) and the cobalt vessel fragment (G51f) with the concentrations of 3130, 5940 and 4511 ppm, except the ASK-G52c. Another blue sample, ASK-G59d, has lower cobalt (39 ppm) concentration with 81 ppm of copper. While some samples have higher concentrations than ASK-G59d, this sample has darker tones compared to the others, which is due to the remarkably low levels of manganese (0.03%). ASK-G82b has the second highest copper content as 570 ppm and it is one of the darkest samples among the products. Another dark green sample is ASK-G37 with the highest iron content (1.4% Fe<sub>2</sub>O<sub>3</sub>) and 124 ppm Cu. ASK-G22a and ASK-G50c have rather high copper (116 and 75

ppm) and iron (III) oxide inclusion above 1%, however, they are not as dark as we expected because of the high manganese concentrations.

Highest iron concentrations of window panes (1.5 and 1.2 %) are seen in the darkest samples, ASK-G40b and ASK-G68. These samples also have rather high copper inclusion 224 ppm and 123 ppm compared to the average value (77 ppm) of the window panes. ASK-G41a is a quite light, green tinted specimen with rather high copper content (144 ppm), which again can be explained by high manganese level.

Droplets and threads of Side do not have dark colors as seen in chunks, but almost half of them contain iron (III) oxide above 1%. The lighter colors are sustained by manganese exceeding 1 percent. However, high copper inclusion can overcome the decolorizing effects of manganese as can be seen in ASK-G72d. This sample has the second highest manganese concentration (1.43%), however, it is the darkest green color compared to other droplets. The rather high copper inclusion (144 ppm) restrains the decolorization. Furthermore, the ideal ratio of iron to manganese is not achieved for decolorization purposes.

Bronze is used as a coloring agent for green and blue colors. To understand the use of bronze, the correlation between copper and tin is inspected. The samples that contain >100ppm of copper are selected. The scatter plot of Sn and Cu (Figure 4.14) reveals that there is a highly strong correlation between these elements. Therefore, the presence of copper might result from the addition of bronze.

Tin is known to be yellow colorant. However, 7 yellow- yellowish green samples from Side (ASK-G44a, ASK-G49a, ASK-G62d, ASK-G79b, ASK-G74a, ASK-G51e, and ASK-G60c) have an insignificant amount of tin. Additionally, silver, which gives the glass a yellow color, is below the detection limits. Hence, the yellow hues do not derive from tin or silver. Nonetheless, the manganese converted  $Fe^{2+}$  that gives blue tones to  $Fe^{3+}$ , which gives a weak yellow hue (Sayre, 1963). For instance, ASK-G51e has a high (1.32%) iron inclusion, however, it has the 4<sup>th</sup> highest manganese

concentration among the Side assemblage, therefore, its yellowish pale green color is clear.

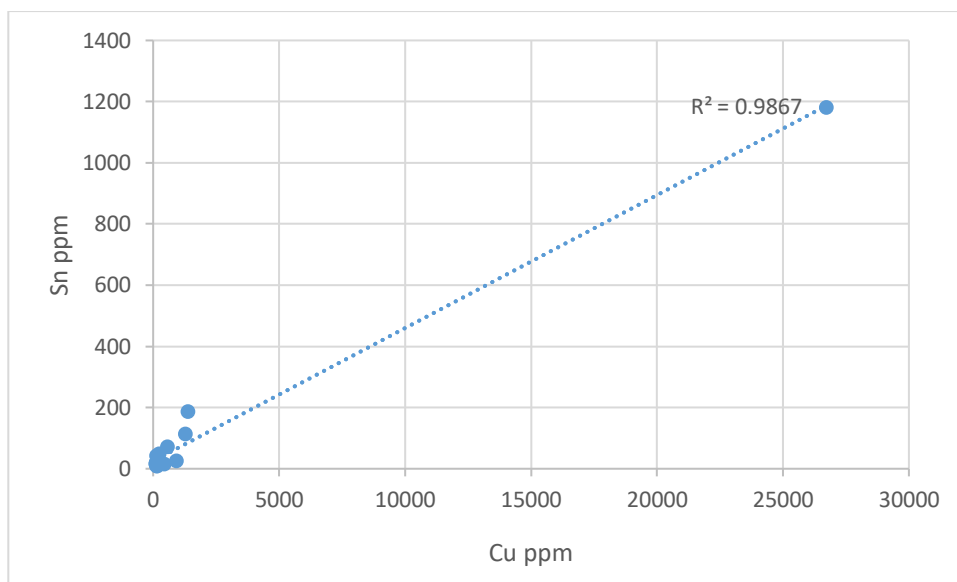


Figure 4.14. Scatter plot of copper and tin for the samples that contain >100 ppm of Cu

As previously mentioned, cobalt is a well-known colorant for the blue color, and it is incorporated into the composition of the glass through minerals. Therefore, the presence of copper, nickel, manganese, iron, zinc, sulfur and arsenic helps us to identify the mineral choice for a coloring agent. The correlation of these elements with cobalt can specify the mineral ores. Scatter graphs (Figure 4.15; Figure 4.16; Figure 4.17) are plotted for the samples which have high cobalt concentration (>100 ppm). The lack of correlation between cobalt and sulfur is an indication that cobaltite ( $\text{CoAsS}$ ) and bieberite ( $\text{CoSO}_4 \cdot 7\text{H}_2\text{O}$ ) were not used as a colorant. Moreover, the high correlations of cobalt with nickel, arsenic, and iron increase the possibility of the use of Skutterudite ( $(\text{Co},\text{Ni},\text{Fe})\text{As}_3$ ) as a cobalt bearing mineral source (Schibille, 2016).

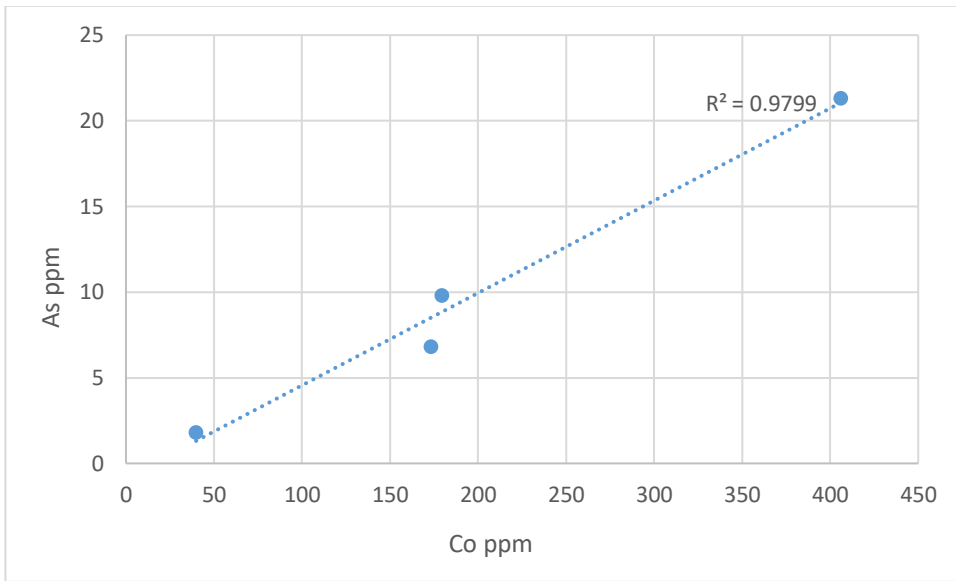


Figure 4.15. Scatter plot of arsenic and cobalt for samples that contain cobalt

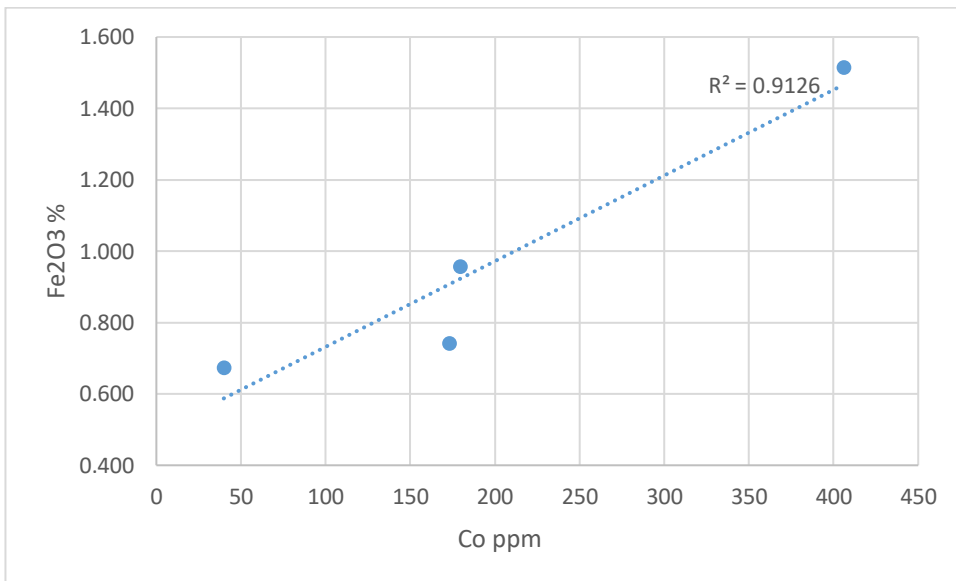


Figure 4.16. Scatter plot of iron oxide and cobalt and cobalt for samples that contain cobalt

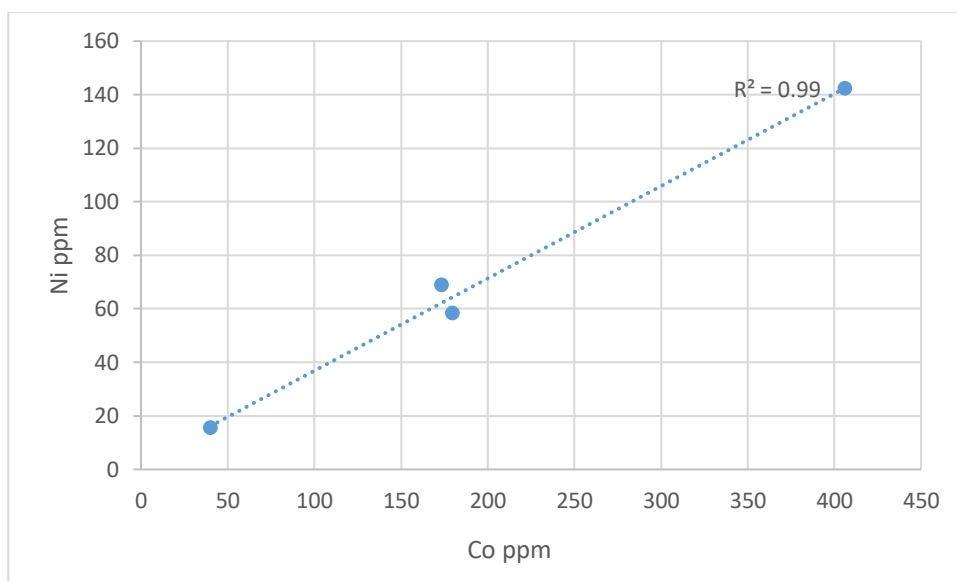


Figure 4.17. Scatter plot of cobalt vs. nickel for cobalt-bearing samples

### 5.3.3. Recycling

As mentioned above (Chapter 2.5), recycling is a problematic issue due to the complications of recycling markers and colorants. Also, there are different opinions about the elevated impurity concentrations which specify recycling. While Jackson and Foster (2014), designate the colorless/naturally colored glass impurity levels as  $\text{Cu} \geq 100$  ppm,  $\text{Pb} \geq 0.1\%$ ,  $\text{Sb} \geq 0.1\%$ , the impurity levels are  $\text{Cu} > 100$  ppm,  $\text{Pb} > 75$  ppm,  $\text{Sn} > 25$  ppm and  $\text{Sb} > 20$  ppm for Rehren and Brüggler (2015). Moreover, Brems and Degryse (2014) assert that glassmaking sands contain an insignificant amount of  $\text{SbO}$ , which is lower than 1.4 ppm and any elevated concentrations may result from the contamination caused by re-melting of different glass cullets, rather than deliberate addition. Further, Cholakova and Rehren (2018) designate the recycling limits of antimony in the range of 20-800 ppm. Additionally, according to Jackson and Paynter (2016), the antimony decolorized glass group contains  $\text{SbO}$  varying between 0.3 and 0.8%.

Although the minimum value for recycled glass is ambiguous, the maximum value can be assigned as 800 ppm. When we designate the minimum level as 20 ppm, 49 samples out of 77 are assumed to be recycled. Figure 4.18 and Figure 4.19 show the correlation of  $K_2O$  vs  $P_2O_5$  and  $CaO$  vs  $P_2O_5$  for 49 samples ( $Sb=20-800$  ppm). Potassium and calcium strongly correlate with phosphorus for recycled glass (Al-Bashaireh et al., 2016). Although not strong, a correlation can be seen in the scatter plots for the 49 samples.

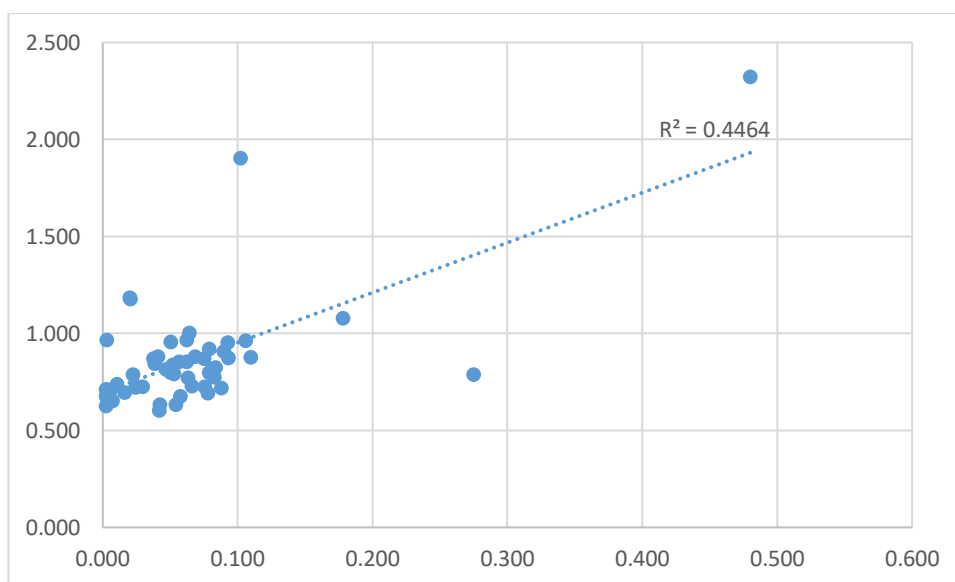


Figure 4.18.  $K_2O$  to  $P_2O_5$  for the samples  $Sb= 20-800$  ppm

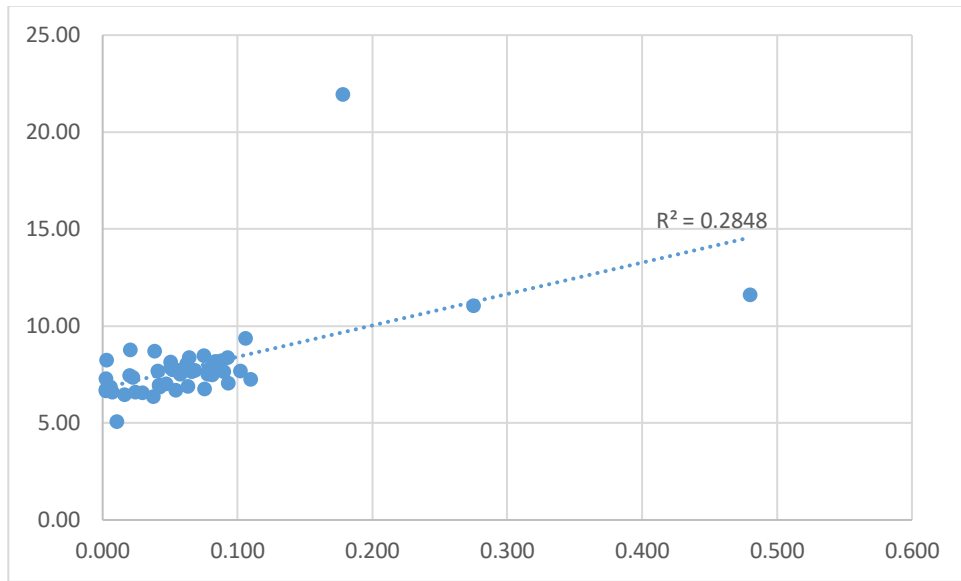


Figure 4.19. CaO to P<sub>2</sub>O<sub>5</sub> for the samples Sb=20-800 ppm

The recycling markers of cobalt, copper, and lead cannot assign recycling for the colored glass. Therefore, these markers can be applied solely for the colorless or the naturally colored glass. Side glass set contains 1 colorless and 24 naturally colored glass. For Pb level of Side samples is measured between 4-317 ppm, with an average of 109 ppm ( $\pm 102$ ). Cu levels are between 6-144 ppm with an average of 43 ppm ( $\pm 39$ ). Sb levels are between 1-7395 ppm, with an average of 657 ppm ( $\pm 1771$ ). When we take out the deliberately antimony-decolorized samples ( $>800$  ppm), only 8 samples out of 25 samples can meet some of the above-mentioned criteria for recycling. These 8 samples tend to show a high correlation between CaO and K<sub>2</sub>O (Figure 4.20) and the high K<sub>2</sub>O samples tend to have higher P<sub>2</sub>O<sub>5</sub> (Figure 4.21), suggesting ash-related contamination (Davis and Freestone, 2018).

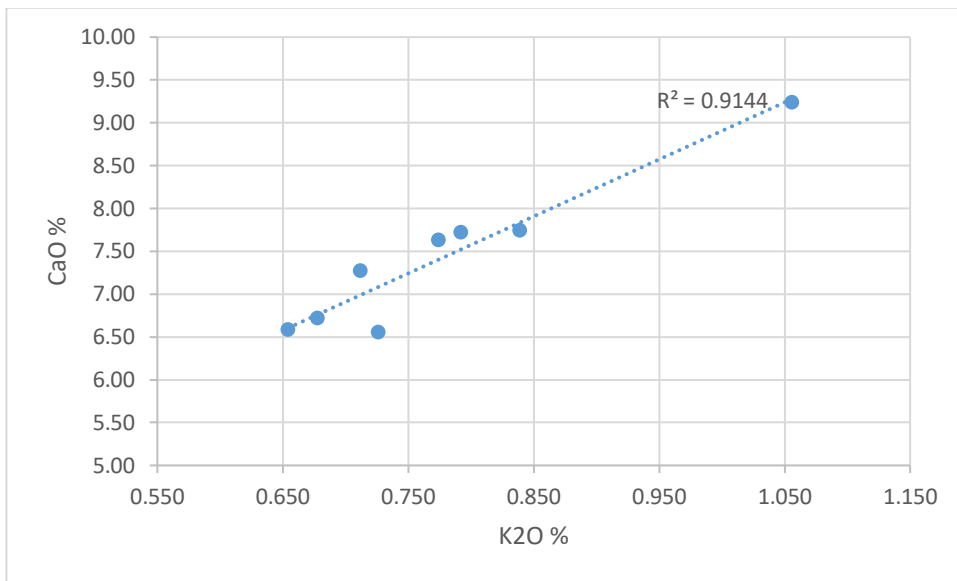


Figure 4.20. The scatter plot of CaO and K<sub>2</sub>O for the 8 recycled colorless/naturally colored glass

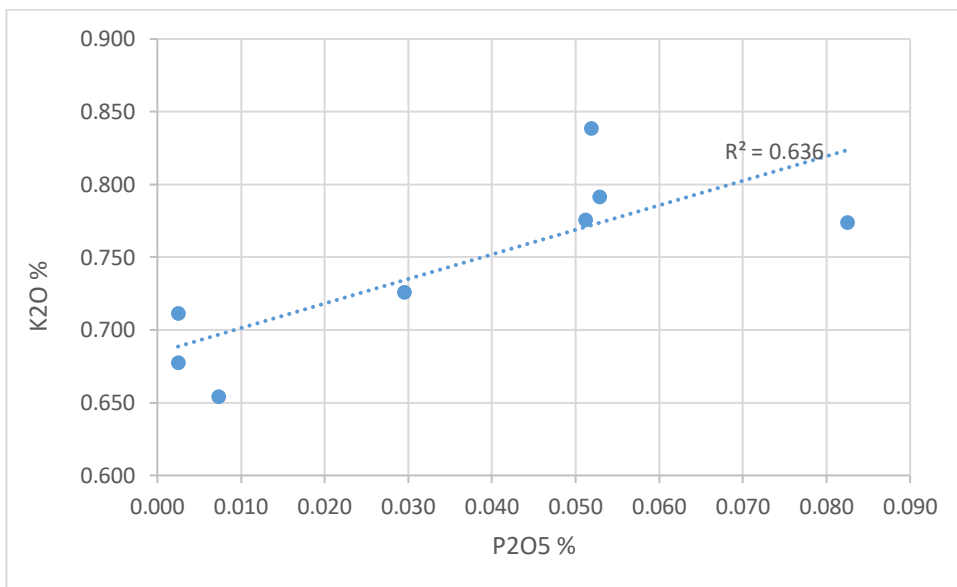


Figure 4.21. The scatter plot of K<sub>2</sub>O and P<sub>2</sub>O<sub>5</sub> for the 8 recycled colorless/naturally colored glass

### 5.3.4. Identification of Compositional Groups

In order to categorize Side glasses into compositional groups, cluster analysis was conducted using R-studio software. The results are shown in a dendrogram, acquired by Ward's method as a clustering algorithm with squared Euclidean distance as the measure of dissimilarity of the data. The dendrogram (Figure 4.22) was performed on elements; MgO, K<sub>2</sub>O, CaO, TiO<sub>2</sub>, MnO, and Fe<sub>2</sub>O<sub>3</sub>. Although Na<sub>2</sub>O and Al<sub>2</sub>O<sub>3</sub> are characteristic elements for identifying the compositional groups, Na<sub>2</sub>O and Al<sub>2</sub>O<sub>3</sub> levels of Side are lower than expected due to the weathered glass structure. The dendrogram acquired by these elements presents five main compositional groups. However, when different levels of antimony are taken into account, 7 different groups emerge within the Side assemblage. These are Roman antimony-decolorized, Roman manganese-decolorized, Roman mixed antimony-manganese decolorized, HIMT(?), Levantine II, high lime, and lead glass (the outlier).

Table 2.1 shows the average elemental composition of different glass groups of Side. It should be noted that silica, soda, and alumina levels are lower compared to the contemporary glass due to the high corrosion levels of Side glass.

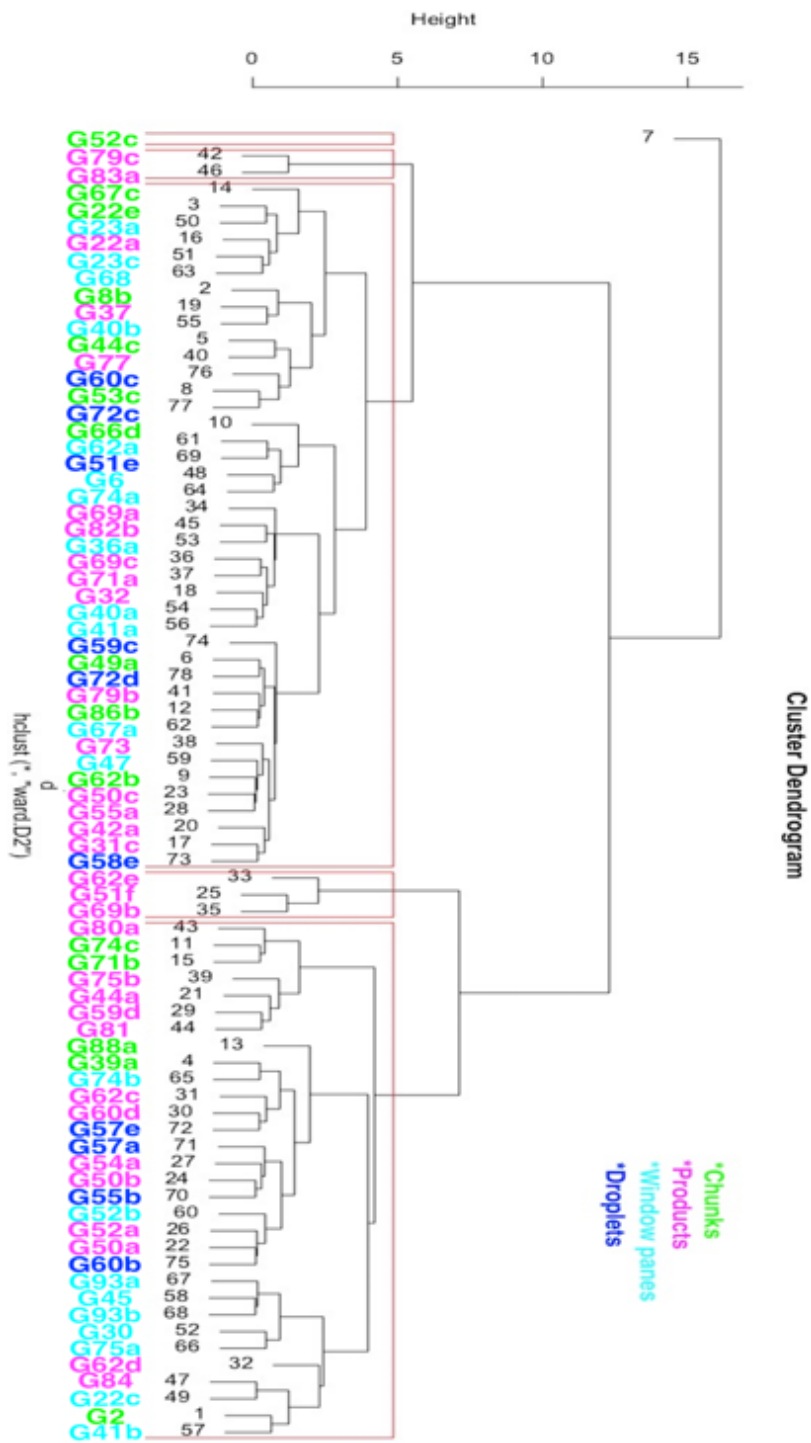


Figure 4. 22. Cluster dendrogram of Side assemblage performed on MgO, K<sub>2</sub>O, CaO, TiO<sub>2</sub>, MnO, and Fe<sub>2</sub>O<sub>3</sub>

Table 2-2 Average elemental compositions of Side glass groups

	Sb-decolorized	Mixed Sb-Mn	High-Mn	High CaO	HIMT (?)	Levantine I	Outlier-Pb glass
Na <sub>2</sub> O	13.410	12.075	11.155	7.907	12.59	11.170	0.089
MgO	0.387	0.765	0.497	0.398	0.70	0.519	0.927
Al <sub>2</sub> O <sub>3</sub>	0.467	0.634	0.886	0.561	0.99	1.038	6.389
SiO <sub>2</sub>	68.885	71.320	68.010	54.047	62.12	65.464	48.08
P <sub>2</sub> O <sub>5</sub>	0.019	0.080	0.040	0.019	0.06	0.068	0.178
SO <sub>3</sub>	0.375	0.359	0.246	0.308	0.32	0.217	0.021
Cl	0.919	0.809	0.759	0.467	0.72	0.747	0.001
K <sub>2</sub> O	0.488	0.881	0.734	0.702	0.85	0.871	1.079
CaO	5.051	6.097	6.658	15.695	7.49	8.135	21.93
TiO <sub>2</sub>	0.108	0.113	0.087	0.112	0.17	0.096	0.531
V <sub>2</sub> O <sub>5</sub>	0.005	0.008	0.009	0.007	0.01	0.005	0.023
Cr <sub>2</sub> O <sub>3</sub>	0.004	0.002	0.001	0.003	0.00	0.004	0.114
MnO	0.020	0.720	2.895	0.455	1.29	0.353	0.109
Fe <sub>2</sub> O <sub>3</sub>	0.541	0.730	0.602	0.745	1.12	0.586	7.166
LOI	8.975	5.700	7.280	18.666	11.58	10.763	13.36
Co	12.6	15.0	29.1	64.1	30.7	24.0	1570.0
Ni	5.7	14.1	23.6	28.3	22.7	13.1	1955.0
Cu	12.0	297.8	80.7	449.0	131.6	79.7	26710.0
Zn	17.4	24.6	15.0	9.0	20.5	10.1	1834.0
Ga	2.9	1.4	2.8	2.5	2.1	3.0	21.0
Ge	0.9	0.6	0.5	0.5	0.7	0.5	5.1
As	143.0	56.9	3.3	4.3	6.3	2.0	128.0
Se	0.3	0.4	0.3	0.5	0.3	0.3	7.4
Br	8.1	8.8	7.3	12.6	10.1	8.7	24.2
Rb	5.6	8.0	10.0	9.8	9.9	10.4	99.1
Sr	409.7	599.3	540.4	489.7	629.6	480.1	218.9
Y	4.4	3.7	5.6	4.0	6.0	5.9	12.0
Zr	61.1	69.3	68.1	82.4	98.3	58.6	256.0
Nb	2.9	7.1	2.8	4.5	4.1	3.5	7.2
Mo	3.0	8.0	7.3	3.5	5.2	3.7	36.8
Cd	7.7	6.1	1.0	1.1	1.1	0.9	2.1
In	3.1	4.0	0.9	0.8	1.1	0.9	2.7
Sn	42.2	58.1	9.3	41.0	20.0	5.5	1181.0
Sb	5388.0	6684.5	107.3	5.9	343.7	14.1	142.6
Te	10.3	3.4	1.4	1.5	1.5	1.3	1.8
I	3.1	3.9	2.7	2.8	2.6	2.4	7.7
Cs	5.0	6.3	4.5	4.8	4.5	4.4	6.9
Ba	129.3	244.7	598.3	203.9	357.3	276.5	135.9
La	9.2	11.3	9.3	15.5	12.6	13.5	29.0
Ce	16.6	32.7	25.9	27.5	21.6	22.2	32.7
Hf	5.3	20.2	6.6	23.3	10.0	6.0	810.0
Ta	2.1	7.5	4.1	8.0	5.2	3.7	160.0
W	1.7	2.4	2.0	2.2	2.1	1.9	28.0
Hg	0.7	0.8	0.7	0.9	0.7	0.7	7.0
Tl	0.7	1.1	0.8	1.6	1.0	0.9	103.6
Pb	146.2	560.6	178.7	1618.9	381.6	258.4	84270.0
Bi	0.8	1.4	0.8	1.8	0.9	0.7	31.0
Th	1.3	3.3	1.7	9.9	3.4	2.3	271.4
U	11.4	9.1	7.1	8.5	8.3	8.3	31.0

### Roman antimony-decolorized glass (Rom Sb)

There are only two samples (ASK-G75b and ASK-G80a) that fit this group. The main separators of this group are the presence of antimony oxide as a decolorizer together with the partial absence of manganese ( $\text{MnO} < 0.03\%$ ). SbO levels are 3381ppm and 7395ppm. The manganese concentrations of the two samples are 0.016% and 0.024%. The two colorless specimens are the rare colorless samples that do not contain blue or green tint in the Side sample set, due to their high antimony and low colorant contents.

Although 13.4% of soda is quite low for the Late Antique glass, the highest level of soda and the lowest levels of alumina (0.4%) and lime (5%) are detected in this group compared to Side assemblage. This group is known to be a non-recycled, primary glass due to the absence of manganese (Schibille et al., 2016). While ASK-G75b does not meet any of the recycling criteria, ASK-G80a has 267 ppm lead content which is higher than the accepted threshold for sand impurities. Hence, we can say that, even if ASK-G80a was not recycled with a manganese-bearing glass, it might be re-melted or recycled with a lead-bearing glass.

### Roman manganese-decolorized glass (Rom Mn)

Inclusion in this group is constrained with manganese contents above the background levels ( $>0.025\%$ ) and antimony levels below the detection limits of XRF. This natron-based group has lower soda (11.15%), higher lime (6.65%) and alumina (0.8%), together with slightly higher  $\text{K}_2\text{O}$  (0.73%), MgO (0.4%) and  $\text{Fe}_2\text{O}_3$  (0.6%) compared to Roman antimony-decolorized type. Rom-Mn is comprised of only 2 samples (ASK-G79c and ASK-G83a) with the highest manganese values (2.9 and 2.8%) compared to the assemblage. The two samples are not colorless but have dark purple, brown colors when in the state of trivalent manganese  $\text{Mn}^{3+}$ . Apart from soda and alumina levels, this type corresponds to the typical Rom Mn glass.

### Roman mixed antimony-manganese decolorized glass (Rom Sb-Mn)

Only two samples (ASK-G81 and ASK-G82b) correspond to this widespread group from the 1<sup>st</sup> to 3<sup>rd</sup> centuries. Presence of manganese and antimony above the detection limits ( $>0.025$  and  $>0.03\%$ ) is the marker of this group. While manganese concentrations of ASK-G81 and ASK-G82b are 0.04% and 1.4%, antimony concentrations are 4451 and 8818 ppm. Rom Sb-Mn glass group is composed by mixing two distinct glass groups, which is decolorized by manganese and antimony separately. Therefore, the base glass components such as soda (12.07%), alumina (0.63%), and manganese (0.72%) levels are also in between the antimony decolorized and manganese decolorized glass groups. Pb levels above 100 ppm (310 and 810 ppm) also verifies the recycling process. Phosphorus concentrations being higher than both Rom-Sb and Rom-Mn groups is an indication of ash-related contamination for staying longer in the furnace environment. Moreover, the iron levels are higher than the two groups, which probably occurs due to contamination from the furnace wall (Freestone, 2008).

### High Iron Manganese Titanium- HIMT (?)

HIMT glass, which spread by the 4th century AD onwards, shows elevated levels of iron ( $> 0.7\%$ ), manganese ( $\sim 1-2\%$ ) and titanium ( $> 0.1\%$ ), at the same time it has high soda ( $>18\%$ ), high magnesia ( $>0.8\%$ ) and low lime ( $\sim 6\%$ ) values (Freestone 1994). HIMT glass has subgroups such as HIMT1 (strong HIMT) and HIMT2 (weak HIMT), the levels of iron, manganese, and titanium of HIMT1, which is higher than HIMT2 glass (Foster and Jackson, 2009). The widely distributed weak HIMT in the 6th and 7th centuries throughout the Empire is similar to Foy's "Group 2" (Foy et al., 2000). In addition to these, the glass with only high iron-manganese-titanium content is not considered HIMT glass unless there is a correlation between Mn, Ti, Zr, and Fe.

This group, which includes the great majority of the samples (41) of Side, resembles the weak HIMT group with its high titanium (0.17%), iron (1.12%), manganese (1.29

wt.%) and low alumina (0.99%) content. Compared to other glass groups, it has the highest Sr (620 ppm) and Zr (98 ppm- except the outlier with 256 ppm) levels.

Interestingly, the scatterplot of  $\text{TiO}_2$  vs Zr, and  $\text{TiO}_2$  vs  $\text{Fe}_2\text{O}_3$  shows strong correlation for the Side glass assemblage (Figure 4.23). However, when a graph is plotted solely by HIMT group, the same correlation does not occur for  $\text{TiO}_2$  vs Zr and  $\text{TiO}_2$  vs  $\text{Fe}_2\text{O}_3$  (Figure 4.24; Figure 4.25). As well, Mn and Fe do not correlate with each other (Figure 4.26). Thus, so-called HIMT2 group does not meet the entire criteria. Moreover, Ceglia et al. (2015) introduce the term HLIMIT glass to the literature as a subgroup to HIMT glass, similar to weak HIMT with the exception of high lime content. Gliozzo and his counterparts present similar glass types to Ceglia's HLIMIT glass, which is signifies as CaO-rich, and CaO-rich/NaO-poor glass. To understand the resemblances between these glass groups, we compared these three samples.  $\text{Fe}_2\text{O}_3/\text{TiO}_2$  versus  $\text{Fe}_2\text{O}_3/\text{Al}_2\text{O}_3$  graph in Figure 4.27 is useful to differentiate compositional groups (Ceglia et al., 2015). Side samples did not follow the same slope of Ceglia's Cypriot samples and Gliozzo et al's Herdonia samples due to different alumina ratios.

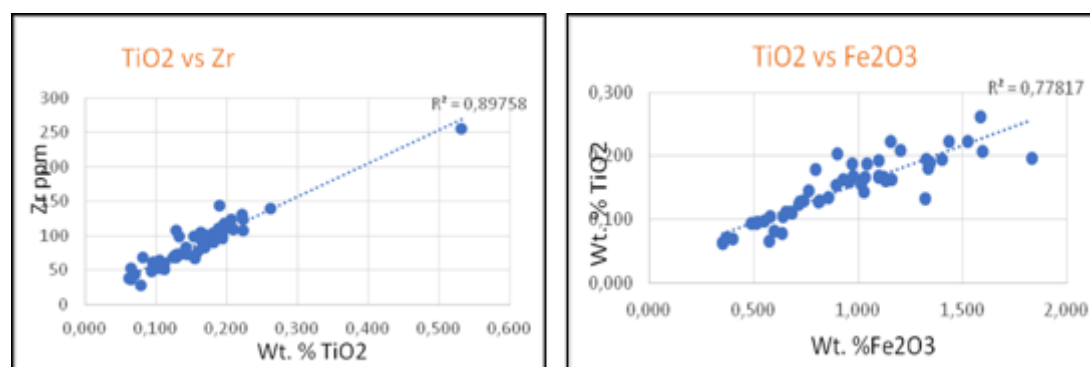


Figure 4. 23. (a) Scatter graph of Zr vs.  $\text{TiO}_2$  for Side assemblage; (b) Scatter graph of  $\text{Fe}_2\text{O}_3$  vs.  $\text{TiO}_2$  for Side assemblage

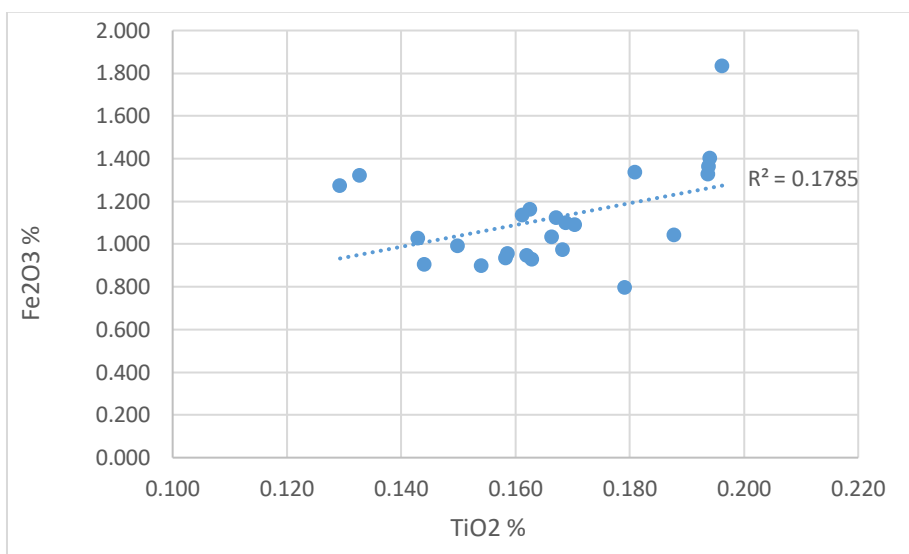


Figure 4. 24. Scatter graph showing Fe<sub>2</sub>O<sub>3</sub> vs TiO<sub>2</sub> concentrations for Side HIMT(?) glasses

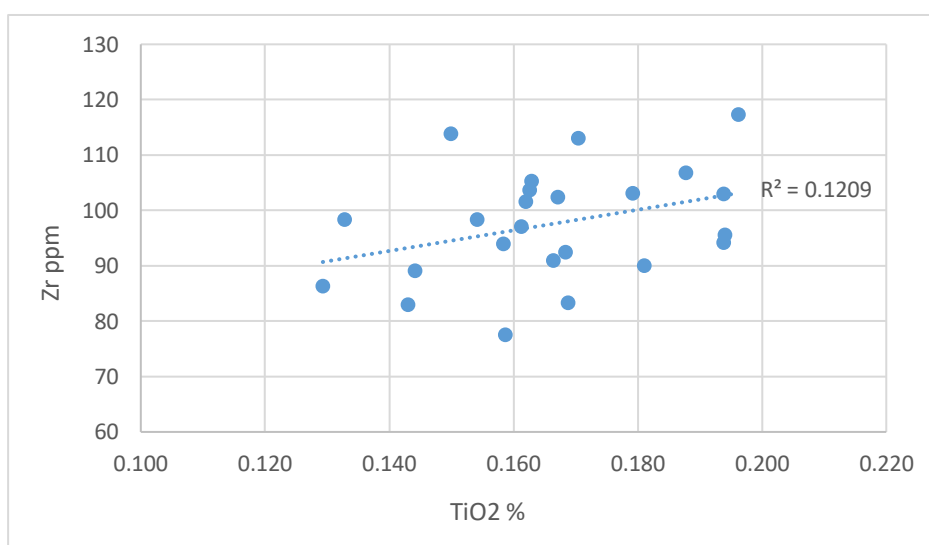


Figure 4. 25. Scatter graph showing Zr vs. TiO<sub>2</sub> concentrations for Side HIMT(?) glasses

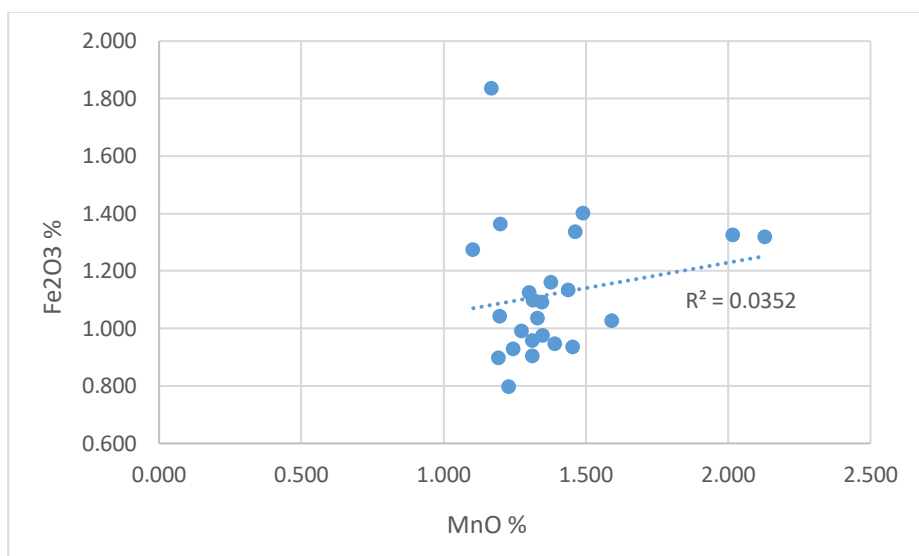


Figure 4. 26. Scatter graph showing Fe<sub>2</sub>O<sub>3</sub> vs MnO concentrations for Side HIMT(?) glasses

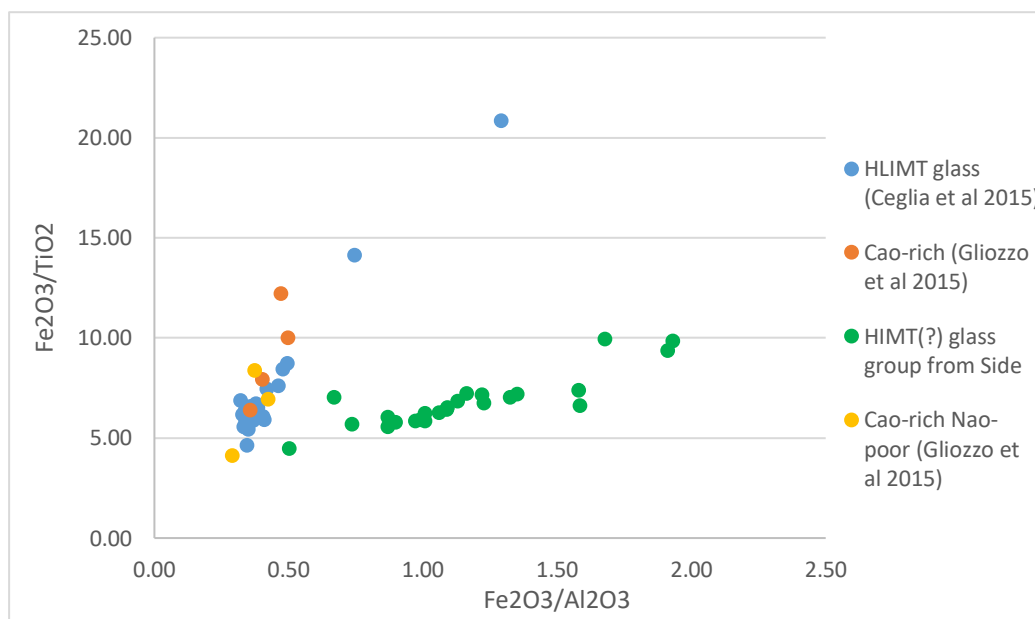


Figure 4. 27. Scatter graph showing Fe<sub>2</sub>O<sub>3</sub>/TiO<sub>2</sub> vs. Fe<sub>2</sub>O<sub>3</sub>/Al<sub>2</sub>O<sub>3</sub> concentration for Side HIMT(?) glasses with HLIMIT glass samples of Ceglia et al, 2015; Cao-rich HIMT and Cao-rich/NaO-poor HIMT glass samples from Gliozzo et al, 2015

Pergamon assemblage presents a sample with a similar composition to HIMT(?) glass group. Whether these glasses were produced in similar regions or not can be investigated through the trace elements. Gliozzo's available trace element data of the CaO-rich and CaO-rich/NaO-poor glass groups together with the Pergamon weak HIMT sample are plotted after the values are normalized to the average continental crust. Figure 4.28 shows that while Pergamon and Gliozzo's samples show similar patterns, HIMT(?) glass from Side has slightly elevated levels of trace elements.

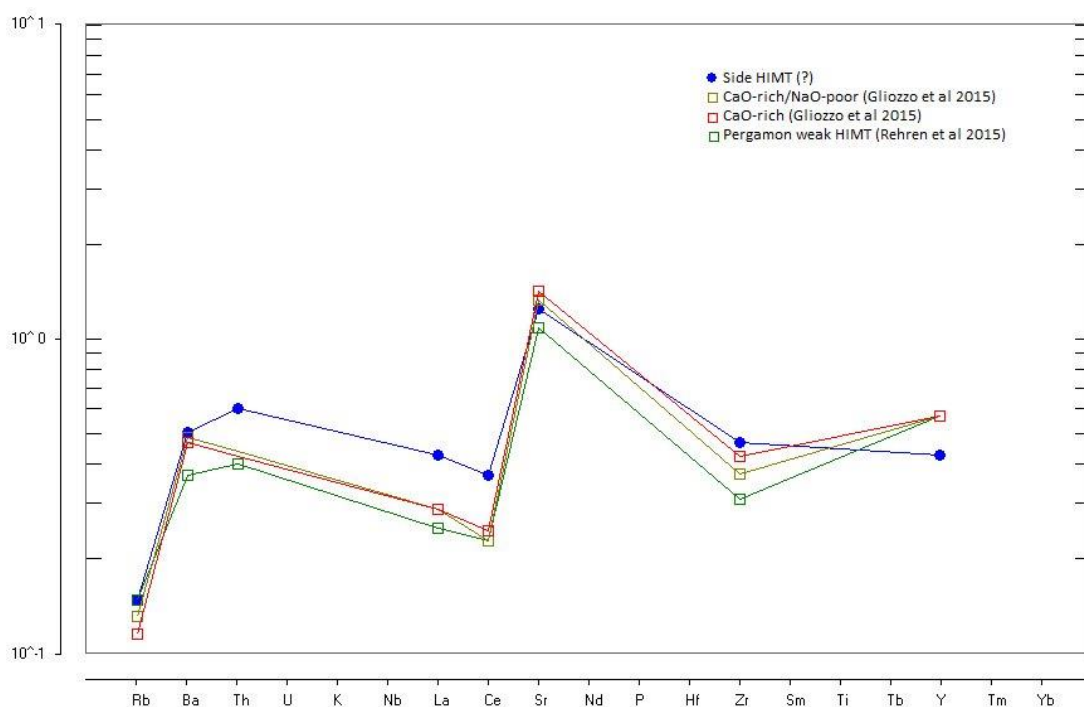


Figure 4.28. Spider diagram showing the trace elements of High CaO HIMT glass samples from Side, Pergamon, and Herdonia

Figure 4.29 presents a scatter graph demonstrating ratios between TiO<sub>2</sub> and Al<sub>2</sub>O<sub>3</sub> with Al<sub>2</sub>O<sub>3</sub> and SiO<sub>2</sub> of variant HIMT samples from Anatolia, such as Sagalassos, Boğazköy-Hattusa, and Pergamon, together with other archaeological sites from Europe and Egypt. Since SiO<sub>2</sub>, Al<sub>2</sub>O<sub>3</sub> and TiO<sub>2</sub> concentrations represent quartz, feldspar and heavy mineral contents respectively, this graph is particularly powerful

in distinguishing production groups. According to the graph, Side HIMT(?) group is pronouncedly dissociated from other glass samples, meaning that Side cannot be associated with any of the HIMT groups.

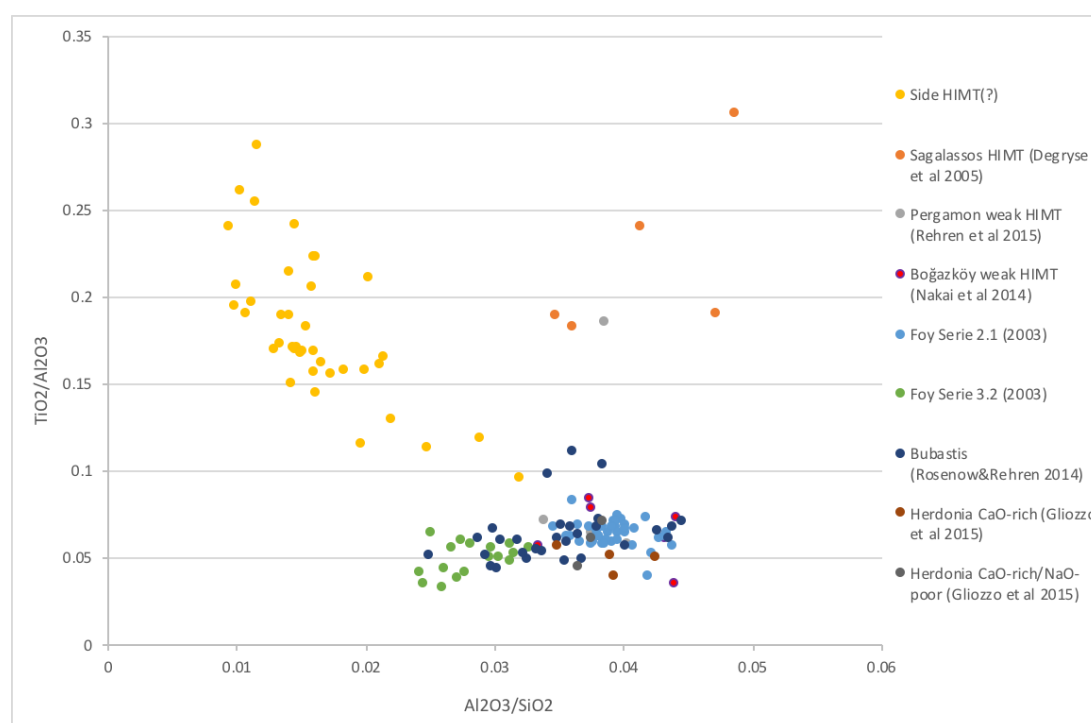


Figure 4.29. The scatter diagram of variant HIMT glass group samples from Anatolia, Europe, and Egypt showing  $TiO_2/Al_2O_3$  vs.  $Al_2O_3/SiO_2$

### Levantine I

Levantine glass, which was produced in the 6th and 7th centuries, is characterized by high lime (~9%), high alumina (~3%) and low soda (~15%), titanium and iron levels (Freestone et al., 2000). The second largest Side glass group (31 samples) resembles the Levantine1 group with its high lime (8.5 wt.%), low titanium (<0.1 wt.%), and low iron (~0.5 wt.%) content. Soda content is extremely low at ~11%, this marginal level is only seen in Freestone's (2000) Bet Eli'ezer assemblage, a further comparison is

presented below. Compared to the other groups (except the outlier), Levantine I glass has marginally the highest concentrations of alumina (1.03%) and the lowest concentrations of titanium (0.09%) and zirconium (58 ppm). This occurs because the feldspar content is richer in its glass-making sand and therefore, the heavy elements such as zirconium and titanium are lower.

The comparison of Levantine glass groups from various Anatolian sites, such as Ephesus, Pergamon, Aphrodisias, Sagalassos, and Boğazköy-Hattusa, is demonstrated in Figure 4.30, which shows  $TiO_2/Al_2O_3$  versus  $Al_2O_3/SiO_2$ , a useful graph for separating glass groups. The Side-Levantine I glass group has similar results only with the samples from Pergamon (Rehren et al, 2015) and Aphrodisias (Brill, 1999). To understand whether these glass groups are made in similar production regions, a spider diagram of the trace elements is needed. However, trace elemental data is not available for the mentioned sites, except Pergamon.

The available trace element data from the primary production sites such as Apollonia and Bet Eli'ezer (current Israel), and a secondary production site, Pergamon (current İzmir) were plotted with a spider diagram after the data were normalized according to the average continental crust (Figure 4.31). The diagram exposes that while the Levantine glass sample from Pergamon and the primary glass from the Levant show close elemental concentrations, Levantine I glass from Side follows a separated line from the other glass groups, which is probably suggesting different production sites.

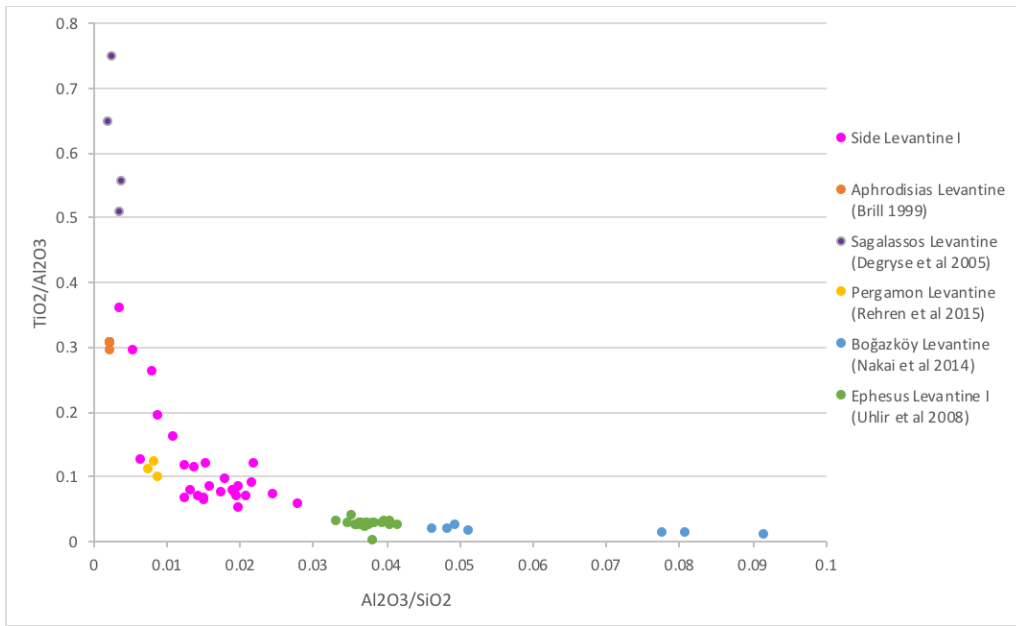


Figure 4.30. The scatter diagram of Levantine glass group samples from various Anatolian sites showing  $TiO_2/Al_2O_3$  vs.  $Al_2O_3/SiO_2$

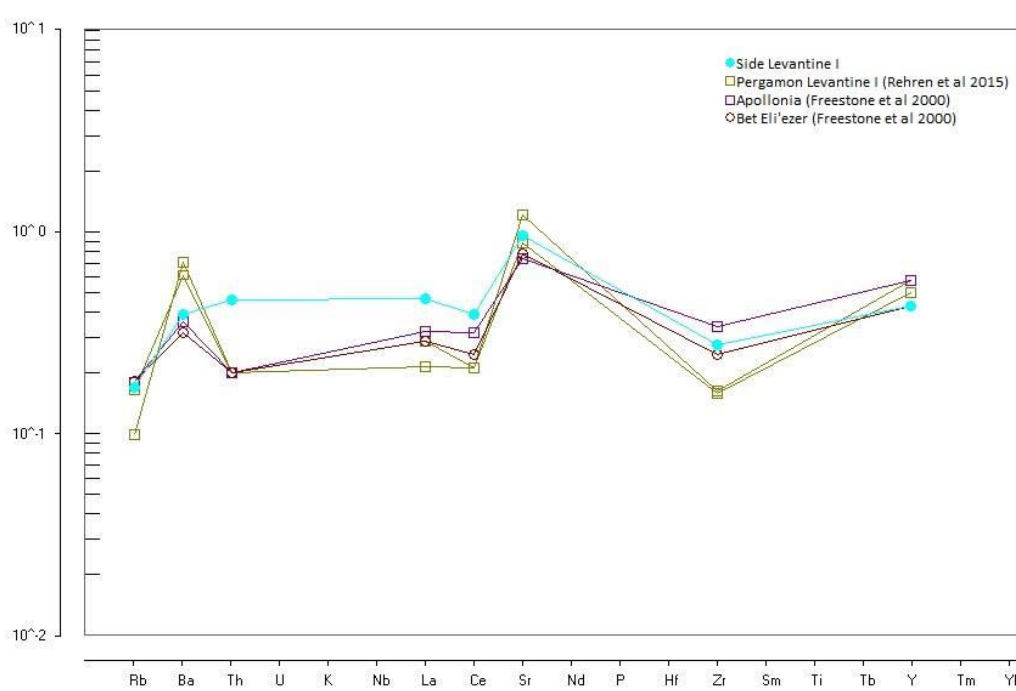


Figure 4.31. The spider diagram showing the trace elements of Levantine glass from Side, Pergamon, Apollonia and Bet Eli'ezer

### High lime glasses (High CaO)

Only three samples emerge in this group. Since the loss on ignition values are remarkably high, commenting on the concentration of this group would not be reliable. However, three samples outstand with their significantly high CaO levels. The average lime concentration is 15.69% which shows the highest values (except ASK-G52c) among Side glass.

### The outlier

ASK-G52c is the sole representative of lead glass with 8.4%. While scarcely any soda (0.08%) content is detected, lime and alumina levels present the highest value (21.9% - 6.38%) in the assemblage. The silica concentration is the lowest value with 48 percent. The alumina levels above %3 do not fit the standards of Roman glass (Freestone, 2008). The extraordinarily high concentration of alumina and extremely low concentration of chlorine (10 ppm) make us think that this specimen is not contemporary with the assemblage. Most likely, it was made in the later periods.

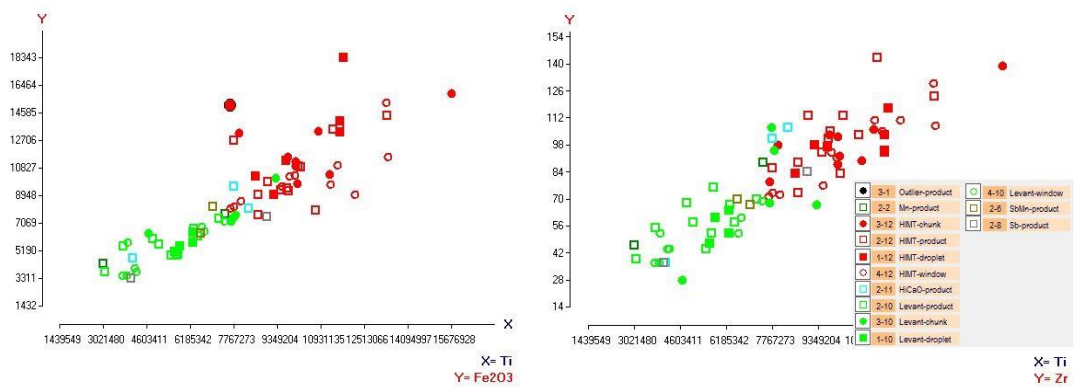


Figure 4.32. (a) Scatter graph showing TiO<sub>2</sub> vs. Fe<sub>2</sub>O<sub>3</sub> for Side glass  
(b) Scatter graph showing TiO<sub>2</sub> vs. Zr for Side glass

The graph (Figure 4.32a-b) that plots  $\text{TiO}_2$  vs.  $\text{Fe}_2\text{O}_3$  and  $\text{TiO}_2$  vs. Zr can demonstrate the differences in silica sources (the outlier is not plotted). Highest values come from HIMT(?) group. Other glass groups do not show any significant clustering. The graphs prove that HIMT(?) and Levantine groups of the Side glass are apparently made from distinct silica sources. As mentioned before, the lower values of the heavy elements can be explained by the comparatively higher feldspar content of Levantine glass.

The trace elements of seven glass groups are demonstrated in the spider diagram (Figure 4.33). It suggests different production regions for every glass group. Except for the outlier, the most distinctive one is the High-CaO group with the highest thorium level.

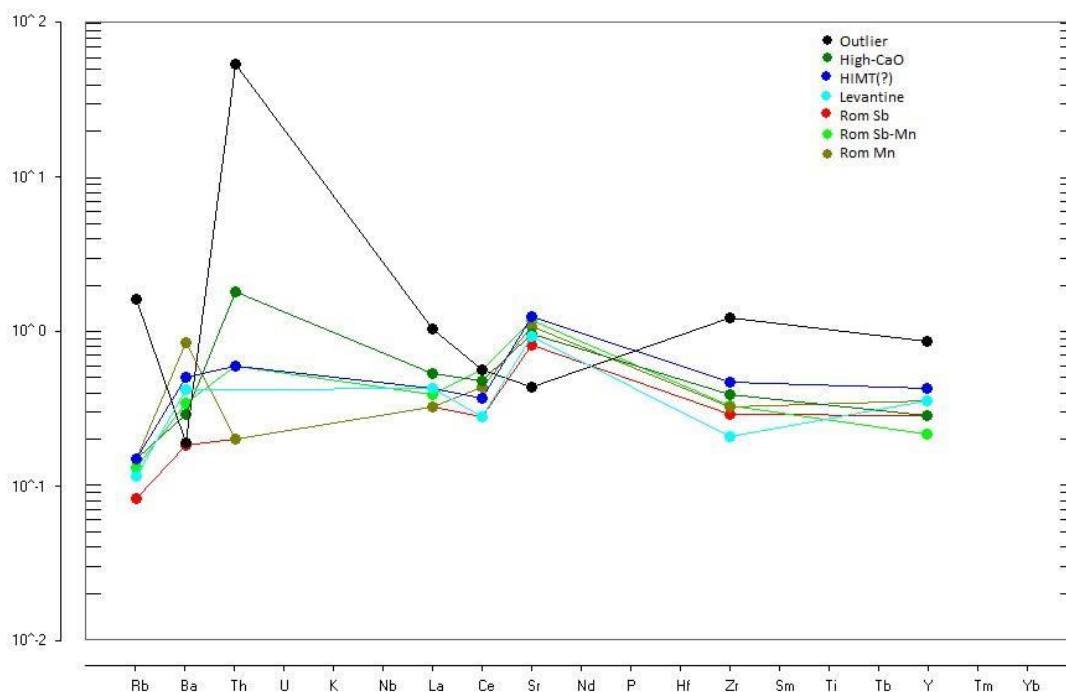


Figure 4.33. Spider diagram showing the trace elements of seven glass groups from Side

#### 1.4. Petrographic Thin-Section Optical Microscopy Analysis

9 clay fragments from the furnaces and crucibles were analyzed by thin section optical microscopy. Petrographic properties of the samples were investigated in terms of rock and mineral contents (Table 4.1). The samples were exposed to heat between 600-900 °C. Two samples (ASK-G88b and ASK-G29) have relatively low temperature values at about 600°C. As mentioned before, Side assemblage contain spilled glass adhered to ground pieces occurred during shaping, such as ASK-G88b and ASK-G29. These clay samples were not exposed to high temperatures at the furnace as in the other samples, but were exposed to the heat of the molten glass, which explains the relatively low heat values.

The structural porosity ratio of the crucibles varies between 3-8%. The mineral and rock structure of the crucibles indicate the origin of the raw materials. Ancient site Side and nearby regions have conglomerate and lime stone rock formation. However, minerals and rock fragment contents of the crucibles showed the volcanic type rock formation, so, the crucibles might be prepared by using clay material which were provided from long distance. Therefore, we can conclude that the crucibles were used on purpose for glass production. The selection of volcanic based rock fragments for clay of the crucibles might be chosen on purpose for exposing to high temperatures.

*Table 4-1 The table showing the porosity, endured temperature, rock and mineral types and the origin of the rocks of the clay samples*

Sample	T (°C)	P (%)	Rocks ve Minerals*	Rock Origin
ASK-B1 ASK-G25b	>900	8	Q,Ch,Pl	Granite
ASK-G4	<800		Q,Ch,Pl,C,Op	Andesite
ASK-G88b	~600	6	Q,Ch,Pl,C,By,Op	Schist
ASK-G29	~600	5	Q,Ch,Pl,By,Op,Sr	Andesite
ASK-G84 ASK-G86a ASK-G90 ASK-G92	>900	3	Q,Ks,Op	Shist (kaoline-illite)

Additionally, according to PED-XRF results (Table B.9), the average value of SiO<sub>2</sub>, CaO, Al<sub>2</sub>O<sub>3</sub>, Fe<sub>2</sub>O<sub>3</sub>, Na<sub>2</sub>O, and MgO of the crucible and kiln fragments is respectively 46.11%, 16.17%, 5.96%, 4.11%, 2.94% and 1.83%. SiO<sub>2</sub>, Na<sub>2</sub>O and Al<sub>2</sub>O<sub>3</sub> contents are high while Fe<sub>2</sub>O<sub>3</sub> concentration is near to the standard values of clay samples. SiO<sub>2</sub> and Al<sub>2</sub>O<sub>3</sub> are representative for the origin of clay, however, the high values of SiO<sub>2</sub> and Al<sub>2</sub>O<sub>3</sub> regarding to the clay content indicate the connections of the samples with glass production, which supports the petrographic analysis.

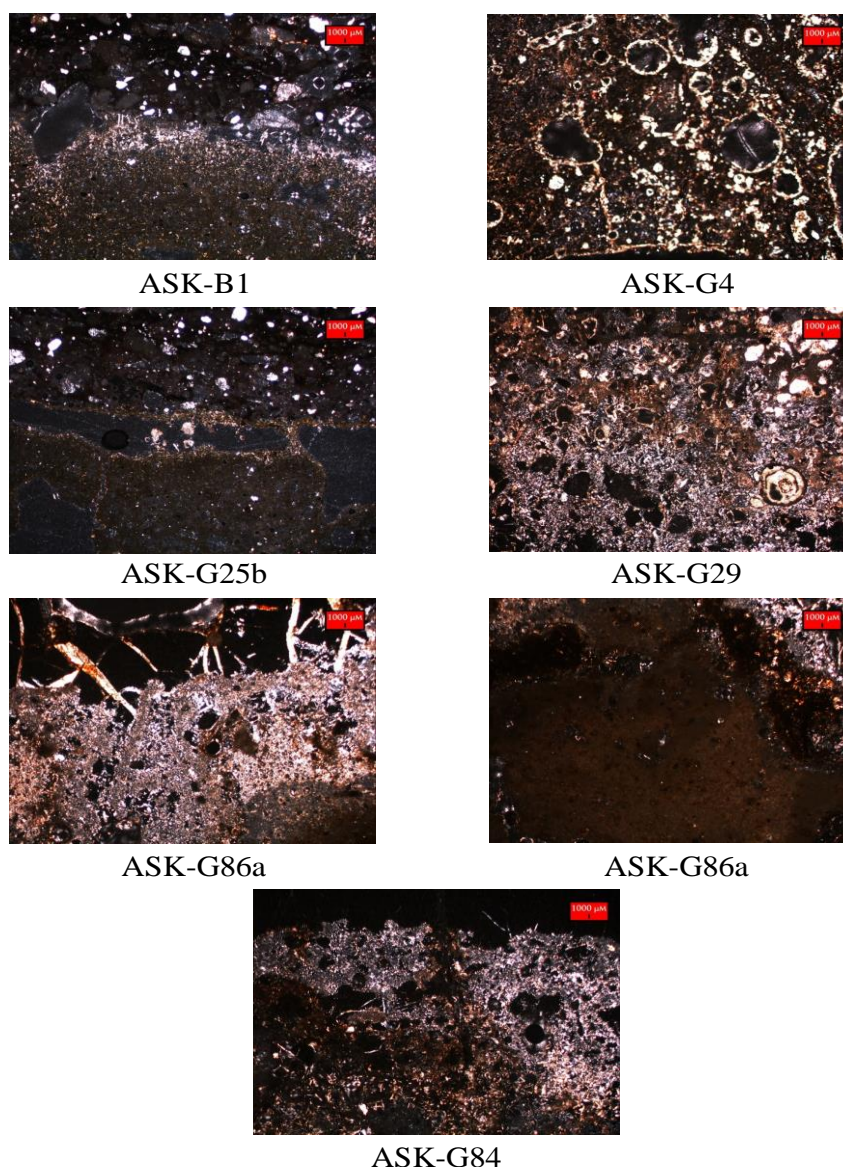


Figure 4.34. Thin section optical microscope photographs of the clay samples

## CHAPTER 6

### CONCLUSION

The investigation of Side glass assemblage was conducted on visual, chemical and petrographic bases. According to the results of the analyses, Side Early Byzantine glass workshop, which was operating between the 4<sup>th</sup> and 7<sup>th</sup> centuries BC, mainly produced glass in compliance with the standards of the period. It is essential to determine the production type of glass workshop.

Visual and optical microscope analyses show that a great majority of the Side glass samples were highly or moderately weathered. Dulling, iridescence, black discoloration, and milky surfaces are the deterioration types which were detected in most of the samples. Optical microscope photographs reveal the seedy structure of Side assemblage, with an exception of few bubble-free samples. The thickness measurements and the bubble shapes reflect that a great number of Side assemblage was shaped by glass blowing as expected from the general trends of the Late Antique period. Although Side assemblage has a wide range of colors, they were generally in blue-green or yellow-green shades, which were the dominant colors of the Late antique glass originating from the primary production centers of Egypt and Levant region.

The petrographic thin section analysis shows that the crucible and furnace fragments were deliberately chosen to endure high temperatures. The volcanic rocks that were used in the crucibles of Side might have brought from distant places since Side and the nearby sites have conglomerate and lime stone rock formation.

The PED-XRF results show that Side assemblage was a soda-lime-silica glass with a homogenous composition, except the outlier sample, ASK-G52c. As it can be understood from the low magnesia and potash levels (both below 1.5 wt.%), Side

glasses were fluxed with natron instead of plant ash. The absence of a correlation between CaO and MgO suggests that the lime source of Side assemblage was the shell fragments naturally occurred in the sand, instead of dolomite. Strontium and zirconium levels reveal that Side assemblage was produced with nautical sand. Although Side glass is a natron-fluxed, soda-lime-silica glass, which is compatible with the period, soda, silica, and alumina levels are lower than expected. While this situation mostly arises from the glass deterioration, the low alumina levels can be explained by the selection of a purer sand source. Also, the glass blowing technique needs lower soda inclusion compared to the casting method.

The main colorants were iron, copper, manganese, and vanadium. According to the graphical correlations, bronze was the source of copper and skutterudite was the source of cobalt. On the other hand, manganese was used as the main decolorant deriving from pyrolusite. The deliberate addition of manganese was detected for the great majority of the Side glass set. Only four samples have been found to include a stronger decolorant, antimony. The used decolorants did not sustain utterly colorless glass due to high iron content which is above 1 wt%. When the 25 colorless or naturally colored glass samples were investigated to understand the recycling conditions, it is been observed that only 8 of them were subjected to recycling.

According to the prevailing aspect of the production models in 1<sup>st</sup> millennium AD, glass that was produced in the great tanks of the primary production centers was shipped to the secondary production centers to be shaped and colored. To understand whether Side glass fits this concept or not, the glass groups were identified with the help of hierarchical cluster analysis. 7 different glass groups were identified; Roman antimony-decolorized, Roman manganese-decolorized, Roman mixed antimony-manganese decolorized, HIMT(?), Levantine II, high lime, and lead glass (ASK-G52c- the outlier). Only four samples were found matching to the Roman Sb and Roman mixed Sb-Mn groups. The great majority of the Side assemblage was classified under HIMT(?) and Levantine I groups.

While Rom Sb, Rom Mn, and Rom Sb-Mn groups fit well to the compositional standards of the period -except the soda and alumina contents-, the classification of the HIMT(?) glass group is a bit problematic. In general, HIMT glass is an Egyptian-origin, widespread Late Antique group, which is recognized with its high iron, manganese, and titanium contents. The HIMT(?) group of Side corresponds most of the standards with its high Fe, Mn and Ti levels. However, it does not meet the correlation criteria between Zr, Ti and Fe required to be HIMT glass. The HIMT group has normally low calcium content, yet the CaO level of Side-HIMT samples was higher than the common HIMT. Although few are encountered, similar glass groups have been identified in the literature. When the high CaO-HIMT samples of Side were compared with its contemporaries from Anatolia and other regions, Side samples fall in a separate glass group. Likewise, similar comparisons were also conducted on the Levantine I glass, which were also dissociated from its contemporaries.

According to Freestone, the Late Antique glass that came to Anatolia was solely made in primary production workshops like the ones in Levant or Egypt, since the size of the kilns and crucibles were quite small to melt glass in Asia Minor. Thus, when we consider the size of its furnace, Side can be regarded as a secondary production site. Although the provenance of Side glass is a bit ambiguous, the great majority of the samples might have come both from Levant and Egypt to be shaped in the secondary glass workshop of Side.

Since boron is a key element for the Asia Minor, further chemical analyses which enable the detection of boron will be helpful for tracing the roots of glass. However, provenance studies are absolutely necessary to understand whether these glasses were produced locally or not. In terms of eliminating the confusion about the provenance of the glass groups, Sr isotope analysis is highly useful to detect the origin of the raw materials.



## REFERENCES

Al-Bashaireh, K., Al-Mustafa, S., Freestone, I. & al-Housan, A. (2016). Composition of Byzantine glasses from Umm el-Jimal, northeast Jordan: Insights into glass origins and recycling. *Journal of Cultural Heritage*. 21. 10.1016/j.culher.2016.04.008.

Akyol, A. A., Gençler G. Ç., Kadioğlu Y. K. & Demirci, Ş. (2008). *Elaiussa-Sebaste Cam Örnekleri Arkeometrik Çalışmalar*. In: T.C. Kültür ve Turizm Bakanlığı, Kültür Varlıkları ve Müzeler Genel Müdürlüğü, 30. Uluslararası Kazı, Araştırma ve Arkeometri Sempozyumu, 24. Arkeometri Sonuçları Toplantısı. Ankara, Türkiye. (T.C. Kültür ve Turizm Bakanlığı Yayın No: 3173 / Kültür Varlıkları ve Müzeler Genel Müdürlüğü Yayın No: 132) 13-28.

Amstock, J. S. (1997). *Handbook of Glass in Construction*. New York: McGraw-Hill.

Arrian. (1999). *Anabasis of Alexander*. Cambridge: Harvard University Press.

Bach, H. & Krause, D. (2010). *Analysis of the composition and structure of glass and glass ceramics*. Berlin: Springer.

Biek, L. & Bayley, J. (1979). Glass and other vitreous materials. *World Archaeology*, 11(1), 1-25. doi:10.1080/00438243.1979.9979746

Bimson, M. & Freestone, I.C. (1985). Discovery of an Islamic Glass-making Site in Middle Egypt (Ashmunein; Bimson and Freestone 1985). *Annales 10e Congres De l'Association Internationale Pour l'Histoire Du Verre*.

Brems, D. & Degryse, P. (2014). Western Mediterranean sands for ancient glass making. In Degryse P. (Ed.), *Glass Making in the Greco-Roman World: Results of the ARCHGLASS project* (pp. 27-50). Leuven (Belgium): Leuven University Press. Retrieved from <http://www.jstor.org/stable/j.ctv2bctjr.7>

Brill, R. H. (1999). *Chemical Analyses of Early Glasses*. Corning (Nueva York): Corning Museum of Glass.

Brill, R. H. (1988). "Scientific Investigations of the Jalame Glass and Related Finds." *Excavations at Jalame: Site of a Glass Factory in Late Roman Palestine*, by Gladys Davidson. Weinberg, Univ. of Missouri Press, pp. 257–294.

Brill, R. H. (2001). *The Glassmakers of Firozabad and the Glassmakers of Kapadwanj: Two Pilot Video Projects*. *Annales Du 15e Congrès De L'Association Internationale Pour L'Histoire Du Verre*. New York: Corning, 267-268.

Brun, N., Mazerolles, L & Pernot, M. (1991). Microstructure of Opaque Red Glass Containing Copper. *Journal of Materials Science Letters*. 10. 1418-1420. 10.1007/BF00735696.

Bosch, C. E. (1957). *Pamphylia Tarihine Dair Tetkikler*. Ankara: Türk Tarih Kurumu Basımevi.

Ceglia, A., Cosyns, P., Nys, K., Terryn, H., Thienpont, H. & Meulebroeck, W. (2015). Late antique glass distribution and consumption in Cyprus: A chemical study. *Journal of Archaeological Science*. 61. 10.1016/j.jas.2015.06.009.

Cholakova, A. & Rehren, T. (2018). A Late Antique Manganese Decolourised Glass Composition: Interpreting patterns and Mechanisms of Distribution. In *Things That Traveled: Mediterranean Glass in the First Millennium CE*. London: UCL Press.

Cosyns, P., Janssens, K., Van der Linden, V. & Schalm, O. (2006). Black glass in the Roman empire: a work in progress. *Interregional Comparisons and Recent Finds, International Colloquium, 13th May 2005*. 1. 30-41.

Çakmaklı, Ö. D. (2014). Roman and Byzantine Glass Workshops in Caria An Assessment of New Finds and Evidence. *Anadolu (Anatolia)*, (40), 131-141. doi:10.1501/Andl\_0000000416

Dardeniz, G. (2016). Glassmaking and/or glassworking: Revisiting scientific and archaeological evidence from the Late Bronze Age Anatolia [Cam üretmek ve/veya Cam işlemek: Anadolu'da Geç Tunç Çağı verilerinin bilimsel ve arkeolojik olarak gözden geçirilmesi]. *Arkeometri Sonuçları Toplantısı*. 31.

Davison, S. (2003). *Conservation and restoration of glass* (2nd ed.). Oxford: Butterworth-Heinemann.

Degryse, P. (2014). Glass making in the Greco-Roman world: Results of the ARCHGLASS project. Leuven, Belgium: Leuven University Press.

Degryse, P. & Poblome, J. (2002). The implications of the use of nepheline for the glass of Roman Sagalassos. In G. Kordas (Ed.), *Hyalos vitrum glass, history, technology and conservation of glass and vitreous materials in the Hellenistic world* (pp. 349-352). Athens: Glasnet Publications.

Degryse, P. & Schneider, J. (2008). Pliny the Elder and Sr-Nd isotopes: Tracing the provenance of raw materials for Roman glass production. *Journal of Archaeological Science*, 35(7), 1993-2000.

Degryse, P., Schneider, J., Poblome, J., Waelkens, M., Haack, U., & Muchez, P. (2005). A geochemical study of Roman to early Byzantine Glass from Sagalassos, South-west Turkey. *Journal of Archaeological Science*, 32(2), 287-299. doi:10.1016/j.jas.2004.09.006

Degryse, P., Scott, R. B., & Brems, D. (2014). The archaeometry of ancient glassmaking: Reconstructing ancient technology and the trade of raw materials. *Perspective*, (2), 224-238. doi:10.4000/perspective.5617

Farnsworth, M., & Ritchie, P. D. (1938). *Spectrographic studies on ancient glass*. Cambridge, MA: William Hayes Fogg Art Museum, Harvard Univ.

Fleming, S & Swann, C. (1999). Roman mosaic glass: a study of production processes, using PIXE spectrometry. *Nuclear Instruments & Methods in Physics Research*

Section B-beam Interactions With Materials and Atoms - NUCL INSTRUM METH PHYS RES B. 150. 622-627. 10.1016/S0168-583X(98)00928-8.

Foy, D., Vichy, M. & Picon, M. (2000). Lingots de verre en Méditerranée occidentale. *Annales Du 14e Congrès De L'Association Pour L'Histoire Du Verre*. 51-57.

Foy, D., Picon, M., Vichy, M. & Thirion-Merle, V. (2003) Caractérisation des verres de la fin de l'Antiquité en Méditerranée occidentale: l'émergence de nouveaux courants commerciaux. In D. Foy and M.-D. Nenna (eds.), *Échanges et commerce du verre dans le monde antique*. Monographies Instrumentum 24, 41–85. Montagnac, Monique Mergoil.

Foster, H. E. & Jackson, C. M. (2009) The composition of 'naturally coloured' late Roman vessel glass from Britain and the implications for models of glass production and supply. *Journal of Archaeological Science* 36, 189–204.

Foster, H. & Jackson, C. (2010). The composition of late Romano-British colourless vessel glass: Glass production and consumption. *Journal of Archaeological Science*. 37. 3068-3080. 10.1016/j.jas.2010.07.007.

Freestone, I. C. (2003). Primary glass sources in the mid-first millenium AD. In *Annales du 15e Congrès de l'Association Internationale pour l'Histoire du Verre*, 111–115. Nottingham, Association Internationale pour l'Histoire du Verre.

Freestone, I. C. (1994) Appendix: Chemical analysis of 'raw' glass fragments. In: Hurst, H.R. (Ed.), *Excavations at Carthage, Vol. II, 1. The Circular Harbour, North Side. The Site and Finds other than Pottery*. British Academy Monographs in Archaeology, No. 4. Oxford University Press, Oxford, pp. 290.

Freestone, I. C. (2004). The Provenance of Ancient Glass through Compositional Analysis. *MRS Proceedings*. 852. 10.1557/PROC-852-OO8.1.

Freestone, I. C. (2006). Glass production in late Antiquity and the early Islamic period. A geochemical perspective. In M. Magetti and B. Messiga (eds.) *Geomaterials in*

*Cultural Heritage*. Geological Society Special Publications 257, 201–216. London, Geological Society.

Freestone, I. C. (2015). The Recycling and Reuse of Roman Glass: Analytical Approaches. *Journal of Glass Studies*, 57, 29-40. Retrieved from <http://www.jstor.org/stable/24726946>

Freestone, I. C., Bimson, M. & Buckton, D. (1990). Compositional categories of Byzantine glass tesserae. *Annales of the 11th Congress of the AIHV, Bâle, August 29-September 3 1988*. 271-281.

Freestone, I. C., Degryse, P., Lankton, J., Gratuze, B., & Schneider, J. (2018). HIMT, glass composition and commodity branding in the primary glass industry. In Rosenow D., Phelps M., Meek A., & Freestone I. (Eds.), *Things that Travelled: Mediterranean Glass in the First Millennium AD* (pp. 159-190). London: UCL Press. Retrieved from <http://www.jstor.org/stable/j.ctt21c4tb3.14>

Freestone, I. C., Gorin-Rosen, Y., Greenwood, R. (2002). Byzantine and early Islamic glassmaking in the Eastern Mediterranean: production and distribution of primary glass. (with R Greenwood and Y Gorin-Rosen). Freestone I C, Greenwood R and Gorin-Rosen Y (2002) Byzantine and Early Islamic Glassmaking in the Eastern Mediterranean: Production and Distribution of Primary Glass. in G. Kordas ( Ed) *Hyalos - Vitrum - Glass*. Athens , 167-174.

Freestone I. C., Gorin-Rosen Y., Hughes M. J. (2000). Primary glass from Israel and the production of glass in late antiquity and the Early Islamic period. In: Nenna M-D (ed) *La route du verre. Ateliers primaires et secondaires du second millénaire av. J.C. au Moyen Âge*. Maison de l'Orient Méditerranéen-Jean Pouilloux, Lyon, pp. 65–83

Freestone, I. C., Wolf, S., & Thirlwall, M. (2005). The production of HIMT glass: Elemental and isotopic evidence. *Annales Du 16e Congrès De L'Association Internationale Pour L'Histoire Du Verre (Corning, New York, 2001)*, 153-157.

Gliozzo, Elisabetta & Turchiano, Maria & Giannetti, F & Santagostino Barbone, A. (2015). Late Antique Glass Vessels and Production Indicators from the Town of

Herdonia (Foggia, Italy): New Data on CaO-Rich/Weak HIMT Glass. *Archaeometry*. n/a-n/a. 10.1111/arc.12219.

Goffer, Z. (2007). *Sand: Glass, Glaze, and Enamel*. In *Archaeological Chemistry*, Z. Goffer (Ed.). doi:10.1002/9780471915256.ch3

Gorin-Rosen, Y. (2000). The ancient glass industry in Israel: Summary of the finds and new discoveries. *La Route du Verre*. 49-64.

Gratuze, B. & Barrandon, J. (1990). Islamic Glass Weights and Stamps: Analysis Using Nuclear Techniques. *Archaeometry*, 32: 155-162. Doi:10.1111/J.1475-4754.1990.Tb00462.X

Harden, D. B., (1959) New Light on Roman and Early Medieval Window Glass, *Glastechnische Berichte*, Vol. VIII, 9-16.

Henderson, J. (1988). Electron probe microanalysis of mixed-alkali glass. *Archaeometry*. 30. 77 - 91. 10.1111/j.1475-4754.1988.tb00436.x.

Henderson, J. (1989). *Scientific analysis in Archaeology and its interpretation*. Oxford: Oxford University Committee for Archaeology.

Henderson, J. (1991). Industrial specialization in late Iron Age Britain and Europe. *Archaeological Journal*, 148(1), 104-148. doi:10.1080/00665983.1991.11021373

Henderson, J. (1995) Le Verre de Dorestad: continuité technologique ou innovation? In D. Foy (ed.) *Le Verre de l'Antiquité Tardive et du Haut Moyen Age*. Typologie-Chronologie-Diffusion, 51-56. Guiry-en-Vexin, Musée archéologique départemental du Val-d'Oise.

Henderson J. (1996). Scientific analysis of selected Fishbourne vessel glass and its archaeological interpretation. In: Cunliffe B., Down A. and Rudkin D. (Eds) *Excavations at Fishbourne 1969-1988*, Chester Excavations 9, 189-92.

Henderson, J. (2007). *The science and archaeology of materials: an investigation of inorganic materials*. London: Routledge.

Henderson, J. (2013). *Ancient glass: an interdisciplinary exploration*. New York: Cambridge University Press.

Henderson, J. (2013b). *Glass and Faience*. In *The Oxford Handbook of the European Bronze Age* (pp. 492-501). Oxford, UK: Oxford University Press. doi:10.1093/oxfordhb/9780199572861.013.0027

Hodges, H. (1992). *Technology in the ancient world*, New York: Barnes and Noble, 2nd edition.

Jackson, C. M. (1996) From Roman to early medieval glasses. Many happy returns or a new birth? In *Annales du 13e Congrès de l'Association Internationale pour l'Histoire du Verre*, 289–301. Lochem, Association Internationale pour l'Histoire du Verre.

Jackson, C. M. (2005). Making Colourless Glass. In *The Roman Period\**. *Archaeometry*, 47(4), 763-780. doi:10.1111/j.1475-4754.2005.00231.x

Jackson, C., & Foster, H. (2014). The last Roman glass in Britain: Recycling at the periphery of the empire. In *Neighbours and Successors of Rome*(pp. 6-14). Oxford, United Kingdom: Oxbow Books.

Jackson, C. M., Paynter, S., Nenna, M., & Degryse, P. (2016). Glassmaking using natron from el-Barnugi (Egypt); Pliny and the Roman glass industry. *Archaeological and Anthropological Sciences*. doi:10.1007/s12520-016-0447-4

Jackson, C. M. & Paynter, S. (2016). A great big melting pot: exploring patterns of glass supply, consumption and recycling in Roman Coppergate, York. *Archaeometry*. doi:10.1111/arcm.12158

Kaczmarczyk, A. (1986). The source of cobalt in ancient Egyptian pigments. In Proceedings of the 24th International Symposium on Archaeometry (pp. 369-376). DC: Smithsonian Institution Press.

Kato, N., Nakai, I., & Shindo, Y. (2009). Change in chemical composition of early Islamic glass excavated in Raya, Sinai Peninsula, Egypt: On-site analyses using a portable X-ray fluorescence spectrometer. *Journal of Archaeological Science*, 36(8), 1698-1707. doi:10.1016/j.jas.2009.03.020

Keller, D., Price, J., & Jackson, C. M. (2014). *Neighbours and successors of Rome: Traditions of glass production and use in Europe and the Middle East in the later 1st millennium AD*. Oxford: Oxbow Books.

Kerr, P.F. (1977) *Optical Mineralogy*, McGraw-Hill Co. First Ed'n., New York.

Kramar, U. (1999). X-Ray Fluorescence Spectrometers. In J. C. Lindon (Ed.), *Encyclopedia of Spectroscopy and Spectrometry* (pp. 2467-2477). Elsevier. doi:10.1006/rwsp.2000.0336

Lambert, J. B. (1998). *Traces of the past: unraveling the secrets of archaeology through chemistry*. Cambridge (Mass.): Perseus.

Lindon, J. C., Tranter, G. E., & Holmes, J. L. (2000). *Encyclopedia of spectroscopy and spectrometry*. San Diego, CA: Academic Press.

Liritzis, I., & Stevenson, C. M. (2012). *Obsidian and ancient manufactured glasses*. Albuquerque: University of New Mexico Press.

Mansel, A. M. (1978). *Side: 1947-1966 yılları kazıları ve araştırmalarının sonuçları*. Ankara: Türk Tarih Kurumu Basımevi.

Mansel, A. M. (1967). *Side Kılavuzu*. Ankara: Türk Tarih Kurumu Basımevi.

Meckel L. et al. (1999) The Chemical Analysis of Glasses, Glass Ceramics, and Related Materials. In: Bach H., Krause D. (eds) Analysis of the Composition and Structure of Glass and Glass Ceramics. Schott Series on Glass and Glass Ceramics (Science, Technology, and Applications). Springer, Berlin, Heidelberg

Mirti, P., Casoli, A. & Appolonia, L. (1993), Scientific Analysis Of Roman Glass From Augusta Praetoria. *Archaeometry*, 35: 225-240. Doi:10.1111/J.1475-4754.1993.Tb01037.X

Mirti, P., Davit, P., Gulmini, M., & Sagui, L. (2001). Glass Fragments from the Crypta Balbi in Rome: The Composition of Eighth-century Fragments. *Archaeometry*, 43(4), 491-502. doi:10.1111/1475-4754.00032

Nakai, I & Matsuzaki, M & Daichi, Sawamura & Abe, Yoshinari & Schachner, A. (2014). Chemical characterization of Roman and early Byzantine glass from bołazköy/hattuša and its vicinity. *Istanbuler Mitteilungen*. 64. 237-261.

Nenna, M.-D & Vichy, Michèle & Picon, Maurice. (1997). L'atelier de verrier de Lyon, du Ier siècle après J.-C. et l'origine des verres "Romains". *Revue d'Archéométrie*. 21. 81-87. 10.3406/arsci.1997.949.

Newton, R. & Davison, S. (1989). Conservation of glass (1st ed). Butterworths, London; Boston

Ohno, Y. (2007). Spectral Color Measurement. In *Colorimetry*, J. Schanda (Ed.). doi:10.1002/9780470175637.ch5

Özgümüş, Ü. (2000). *Anadolu Camcılığı*. İstanbul: Pera Yayıncılık ve Kitapçılık.

Paynter, S. (2006). Analyses of colourless Roman glass from Binchester, County Durham. *Journal of Archaeological Science*. 33. 1037-1057. 10.1016/j.jas.2005.10.024.

Paynter, S. (2008). Experiments in the Reconstruction of Roman Wood-Fired Glassworking Furnaces: Waste Products and Their Formation Processes. *Journal of Glass Studies*, 50, 271-290. Retrieved June 7, 2018.

Peltenburg, E. J. (1987) Early Faience: Recent Studies, Origins and Relations with Glass. British Museum.

Pollard, A. M. (1979), X-Rays Fluorescence and Surface Studies of Glass with Application to the Durability of Medieval Window Glass, Ph.D. thesis, Univ. York.

Pollard, A. M., & Heron, C. (2008). The Chemistry, Corrosion and Provenance of Archaeological Glass. In *Archaeological Chemistry* (2nd ed., pp. 144-187). Cambridge, UK: The Royal Society of Chemistry.

Pusch, E. & Rehren, T. (2007). Hochtemperatur-Technologie in der Ramses-Stadt Rubinglas für den Pharao.

Rapp, G. (2002) *Archaeomineralogy*. Springer-Verlag, Berlin. Doi: 10.1007/978-1-4020-4409-0\_12.

Rehren, T. & Brüggler, M. (2015). Composition and production of late antique glass bowls type Helle. *Journal of Archaeological Science: Reports*. 3. 171-180. 10.1016/j.jasrep.2015.05.021.

Rehren, T. & Cholakova, A. (2010). The early Byzantine HIMT glass from Dichin, Northern Bulgaria / Ранновизантийско Стъкло тип НІМТ от Градището При С. Дичин. *Interdiscip. Stud.*. 22.

Rehren, T., & Freestone, I. C. (2015). Ancient glass: From kaleidoscope to crystal ball. *Journal of Archaeological Science*, 56, 233-241. doi:10.1016/j.jas.2015.02.021

Rehren, T., Connolly, P., Schibille, N., & Schwarzer, H. (2015). Changes in glass consumption in Pergamon (Turkey) from Hellenistic to late Byzantine and Islamic times. *Journal of Archaeological Science*, 55, 266-279. doi:10.1016/j.jas.2014.12.025

Rincon, J. M., & Romero, M. (1999). *Characterization Techniques of Glasses and Ceramics*. Berlin: Springer.

Rooksby, H. P. (1976). In Butcher, S. A. et al., Composition of the enamels on the brooches found at Nornour, Isles of Scilly, i963-7. Proc. Archaeometry Conf. (forthcoming)

Rosenow, D. & Rehren, T. (2014). Herding cats – Roman to Late Antique glass groups from Bubastis, northern Egypt. *Journal of Archaeological Science*. 49. 170–184. 10.1016/j.jas.2014.04.025.

Römich, H. (2006). Glass and Ceramics. In E. May & M. Jones (Eds.), *Conservation Science- Heritage Materials* (pp. 160-185). Dorset, UK: The Royal Society of Chemistry.

Santagostino B., Gliozzo, E., D'acapito, F., Memmi Turbanti, I., Turchiano, M. & Volpe, G. (2008), The Sectilia Panels Of Faragola (Ascoli Satriano, Southern Italy): A Multi-Analytical Study Of The Red, Orange And Yellow Glass Slabs. *Archaeometry*, 50: 451-473. Doi:10.1111/J.1475-4754.2007.00341.X

Sayre, E. V., & Smith, R. W. (1961). Compositional Categories of Ancient Glass. *Science*, 133(3467), 1824-1826. doi:10.1126/science.133.3467.1824

Sayre, E.V., & Smith, R.W. (1974). Analytical studies of ancient Egyptian glass (BNL--18562). United States.

Schibille, N., Marii, F. & Rehren, T. (2008). Characterization and provenance of Late Antique window glass from the Petra church in Jordan. *Archaeometry*. 50. 627 - 642. 10.1111/j.1475-4754.2007.00346.x.

Schibille N, Meek A, Tobias B, Entwistle C, Avisseau-Broustet M, et al. (2016) Comprehensive Chemical Characterisation of Byzantine Glass Weights. *PLOS ONE* 11(12): e0168289. <https://doi.org/10.1371/journal.pone.0168289>

Schibille, N., Sterrett-Krause, A. & Freestone, I. C. (2017). Glass groups, glass supply and recycling in Late Roman Carthage. *Archaeological and Anthropological Sciences*, 9, 1223-1241. 10.1007/s12520-016-0316-1.

Shortland, A. J. (2004). Evaporites Of The Wadi Natrun: Seasonal And Annual Variation And Its Implication For Ancient Exploitation. *Archaeometry*, 46: 497-516.  
D

Shortland, A. J. (2012). Lapis lazuli from the kiln: Glass and glassmaking in the late Bronze Age. Leuven: Leuven University Press.

Shugar, A. N. (2000). Byzantine Opaque Red Glass Tesserae From Beit Shean, Israel. *Archaeometry*, 42(2), 375–384. <https://doi.org/10.1111/J.1475-4754.2000.Tb00888.X>

Silvestri, A. (2008). The colourless glass of Iulia Felix. *Journal of Archaeological Science*, 35, 331-341.

Soykal- Alanyali, F. (n.d.). The urban change and transformation of the theater and its surroundings in the light of the side Dionysos (?) Temple. Olba, 24, 419–450. Retrieved from <http://0-search.ebscohost.com.library.metu.edu.tr/login.aspx?direct=true&AuthType=ip&db=edselc&AN=edselc.2-52.084976608652&site=eds-live>

Strabo (1917). *Geography*. Vol. I. Translated by Horace Leonard Jones. London: William Heinemann. p. xxv-xxvi..

Streli, C., Wobrauschek, P. & Kregsamer, P. (1999). X-Ray Fluorescence Spectroscopy, Applications. In J. C. Lindon (Ed.), *Encyclopedia of Spectroscopy and Spectrometry* (pp. 2467-2477). Elsevier. doi:10.1006/rwsp.2000.0336

Tal, O., Jackson-Tal, R. E., & Freestone, I. C. (2008). Glass from a Late Byzantine Secondary Workshop at Ramla (South), Israel. *Journal of Glass Studies*, 50, 81-95.

doi:[http://archaeology.tau.ac.il/arch\\_files/info/orens%20papers/jgs50\\_Tal-jacksontal-freestone.pdf](http://archaeology.tau.ac.il/arch_files/info/orens%20papers/jgs50_Tal-jacksontal-freestone.pdf)

Taştemür, E. (2018). Antik Cam Fırınları ve Anadolu Örnekleri. *TUBA-AR*, (22), 203-119. doi:10.22520/tubaar.2018.22.012

Tek, A. T. (2010). 2009 Yılı Side Tiyatrosu ve Çevresi Çalışmaları: Cam Çalışmaları (H. S. Alanyalı, Ed.). In 32. Kazı Sonuçları Toplantısı (Vol. 2, pp. 436-452). Ankara, Turkey: T.C. Kültür Ve Turizm Bakanlığı Kültür Varlıkları ve Müzeler Genel Müdürlüğü.

Tek, A. T. (2014). Side 2013 Yılı Kazı ve Araştırmaları: Cam Çalışmaları (H. S. Alanyalı, Ed.). In 36. Kazı Sonuçları Toplantısı (Vol. 1, pp. 273-298). Ankara, Turkey: T.C. Kültür Ve Turizm Bakanlığı Kültür Varlıkları ve Müzeler Genel Müdürlüğü.

Tite, M. (1987), Characterisation Of Early Vitreous Materials. *Archaeometry*, 29: 21-34. Doi:10.1111/J.1475-4754.1987.Tb00394.X

Turner, W. E. (1956). Studies in ancient glasses and glassmaking processes: Raw materials and melting processes. Place of publication not identified: Publisher not identified.

Uhlig, S. (1999) Recent Advances in X-Ray Fluorescence (XRF) Analysis. In: Rincon J.M., Romero M. (eds) *Characterization Techniques of Glasses and Ceramics*. Springer, Berlin, Heidelberg

Uhlig, K., Melcher, M., Czurda-Ruth, B., Schreiner, M., & Krinzinger, F. (2006). Scientific Investigations on Ancient Glasses from Hanghaus I in Ephesos/Turkey using SEM/EDX and  $\mu$ -XRF. *36th INTERNATIONAL SYMPOSIUM ON ARCHAEOMETRY*. Retrieved November 19, 2018.

Uhlig, K., Melcher, M., Schreiner, M., Czurda-Ruth, B. & Krinzinger, F. (2008). SEM/EDX and  $\mu$ -XRF investigations on ancient glass from Hanghaus 1 in Ephesos/Turkey. *Glass in Byzantium - Production, Usage, Analyses*.

Valentin, B. (2010). X-Ray Fluorescence (XRF) Analysis. In *Analysis of the Composition and Structure of Glass and Glass Ceramics*. Mainz: Springer.

Wadia, D. N. (1975). *Geology of India*. New Delhi: Tata McGraw-Hill.

Wainwright, I. N. M., Taylor, J. M. & Harley R.D. (1986), Lead antimoniate yellow, in Feller, R. (ed.), *Artists Pigments*, Cambridge Univ. Press, New York, pp. 219– 223.

Wedepohl, K. H., Simon, K., & Kronz, A. (2011). Data On 61 Chemical Elements For The Characterization Of Three Major Glass Compositions In Late Antiquity And The Middle Ages. *Archaeometry*, 53(1), 81-102. doi:10.1111/j.1475-4754.2010.00536.x

West, L. (1932). The Economic Collapse of the Roman Empire. *The Classical Journal*, 28(2), 96-106. Retrieved from <http://www.jstor.org/stable/3290252>

Wight, K. (2011). *Molten color glassmaking in antiquity*. Los Angeles: J. Paul Getty Museum.

Whitehouse, D. (2012). *Glass: A Short History*. Washington, DC: Smithsonian Books.

Zecchin, L. (1987). *Vetro e vetrai di Murano: Studi sulla storia del vetro*. Venezia: Arsenale Editrice.

## APPENDICES

### A. FIGURES

Figure A.1. Chunks

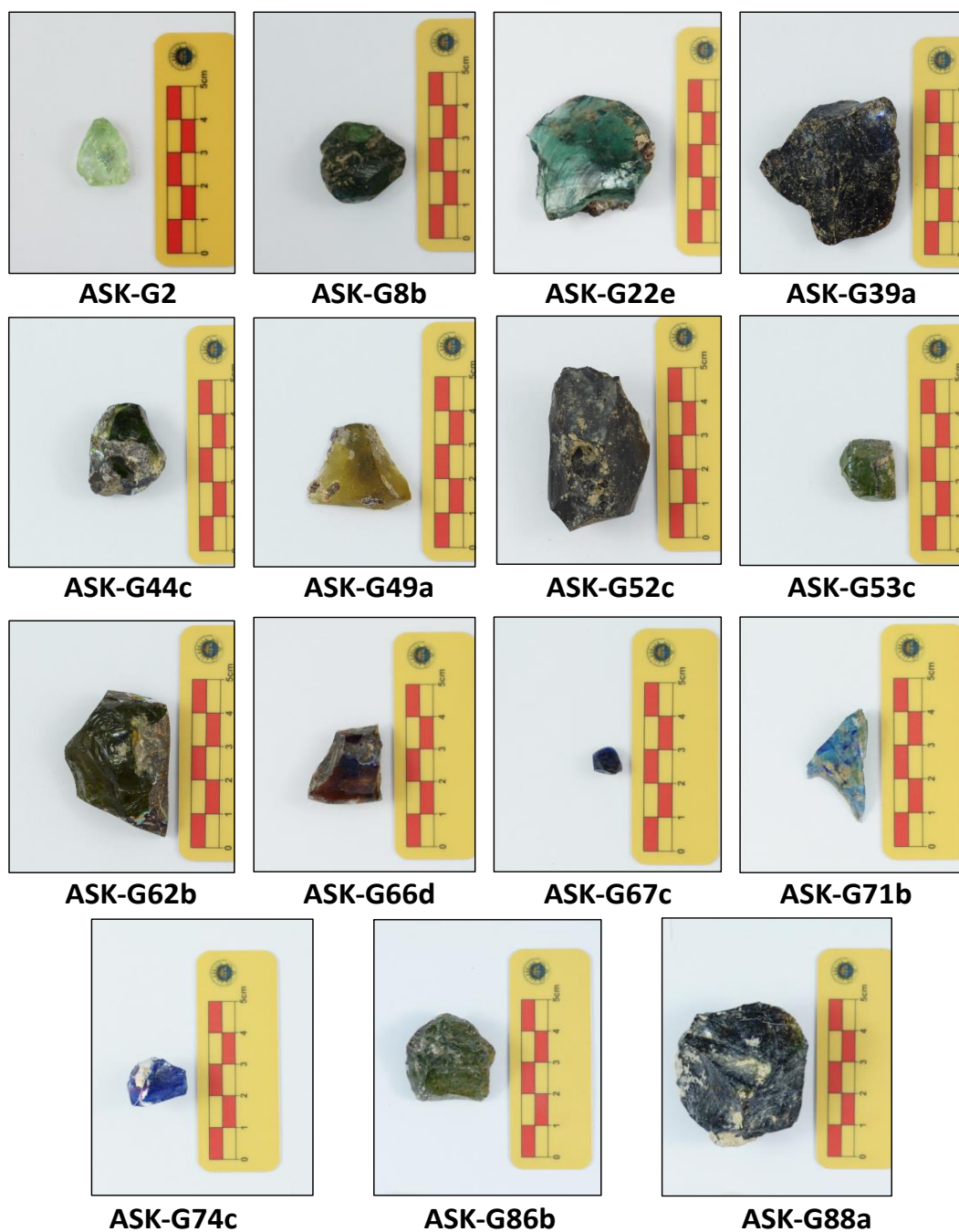


Figure A.2. Products



**ASK-G22a**



**ASK-G31c**



**ASK-G32**



**ASK-G37**



**ASK-G42**



**ASK-G44a**



**ASK-G50a**



**ASK-G50b**



**ASK-G50c**



**ASK-G51f**



**ASK-G52a**



**ASK-G54a**

Figure A.2. (continued) Products



**ASK-G55a**



**ASK-G59d**



**ASK-G60d**



**ASK-G62c**



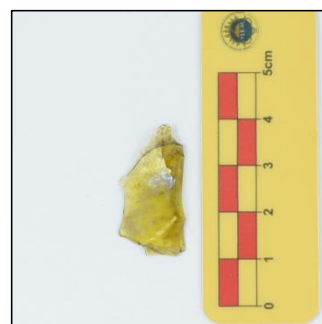
**ASK-G62d**



**ASK-G62e**



**ASK-G69a**



**ASK-G69b**



**ASK-G69c**



**ASK-G71a**

Figure A.2. (continued) Products



**ASK-G73**



**ASK-G75b**



**ASK-G77**



**ASK-G79b**



**ASK-G79c**



**ASK-G80a**



**ASK-G81**



**ASK-G82b**

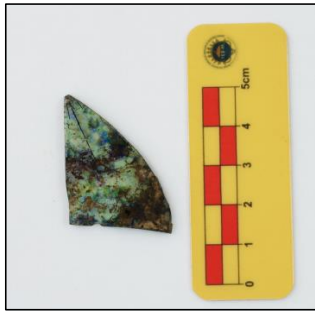


**ASK-G83a**



**ASK-G84**

Figure A.3. Window panes



**ASK-G6**



**ASK-G22c**



**ASK-G23a**



**ASK-G23c**



**ASK-G30**



**ASK-G36a**



**ASK-G40a**



**ASK-G40b**



**ASK-G41a**



**ASK-G41b**



**ASK-G45**



**ASK-G47**

Figure A.3. (continued) Window panes



**ASK-G52b**



**ASK-G62a**



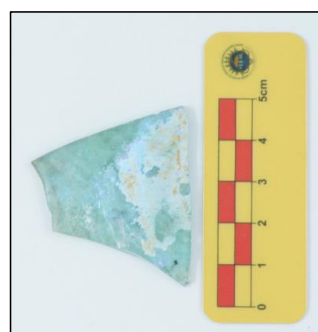
**ASK-G67a**



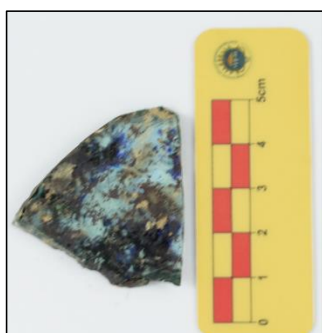
**ASK-G68**



**ASK-G74a**



**ASK-G74b**



**ASK-G75a**



**ASK-G93a**



**ASK-G93b**

Figure A.4. Droplets and Threads



**ASK-G51e**



**ASK-G55b**



**ASK-G57a**



**ASK-G57e**



**ASK-G58e**



**ASK-G59c**



**ASK-G60b**



**ASK-G60c**



**ASK-G72c**



**ASK-G72d**

Figure A.5. Kiln and crucible fragments



**ASK-G4**



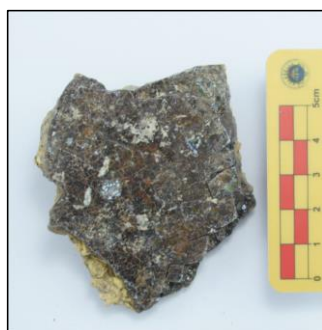
**ASK-G24**



**ASK-G25b1**



**ASK-G25b2**



**ASK-G86a**



**ASK-G88b**



**ASK-G90**

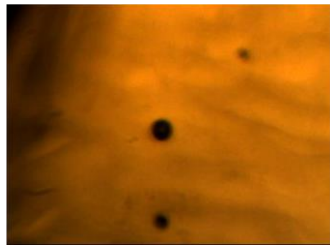


**ASK-G92**

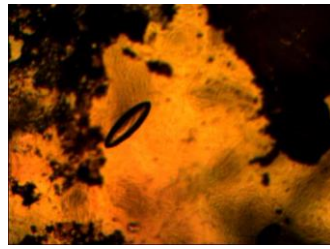


**ASK-B1**

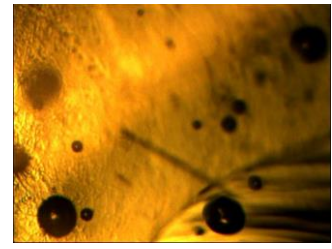
Figure A. 6. Optical Microscope Photographs of Side Samples



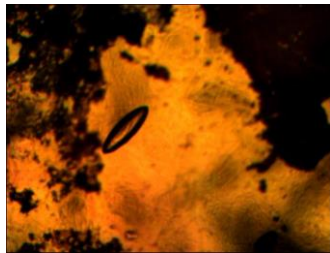
ASK-G2



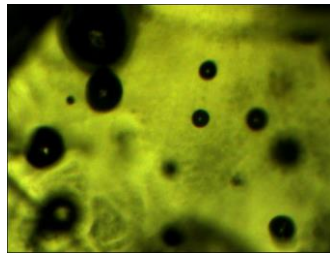
ASK-G6



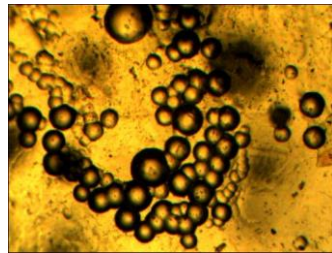
ASK-G8b



ASK-G22c



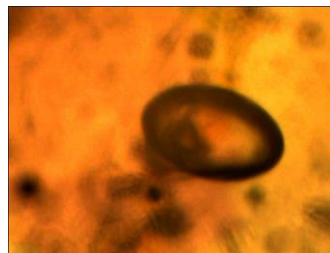
ASK-G22e



ASK-G23a



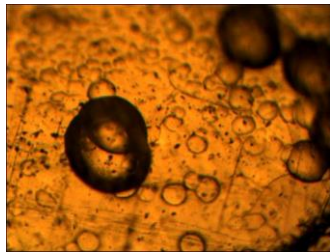
ASK-G23c



ASK-G30



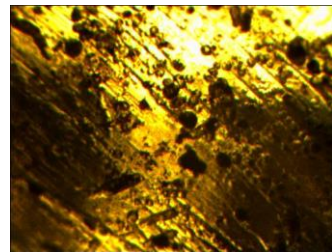
ASK-G31c



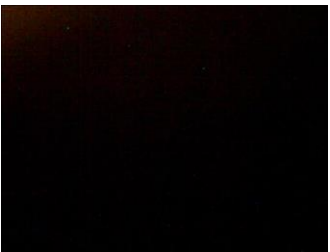
ASK-32



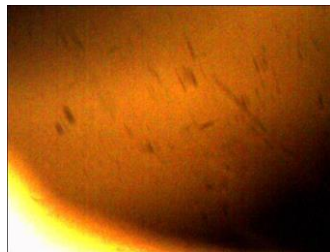
ASK-G36a



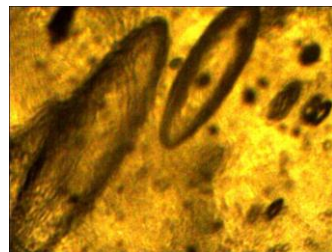
ASK-G37



ASK-G39a



ASK-G40a



ASK-G40b

Figure A. 6. (continued) Optical Microscope Photographs of Side Samples



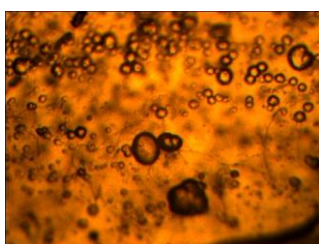
ASK-G41a



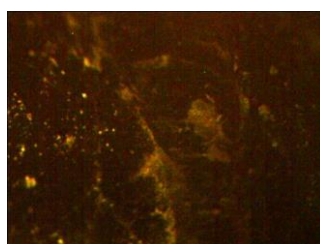
ASK-G41b



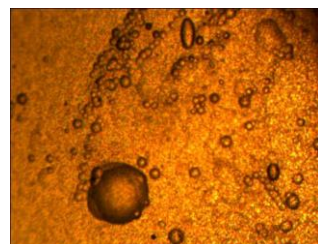
ASK-G42



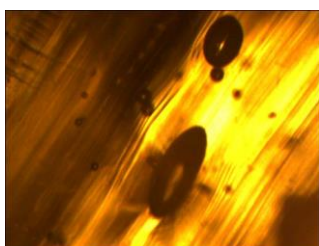
ASK-G44a



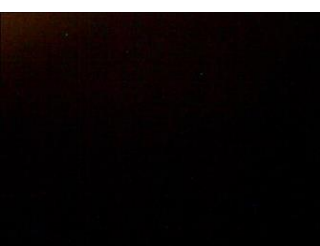
ASK-G44c



ASK-G45



ASK-G47



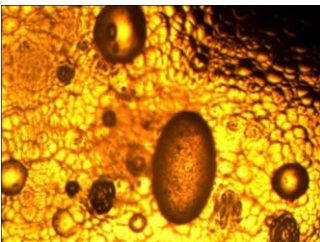
ASK-G49a



ASK-G50a



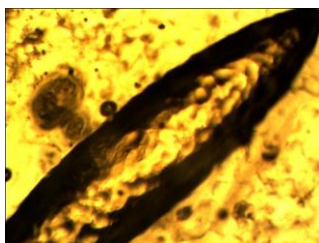
ASK-50b



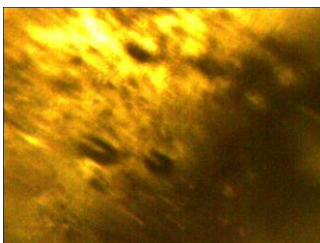
ASK-G50c



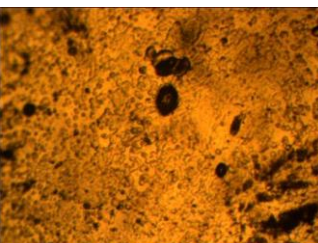
ASK-G51e



ASK-G51f

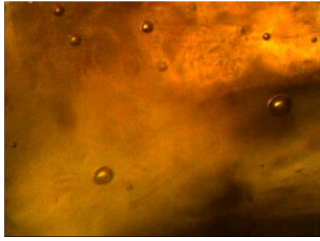


ASK-G52a

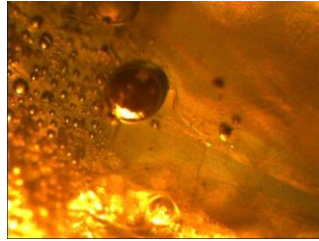


ASK-G52b

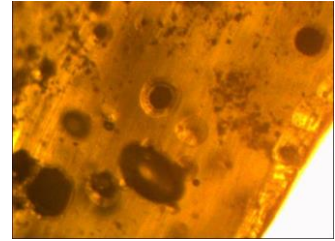
Figure A. 6. (continued) Optical Microscope Photographs of Side Samples



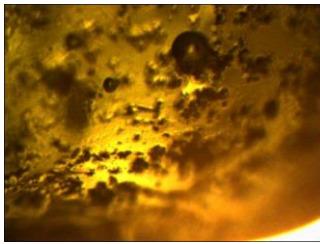
ASK-G53c



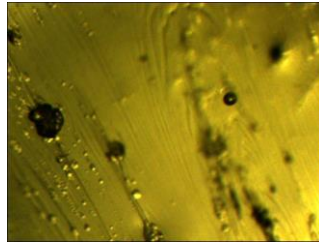
ASK-G54a



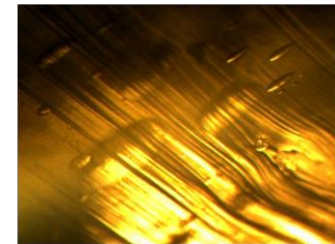
ASK-G55a



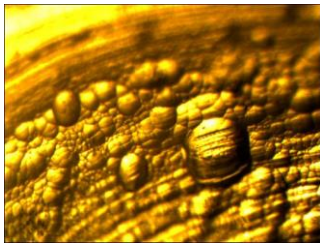
ASK-G55b



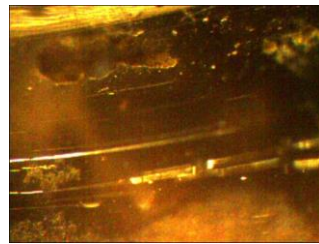
ASK-G57a



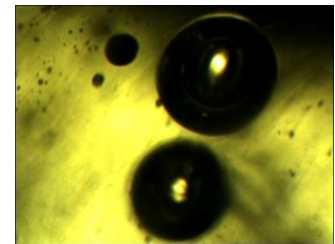
ASK-G57e



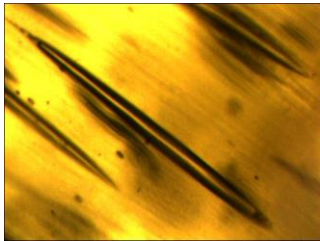
ASK-G58e



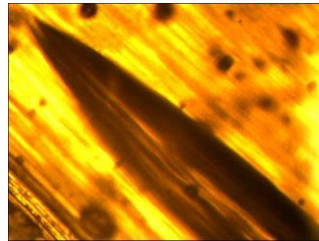
ASK-G59c



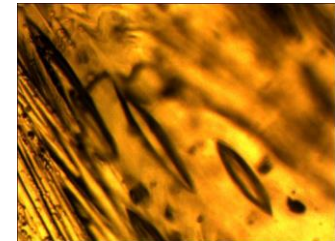
ASK-G59d



ASK-60b



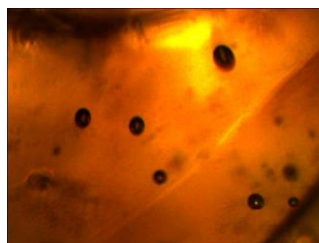
ASK-G60c



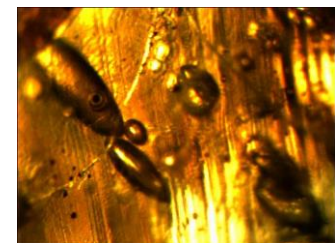
ASK-G60d



ASK-G62a



ASK-G62b

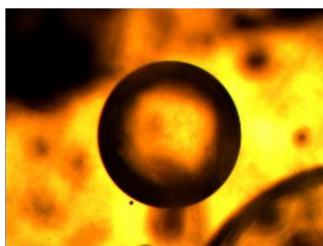


ASK-G62c

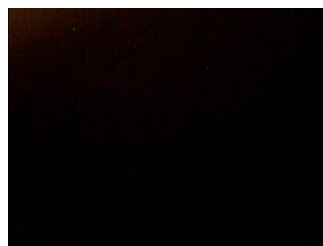
Figure A. 6. (continued) Optical Microscope Photographs of Side Samples



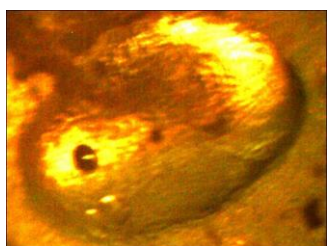
ASK-G62d



ASK-G62e



ASK-G67c



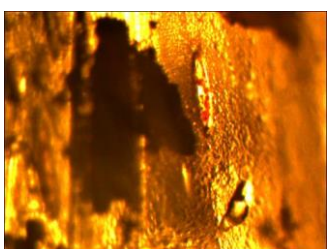
ASK-G69a



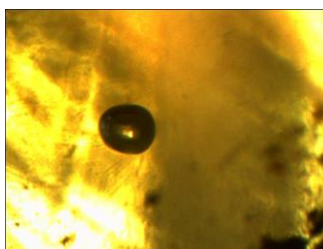
ASK-G69b



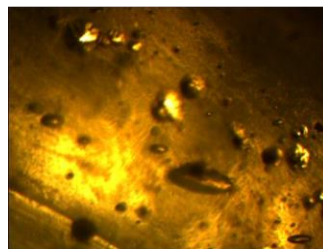
ASK-G69c



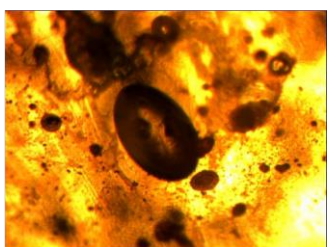
ASK-G71a



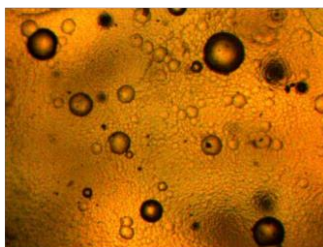
ASK-G71b



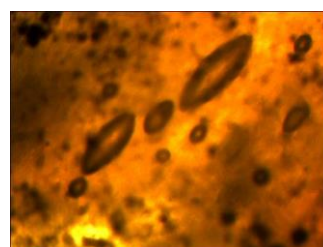
ASK-G72d



ASK-73



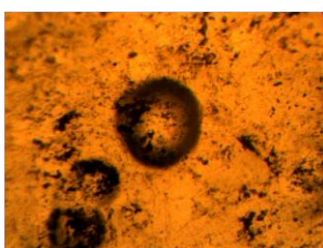
ASK-G74a



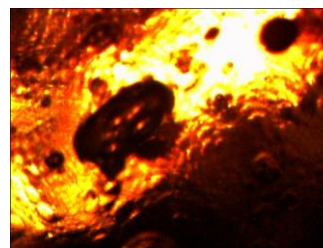
ASK-G74b



ASK-G75a

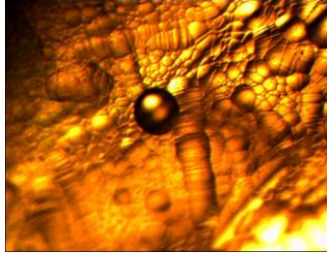


ASK-G75b



ASK-G77

Figure A. 6. (continued) Optical Microscope Photographs of Side Samples



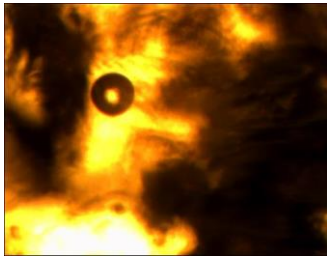
ASK-G79b



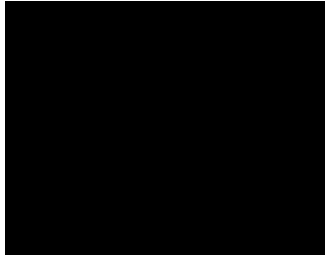
ASK-G79c



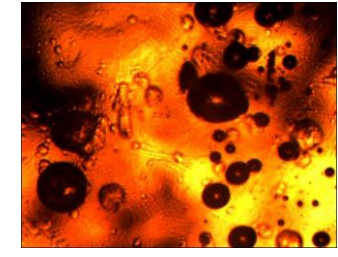
ASK-G80a



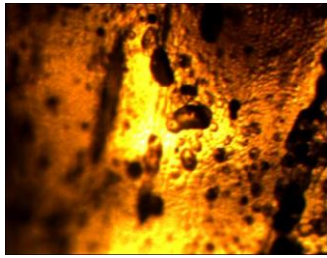
ASK-G81



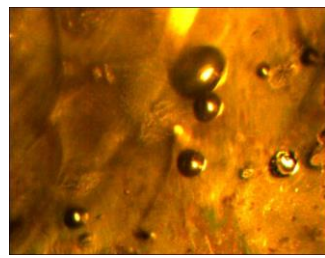
ASK-G82b



ASK-G83a



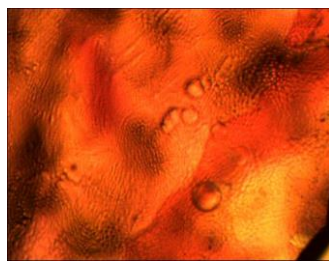
ASK-G84



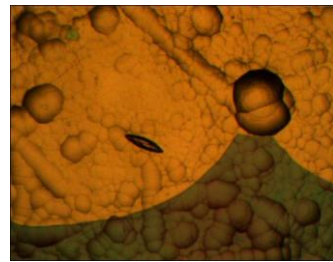
ASK-G86b



ASK-G88a



ASK-93a



ASK-G93b

## B. TABLES

Table B.1. The documentation of the Side sample set classified into groups

Sample No	Description	Region	Excavation Date	Depth	Sondage No	Batch No
ASK-G2	Chunk piece	Dionysus Temple	5.08.2009		3	K45
ASK-G8b	Chunk piece	Dionysus Temple	6.08.2009		3	K47
ASK-G22e	Chunk	Dionysus Temple	4.08.2009		3	K42
ASK-G39a	Chunk	Dionysus Temple	2012	12.19-11.38	2	K9
ASK-G44c	Chunk	Theatre	2009		2f	K60
ASK-G49a	Chunk piece	Theatre	9.08.2009	11.97-11.82	2e	K23
ASK-G52c	Chunk	Theatre	2009		2e	K72
ASK-G53c	Chunk piece	Theatre	11.08.2009	11.88-11.71	2e	K105
ASK-G62b	Chunk	Theatre	23.07.2009	13.08-12.72	2b	K4
ASK-G66d	Chunk piece	Theatre	2009		2d	K38
ASK-G67c	Small chunk piece	Theatre	2009		2d	K36
ASK-G71b	Small chunk piece	Theatre	1.07.1905		2d	K32
ASK-G74c	Small chunk piece	Theatre	2012		N	cleanup
ASK-G86b	Chunk piece	Theatre	2009	13.41-13.33	3b	K101
ASK-G88a	Chunk	Theatre	2009			depo
ASK-G22a	Vessel fragment	Dionysus Temple	4.08.2009		3	K42
ASK-G31c	Vessel body piece	Dionysus Temple	2010		8	K131
ASK-G32	Vessel fragment	Dionysus Temple	2010		8	K131
ASK-G37	Handle	Dionysus Temple	2010		SW corner	K62
ASK-G42a	Base fragment	APS	2013	6.54-6.10	1A	K4
ASK-G44a	Vessel fragment	Theatre	2009		2f	K60
ASK-G50a	Neck piece	Theatre	8.09.2009	12.41-12.33	2e	K89
ASK-G50b	Neck piece	Theatre	8.09.2009	12.41-12.33	2e	K89
ASK-G50c	Vessel fragment	Theatre	8.09.2009	12.41-12.33	2e	K89
ASK-G51f	Vessel fragment	Theatre	2009		2e	K75
ASK-G52a	Neck piece	Theatre	2009		2e	K72
ASK-G54a	Neck piece	Theatre	6.08.2009		2e	K82
ASK-G55a	Base piece	Theatre	9.08.2009	12.15-12.06	2e	K98
ASK-G59d	Oil-lamp piece	Theatre	8.08.2009	12.24-12.15	2e	K85
ASK-G60d	Rim piece	Theatre	5.08.2009		2e	K77
ASK-G62c	Vessel fragment	Theatre	23.07.2009	13.08-12.72	2b	K4
ASK-G62d	Vessel fragment	Theatre	23.07.2009	13.08-12.72	2b	K4
ASK-G62e	Vessel fragment	Theatre	23.07.2009	13.08-12.72	2b	K4
ASK-G69a	Handle piece	Theatre	2009		2d	K29
ASK-G69b	Vessel fragment	Theatre	2009		2d	K29
ASK-G69c	Base piece	Theatre	2009		2d	K29
ASK-G71a	Handle piece	Theatre	2009		2d	K32
ASK-G73	Base fragment	Theatre	2012		N	cleanup
ASK-G75b	Vessel fragment	N2	2012	3.29-3.02	4	K32
ASK-G77	Base fragment	N2	2012			K51
ASK-G79b	Base fragment	N2	2012	12.34-12.22	3a	K22
ASK-G79c	Base fragment	N2	2012	12.34-12.22	3a	K22
ASK-G80a	Vessel fragment	TT	2012		9	K10
ASK-G81	Vessel fragment	TT	2012		10	K66
ASK-G82b	Two colored vessel fragment	MZ	2012	12.22-12.66	3a1	K24
ASK-G83a	Base piece	MZ	2012	12.34-12.22	3a	K22
ASK-G84	Rim piece	MZ	2012	12.34-12.22	3a	K22

Table B.1 (continued)

Sample No	Description	Region	Excavation Date	Depth	Sondage No	Batch No
ASK-G6	Window pane	Dionysus Temple	1.07.2009	11.99-11.95	2	K26
ASK-G22c	Window pane	Dionysus Temple	4.08.2009		3	K42
ASK-G23a	Window pane	Dionysus Temple	8.08.2009		4	K55
ASK-G23c	Window pane	Dionysus Temple	8.08.2009		4	K55
ASK-G30	Window pane	Dionysus Temple	2010		7d2	K22
ASK-G36a	Window pane	Dionysus Temple	2010		2	K14
ASK-G40a	Weathered window pane	Dionysus Temple	2012	12.34-12.13	2	K8
ASK-G40b	Window pane	Dionysus Temple	2012	12.34-12.13	2	K8
ASK-G41a	Weathered window pane	Dionysus Temple	2010	11.88-11.77	3	K11
ASK-G41b	Window pane	Dionysus Temple	2010	11.88-11.77	3	K11
ASK-G45	Window pane	Theatre	2009		2f	K63
ASK-G47	Weathered window pane	Theatre	8.08.2009	12.24-12.15	2e	K95
ASK-G52b	Window pane	Theatre	2009		2e	K72
ASK-G62a	Window pane	Theatre	23.07.2009	13.08-12.72	2b	K4
ASK-G67a	Window pane	Theatre	2009		2d	K36
ASK-G68	Window pane	Theatre	2009		2d	K43
ASK-G74a	Window pane	Theatre	2012		N	Cleanup
ASK-G74b	Window pane	Theatre	2012		N	Cleanup
ASK-G75a	Window pane	N2	2012	3.29-3.02	4	K32
ASK-G93a	Weathered window pane	Theatre	2009		2f	K62
ASK-G93b	Window pane	Theatre	2009		2f	K62
ASK-G51e	Droplet	Theatre	2009		2e	K75
ASK-G55b	Droplet	Theatre	9.08.2009	12.15-12.06	2e	K98
ASK-G57a	Droplet	Theatre	8.08.2009	14.41-12.33	2e	K89
ASK-G57e	Thread	Theatre	8.08.2009	14.41-12.33	2e	K89
ASK-G58e	Droplet	Theatre	7.08.2009		2e	K89
ASK-G59c	Thread	Theatre	8.08.2009	12.24-12.15	2e	K85
ASK-G60b	Droplet	Theatre	5.08.2009		2e	K77
ASK-G60c	Thread	Theatre	5.08.2009		2e	K77
ASK-G72c	Droplet	Theatre	2009		2d	K39
ASK-G72d	Droplet-waste glass	Theatre	2009		2d	K39
ASK-G4	Lump	Dionysus Temple	1.07.2009	11.86-11.75	2	K30
ASK-G24	Glass with clay	Dionysus Temple	2010	11.56-11.45	7d2	K122
ASK-G25b	Two-layered kiln and clay fragment	Dionysus Temple	2010	11.54-11.31	4	K28
ASK-G29	Kiln fragment with glass	Dionysus Temple	2010	11.57-11.36	7g	K84
ASK-G86a	Crucible piece	Theatre	2009	13.41-13.33	3b	K101
ASK-G88b	Glass with clay	Theatre	2009		old material	depo
ASK-G90	Crucible piece	Dionysus Temple	2009	13.12-12.90	3b	K108
ASK-G92	Crucible piece	Theatre	11.08.2009		3b	

Table B.2 The color analysis and the thickness of the Side set

Sample No	L	a	b	Color	Thickness
ASK- G2	69,0398	-16,9344	25,8385	light green	13.040-15.226
ASK- G6	35,6313	-13,1313	16,4345	light green	2.339-2.466
ASK- G8b	22,1518	-19,9817	16,7633	dark green	15.655-13.867
ASK- G22c	49,8119	-10,4957	13,0692	light green	2.958-2.98
ASK- G22e	15,1799	-10,4580	2,6973	green	5.148-15.326
ASK- G23a	45,1018	-25,7733	4,1921	blue-green	2.318-3.446
ASK- G23c	39,8068	-18,9319	5,6818	blue-green	-
ASK- G30	75,9226	-25,2858	5,6054	light blue	2.496-2.267
ASK- G31c	27,7686	-0,1154	11,483	covered with corrosion	3.277-3.681
ASK- G32	69,5412	-7,1634	12,5341	colorless - green tint	0.807-0.813
ASK- G36a	65,2623	-6,2706	13,5961	pale green	1.736-2.073
ASK- G37	23,1373	-16,0171	14,3803	green	4.619-8.680
ASK- G39a	0,7706	4,9706	-11,1147	navy	13.802-17.122
ASK- G40a	59,7805	-15,5387	-0,8636	blue green	2.810
ASK- G40b	38,0263	-20,5082	10,4525	green	2.890-3.353
ASK- G41a	71,2475	-12,0891	16,539	pale green	1.854-2.104
ASK- G41b	69,4737	-20,4898	4,9794	colorless - blue tint	1.932-2.318
ASK- G42	58,1477	-6,326	19,7814	light green	4.047-5.685
ASK- G44a	56,8774	-6,3686	38,2496	light olive	0.779-1.356
ASK- G44c	32,1291	-12,0541	23,1618	green	12.402-16.954
ASK- G45	71,163	-12,2977	-1,7862	colorless - blue tint	1.684-2.822
ASK- G47	36,3091	-15,1296	30,9042	olive green	3.471-3.988
ASK- G49a	33,676	1,2364	41,4762	olive green	3.979-17.216
ASK- G50a	62,3608	-22,1781	-2,2404	blue	2.481-5.145
ASK- G50b	62,3608	-22,1781	-2,2404	blue	0.93-2.835
ASK- G50c	42,9807	-11,8841	26,2759	khaki	2.797-3.849
ASK- G51e	40,3592	-4,6094	31,9899	olive green	3.6-8.383
ASK- G51f	27,5506	1,4729	-21,6086	blue	1.239-2.443
ASK- G52a	29,4684	-16,3825	7,7364	green	2.835-5.004
ASK- G52b	76,1233	-16,0227	6,0657	colorless - green tint	3.942-7.89
ASK- G53c	30,4679	-12,1487	28,8121	dark green	9.544-12.09
ASK- G54a	58,8184	-16,8842	0,5458	light blue	1.786-2.323
ASK- G55a	41,8942	-6,9487	4,6667	pale green	4.34-5.541
ASK- G55b	42,7149	-13,4896	4,5304	blue-green	8.692-12.827
ASK- G57a	55,0343	-21,1531	0,0423	blue	1.426-18.501
ASK- G57e	61,0388	-16,0936	8,9648	pale blue	3.805-8.344

Table B.2 (continued)

Sample No	L	a	b	Color	Thickness
ASK- G58e	27,5437	-10,8213	17,8581	green	5.176-17.576
ASK- G59c	45,5014	-7,3086	-9,3863	blue	1.872-4.831
ASK- G59d	39,4386	-6,2885	-26,102	blue	9.088-10.426
ASK- G60b	49,7435	-24,8271	-3,8125	blue-green	4.248-13.302
ASK- G60c	33,959	-6,7881	23,9297	olive green	5.749-6.34
ASK- G60d	44,138	-17,7688	11,9337	blue-green	2.405-6.763
ASK- G62a	50,9458	-9,065	17,0416	green	2.696-2.72
ASK- G62b	21,5797	-7,024	19,4807	green	14.843-18.784
ASK- G62c	35,3799	-17,9653	1,6946	blue-green	3.921-8.471
ASK- G62d	63,2664	-2,2852	24,2336	colorless - yellow tint	-
ASK- G62e	65,4546	-12,3628	27,5252	light green	2.195-3.812
ASK- G67c	3,9339	5,6569	-18,9448	navy	11.015-11.453
ASK- G69a	32,1715	-4,1776	13,1002	green	1.215-12.705
ASK- G69b	32,7975	-0,7699	41,3209	olive green	-
ASK- G69c	32,4592	-6,614	8,3924	olive green	-
ASK- G71a	35,5945	-4,4742	17,8261	olive green	3.921-8.037
ASK- G71b	24,1585	-3,2101	-15,8644	blue	2.239-9.613
ASK- G72d	20,2629	-11,1663	9,9242	dark green	5.74-15.084
ASK- G73	47,27	-3,7955	19,61	light olive	2.383-7.314
ASK- G74a	50,0089	-7,1219	34,308	light olive	1.589-3.834
ASK- G74b	53,0979	-15,2586	6,0194	blue-green	2.345-2.881
ASK- G74c	14,6929	7,9248	-21,9679	navy	5.335-11.075
ASK- G75a	55,8771	-10,9007	8,4196	pale blue	4.194-4.631
ASK- G75b	74,2017	-3,164	19,872	colorless - yellow tint	1.049-2.319
ASK- G77	46,6045	-11,6139	23,1194	green	3.334-5.167
ASK- G79b	43,6315	-1,0164	36,065	olive green	2.966-5.188
ASK- G79c	25,2204	2,0611	16,4029	dark amber-brown	1.859-4.469
ASK- G80a	66,1006	-4,5597	19,2912	light olive	1.323-2.945
ASK- G81	40,8943	-0,9626	16,7578	colorless - yellow tint	1.178-3.495
ASK- G82b	6,0376	4,2346	2,6569	brown	2.955-3.411
ASK- G83a	12,0369	8,6053	5,0348	dark amber-brown	5.995-7.249
ASK- G84	35,2929	-4,0827	20,4503	olive green	2.503-5.938
ASK- G86b	22,0619	-6,7819	18,2653	green	7.903-18.473
ASK- G88a	7,8147	0,5295	-1,4111	dark green	23.271-27.429
ASK- G93a	43,2333	-14,3429	-1,4097	colorless - blue tint	1.11-3.766
ASK- G93b	50,5637	-9,3854	1,8003	colorless - blue tint	1.493-2.756

Table B.3. Color Schema of Side Samples by Chromamateric Analysis

		
ASK-G2	ASK-G6	ASK-G8b
		
ASK-G22c	ASK-G22e	ASK-G23a
		
ASK-G23c	ASK-G30	ASK-G31c
		
ASK-G32	ASK-G36a	ASK-G37
		
ASK-G39a	ASK-G40a	ASK-G40b
		
ASK-G41a	ASK-G41b	ASK-G42a
		
ASK-G44a	ASK-G44c	ASK-G45
		
ASK-G47	ASK-G49a	ASK-G50a
		
ASK-50b	ASK-50c	ASK-51e
		
ASK-G51f	ASK-G52a	ASK-52b
		
ASK-53c	ASK-G54a	ASK-G55b
		
ASK-57a	ASK-G57e	ASK-G58e

Table B.3. (continued) Color Schema of Side Samples by Chromamateric Analysis

		
ASK-G59c	ASK-G59d	ASK-G60b
		
ASK-G60c	ASK-G60d	ASK-G62a
		
ASK-G62b	ASK-G62c	ASK-G62d
		
ASK-G62e	ASK-G67c	ASK-G69a
		
ASK-G69b	ASK-G69c	ASK-G71a
		
ASK-G71b	ASK-G72d	ASK-G73
		
ASK-G74a	ASK-G74b	ASK-G74c
		
ASK-G75a	ASK-G75b	ASK-G77
		
ASK-79b	ASK-79c	ASK-G80a
		
ASK-G81	ASK-G82b	ASK-83a
		
ASK-84	ASK-G86b	ASK-G88a
		
	ASK-G93a	ASK-G93b

Table B.4. PED-XRF results for the chunks

Element	Dimension	ASK-G2	ASK-G8b	ASK-G22e	ASK-G39a	ASK-G44c	ASK-G49a
<b>Na<sub>2</sub>O</b>	%	10,00	11,51	13,15	12,16	14,56	16,39
<b>MgO</b>	%	0,265	0,629	0,645	0,723	1,126	1,020
<b>Al<sub>2</sub>O<sub>3</sub></b>	%	0,217	1,244	1,072	1,429	1,197	0,952
<b>SiO<sub>2</sub></b>	%	56,96	61,29	66,49	65,87	64,81	64,68
<b>P<sub>2</sub>O<sub>5</sub></b>	%	0,003	0,050	0,062	0,176	0,106	0,075
<b>SO<sub>3</sub></b>	%	0,294	0,179	0,197	0,125	0,469	0,431
<b>Cl</b>	%	0,860	0,755	0,760	0,703	0,616	0,516
<b>K<sub>2</sub>O</b>	%	1,230	0,955	0,965	1,712	0,963	0,872
<b>CaO</b>	%	6,35	7,84	8,02	9,58	9,36	8,45
<b>TiO<sub>2</sub></b>	%	0,078	0,262	0,167	0,128	0,188	0,163
<b>V<sub>2</sub>O<sub>5</sub></b>	%	0,009	0,010	0,007	0,006	0,009	0,011
<b>Cr<sub>2</sub>O<sub>3</sub></b>	%	0,002	0,005	0,005	0,007	0,004	0,004
<b>MnO</b>	%	0,870	0,891	0,914	0,275	1,197	1,377
<b>Fe<sub>2</sub>O<sub>3</sub></b>	%	0,635	1,587	1,098	0,721	1,042	1,161
<b>LOI</b>	%	22,23	12,79	6,45	6,39	4,35	3,9
<b>Co</b>	ppm	8,2	24,1	12,3	16,9	27,8	19,3
<b>Ni</b>	ppm	7	17,4	12,9	15,3	26,3	27,8
<b>Cu</b>	ppm	17,9	94,4	116,1	63,1	57,4	68,4
<b>Zn</b>	ppm	10,8	22,9	15,2	8,3	22,1	24,7
<b>Ga</b>	ppm	2,7	1,8	1	1,3	2,1	3,2
<b>Ge</b>	ppm	0,6	0,6	0,6	0,7	0,4	0,3
<b>As</b>	ppm	2,1	5,5	2,8	3,6	4,4	2,8
<b>Se</b>	ppm	0,2	0,3	0,3	0,4	0,3	0,3
<b>Br</b>	ppm	8,3	9,1	9	7,3	10,5	8,5
<b>Rb</b>	ppm	5,2	11,9	11,8	18,1	9,3	8,1
<b>Sr</b>	ppm	358,5	487	500,9	502,7	836,6	793,7
<b>Y</b>	ppm	4	7,2	6,3	6	5,4	6,2
<b>Zr</b>	ppm	28,7	139,4	88,8	68,4	106,8	103,7
<b>Nb</b>	ppm	1,2	2,6	2,7	3	2,9	3
<b>Mo</b>	ppm	1,8	4,8	2,8	7,6	3,2	11,4
<b>Cd</b>	ppm	0,5	0,8	0,8	0,8	0,8	0,8
<b>In</b>	ppm	0,6	0,8	0,9	0,8	0,8	0,9
<b>Sn</b>	ppm	3,8	14,8	20,5	20,1	9,9	10,3
<b>Sb</b>	ppm	0,6	35,9	84,7	17,8	60,7	78,1
<b>Te</b>	ppm	0,9	1,3	1,2	1,2	1,1	1,2
<b>I</b>	ppm	1,7	2,3	2,3	2,2	2	2,2
<b>Cs</b>	ppm	2,9	4	3,9	3,6	3,5	3,8
<b>Ba</b>	ppm	119,4	391,4	476,7	313,9	254,8	355,5
<b>La</b>	ppm	13,4	8,4	8,1	11,5	9,5	14,8
<b>Ce</b>	ppm	17,3	12	25,6	15,3	23,7	31,4
<b>Hf</b>	ppm	2,2	8,4	8,5	7,3	6,3	5,4
<b>Ta</b>	ppm	2,1	4,8	5,4	4,1	4	4,2
<b>W</b>	ppm	1,5	1,9	1,9	1,7	2	2
<b>Hg</b>	ppm	0,5	0,6	0,7	0,7	0,6	0,6
<b>Tl</b>	ppm	0,4	0,9	1,1	1,6	1,1	0,8
<b>Pb</b>	ppm	28,6	236,1	445,5	916,5	204,9	135,3
<b>Bi</b>	ppm	0,4	0,9	1,2	0,7	0,8	0,7
<b>Th</b>	ppm	0,5	2,4	4,4	7,1	1,4	1,5
<b>U</b>	ppm	4,6	6,4	5,9	7,8	7,3	6,7

Table B. 4. (continued)

Element	Dimension	ASK-G52c	ASK-G53c	ASK-G62b	ASK-G66d	ASK-G67C	ASK-G71B
Na <sub>2</sub> O	%	0,089	12,71	13,770	10,380	10,22	11,83
MgO	%	0,927	0,865	0,994	0,832	0,54	0,525
Al <sub>2</sub> O <sub>3</sub>	%	6,389	0,845	0,915	0,786	0,622	0,674
SiO <sub>2</sub>	%	48,08	59,59	58,89	53,59	61,43	75,16
P <sub>2</sub> O <sub>5</sub>	%	0,178	0,064	0,081	0,066	0,0424	0,01035
SO <sub>3</sub>	%	0,021	0,308	0,385	0,251	0,066	0,4396
Cl	%	0,001	0,512	0,646	0,609	0,6459	0,6466
K <sub>2</sub> O	%	1,079	1,003	0,818	0,728	0,6321	0,7379
CaO	%	21,93	8,37	7,47	7,62	6,839	5,045
TiO <sub>2</sub>	%	0,531	0,181	0,167	0,133	0,128	0,1305
V <sub>2</sub> O <sub>5</sub>	%	0,023	0,011	0,011	0,008	0,0079	0,0065
Cr <sub>2</sub> O <sub>3</sub>	%	0,114	0,002	0,001	0,005	0,00184	0,00767
MnO	%	0,109	1,464	1,302	2,130	0,4236	0,2186
Fe <sub>2</sub> O <sub>3</sub>	%	7,166	1,335	1,124	1,319	1,514	0,7613
LOI	%	13,36	12,75	13,43	21,54	15,93	3,54
Co	ppm	1570	24,4	16,9	27,2	405,9	71,8
Ni	ppm	1955	30,9	22,8	36,1	142,2	27,7
Cu	ppm	26710	90,2	66,4	66,1	1386	438,6
Zn	ppm	1834	28	22,1	32,9	11	0,2
Ga	ppm	21	1,8	0,7	3,5	3,6	1,5
Ge	ppm	5,1	0,3	1	0,4	5	0,6
As	ppm	128	4,1	6	6,3	21,3	4,2
Se	ppm	7,4	0,3	0,3	0,3	1	0,4
Br	ppm	24,2	8,2	9,4	10,8	12,2	17,7
Rb	ppm	99,1	12,6	9,5	8,9	14,3	9,9
Sr	ppm	218,9	698,3	680,4	926,3	668,5	522,4
Y	ppm	12	6,8	5,5	6	1,5	5,6
Zr	ppm	256	90	102,4	98,4	79,3	95,8
Nb	ppm	7,2	4,5	5,9	6,1	3	2,7
Mo	ppm	36,8	3,1	3,3	8,1	6,1	2,7
Cd	ppm	2,1	0,9	2,4	0,9	1,2	0,9
In	ppm	2,7	1,1	1	1,1	1,4	0,9
Sn	ppm	1181	11,6	11,4	4,1	186,9	14,3
Sb	ppm	142,6	149,5	142,1	207,8	159,3	26,2
Te	ppm	1,8	1,5	2	1,5	1,4	1,5
I	ppm	7,7	2,5	2,2	2,6	3,3	2,6
Cs	ppm	6,9	4,5	3,5	4,7	4,5	4,6
Ba	ppm	135,9	392,3	360,6	549,7	220	211,2
La	ppm	29	14,3	7,3	13,1	14,2	9,8
Ce	ppm	32,7	26,7	10	31,8	13	23,1
Hf	ppm	810	9,7	11	6,4	59	21,1
Ta	ppm	160	4,8	4,2	4,3	19	9,7
W	ppm	28	2,1	2	2,3	3,7	2,2
Hg	ppm	7	0,7	0,6	0,7	1,6	0,8
Tl	ppm	103,6	1,2	0,5	0,9	4,3	1,8
Pb	ppm	84270	179,6	200,4	142,2	5940	1165
Bi	ppm	31	0,9	0,8	0,8	4	1,6
Th	ppm	271,4	0,7	1,5	1	39,5	8,2
U	ppm	31	6,3	24,9	6,6	6,9	9,8

Table B.3. (continued)

Element	Dimension	ASK-G74c	ASK-G86b	ASK-G88a	Mean	Sdev
Na <sub>2</sub> O	%	14,490	15,160	9,480	<b>11,73</b>	<b>3,82</b>
MgO	%	0,588	0,913	0,887	<b>0,77</b>	<b>0,23</b>
Al <sub>2</sub> O <sub>3</sub>	%	0,4933	1,085	1,305	<b>1,28</b>	<b>1,45</b>
SiO <sub>2</sub>	%	60,2	62,59	58,99	<b>61,24</b>	<b>6,17</b>
P <sub>2</sub> O <sub>5</sub>	%	0,020	0,083	0,480	<b>0,10</b>	<b>0,12</b>
SO <sub>3</sub>	%	0,534	0,413	0,298	<b>0,29</b>	<b>0,15</b>
Cl	%	0,780	0,740	0,603	<b>0,63</b>	<b>0,20</b>
K <sub>2</sub> O	%	0,693	0,824	2,324	<b>1,04</b>	<b>0,44</b>
CaO	%	5,05	8,15	11,59	<b>8,78</b>	<b>4,01</b>
TiO <sub>2</sub>	%	0,129	0,168	0,155	<b>0,18</b>	<b>0,11</b>
V <sub>2</sub> O <sub>5</sub>	%	0,005	0,008	0,002	<b>0,01</b>	<b>0,00</b>
Cr <sub>2</sub> O <sub>3</sub>	%	0,002	0,002	0,013	<b>0,01</b>	<b>0,03</b>
MnO	%	0,047	1,348	0,356	<b>0,86</b>	<b>0,61</b>
Fe <sub>2</sub> O <sub>3</sub>	%	0,742	0,974	1,014	<b>1,48</b>	<b>1,60</b>
LOI	%	16,23	7,54	12,50	<b>11,53</b>	<b>6,03</b>
Co	ppm	173,2	25,6	21,5	<b>163,01</b>	<b>402,78</b>
Ni	ppm	68,9	21	33,3	<b>162,97</b>	<b>496,84</b>
Cu	ppm	912,8	64,5	114,1	<b>2017,73</b>	<b>6841,94</b>
Zn	ppm	0,3	22,1	8,7	<b>137,55</b>	<b>469,41</b>
Ga	ppm	2,3	3	1,2	<b>3,38</b>	<b>4,96</b>
Ge	ppm	0,6	0,5	0,5	<b>1,15</b>	<b>1,59</b>
As	ppm	6,8	2,7	2,5	<b>13,54</b>	<b>32,00</b>
Se	ppm	0,6	0,2	0,3	<b>0,84</b>	<b>1,83</b>
Br	ppm	16,5	10,2	7	<b>11,26</b>	<b>4,72</b>
Rb	ppm	10,6	9,2	22,3	<b>17,39</b>	<b>22,99</b>
Sr	ppm	412,6	713,7	481,3	<b>586,79</b>	<b>193,09</b>
Y	ppm	5	5,7	6,8	<b>6,00</b>	<b>2,15</b>
Zr	ppm	107,1	92,5	67,7	<b>101,67</b>	<b>49,15</b>
Nb	ppm	4,6	3	2,9	<b>3,69</b>	<b>1,63</b>
Mo	ppm	3,1	3,2	5	<b>6,87</b>	<b>8,68</b>
Cd	ppm	1,2	0,8	0,8	<b>1,05</b>	<b>0,52</b>
In	ppm	0,9	0,9	0,8	<b>1,04</b>	<b>0,49</b>
Sn	ppm	25,9	11	15,4	<b>102,73</b>	<b>301,68</b>
Sb	ppm	3,8	170,7	25,8	<b>87,04</b>	<b>69,11</b>
Te	ppm	1,2	1,2	1,2	<b>1,35</b>	<b>0,28</b>
I	ppm	2,2	2,1	2,2	<b>2,67</b>	<b>1,44</b>
Cs	ppm	3,7	3,6	3,6	<b>4,09</b>	<b>0,92</b>
Ba	ppm	177,7	309,8	303,6	<b>304,83</b>	<b>121,88</b>
La	ppm	21,4	12	18	<b>13,65</b>	<b>5,70</b>
Ce	ppm	23,9	18,9	31,3	<b>22,45</b>	<b>7,68</b>
Hf	ppm	42	8,4	7,5	<b>67,55</b>	<b>205,98</b>
Ta	ppm	14	4,1	5,4	<b>16,67</b>	<b>39,90</b>
W	ppm	2,5	1,9	2,1	<b>3,85</b>	<b>6,70</b>
Hg	ppm	0,9	0,6	0,7	<b>1,15</b>	<b>1,64</b>
Tl	ppm	2,8	0,8	1,1	<b>8,19</b>	<b>26,41</b>
Pb	ppm	3130	157,6	414,2	<b>6504,39</b>	<b>21571,65</b>
Bi	ppm	2,6	0,8	0,7	<b>3,19</b>	<b>7,75</b>
Th	ppm	21	1,8	2,4	<b>24,32</b>	<b>69,15</b>
U	ppm	11,2	6,7	7,4	<b>9,97</b>	<b>7,55</b>

Table B.5. PED-XRF results for the products

Element	Dimension	ASK-G22a	ASK-G31c	ASK-G32	ASK-G37	ASK-G42a	ASK-G44a
Na <sub>2</sub> O	%	9,380	12,430	14,930	14,390	12,260	3,070
MgO	%	0,440	0,655	0,635	0,638	0,582	0,338
Al <sub>2</sub> O <sub>3</sub>	%	0,852	1,259	1,254	0,924	1,585	0,696
SiO <sub>2</sub>	%	52,26	56,83	63,35	63,5	63,87	54,71
P <sub>2</sub> O <sub>5</sub>	%	0,030	0,078	0,054	0,076	0,057	0,021
SO <sub>3</sub>	%	0,166	0,360	0,404	0,253	0,357	0,020
Cl	%	0,634	0,598	0,774	0,821	0,649	0,304
K <sub>2</sub> O	%	0,726	0,693	0,635	0,725	0,674	0,745
CaO	%	6,55	7,50	6,67	6,74	7,49	6,87
TiO <sub>2</sub>	%	0,190	0,163	0,144	0,223	0,179	0,081
V <sub>2</sub> O <sub>5</sub>	%	0,009	0,007	0,009	0,012	0,009	0,006
Cr <sub>2</sub> O <sub>3</sub>	%	0,004	0,002	0,004	0,006	0,004	0,001
MnO	%	0,858	1,245	1,117	1,240	1,230	0,035
Fe <sub>2</sub> O <sub>3</sub>	%	1,345	0,927	0,762	1,437	0,797	0,598
LOI	%	26,56	17,25	9,25	9,01	10,26	32,51
Co	ppm	26,7	10,5	25	17,7	12,4	20,4
Ni	ppm	17,3	16	11,2	17,9	12,8	9,6
Cu	ppm	116,8	147,4	41,4	124,9	30,3	22,7
Zn	ppm	24,4	17,8	20,4	51,1	12,2	9,5
Ga	ppm	1,6	2,4	1,9	0,9	3,9	4,4
Ge	ppm	0,4	1	0,6	1,1	0,5	0,4
As	ppm	5	2,6	1,1	3,7	4,4	1
Se	ppm	0,3	0,3	0,2	0,3	0,2	0,3
Br	ppm	9	8,9	9,6	8	8,6	7,3
Rb	ppm	10,7	8,7	8,1	10,7	8,1	12
Sr	ppm	496,9	659,9	534	462,4	578,5	459,9
Y	ppm	7,2	5,5	5,3	6,8	5,7	4,8
Zr	ppm	143,3	105,3	73,1	123,2	103,1	68,7
Nb	ppm	9,8	4,8	3	3,7	4,5	6,5
Mo	ppm	8,5	2,4	2,8	3,2	3,1	4,5
Cd	ppm	1,5	0,8	0,8	0,8	0,8	0,9
In	ppm	1,1	1	0,8	0,8	1	2,1
Sn	ppm	21,6	15	5,6	42,4	11,7	4,8
Sb	ppm	65,2	216,6	32,4	41,8	209,5	2,1
Te	ppm	1,6	1,2	1,2	1,2	1,2	2,7
I	ppm	2,8	2,2	2,1	2,2	2,1	4,6
Cs	ppm	4,7	3,7	3,6	3,6	3,6	8,5
Ba	ppm	453,2	287,7	339,1	377,6	251,9	298,9
La	ppm	15,7	11,7	7,4	7,4	13,2	19
Ce	ppm	25,6	20,8	10	11,5	16,3	26
Hf	ppm	10,4	4,4	7,3	9,4	4,8	2,7
Ta	ppm	5,3	5,8	3,3	5,4	3	3,1
W	ppm	2,3	2	1,7	2,2	1,7	2,3
Hg	ppm	0,6	0,6	0,6	0,7	0,6	0,7
Tl	ppm	1,3	1	0,7	1,1	0,5	0,8
Pb	ppm	317,1	125	92	352	56,1	62,4
Bi	ppm	0,5	0,7	0,6	1	0,6	0,8
Th	ppm	2,5	1,2	1,8	4,6	1,4	0,7
U	ppm	8,6	7	6,6	7,6	7,6	11,6

Table B.5. (continued)

Element	Dimension	ASK-G50a	ASK-G50b	ASK-G50c	ASK-G51f	ASK-G52a	ASK-G54a
<b>Na<sub>2</sub>O</b>	%	12,850	12,310	15,050	9,450	13,920	7,660
<b>MgO</b>	%	0,555	0,634	0,932	0,287	0,589	0,331
<b>Al<sub>2</sub>O<sub>3</sub></b>	%	1,281	1,413	1,006	0,471	1,238	1,013
<b>SiO<sub>2</sub></b>	%	66,22	71,890	62,34	60,190	70,270	63,080
<b>P<sub>2</sub>O<sub>5</sub></b>	%	0,073	0,073	0,083	0,002	0,053	0,029
<b>SO<sub>3</sub></b>	%	0,158	0,322	0,391	0,375	0,239	0,197
<b>Cl</b>	%	0,697	0,737	0,768	0,574	0,838	0,494
<b>K<sub>2</sub>O</b>	%	0,844	0,820	0,774	0,657	0,733	0,825
<b>CaO</b>	%	8,37	9,195	7,63	14,917	8,113	9,790
<b>TiO<sub>2</sub></b>	%	0,095	0,096	0,169	0,130	0,091	0,084
<b>V<sub>2</sub>O<sub>5</sub></b>	%	0,005	0,006	0,010	0,007	0,005	0,001
<b>Cr<sub>2</sub>O<sub>3</sub></b>	%	0,002	0,005	0,006	0,005	0,003	0,003
<b>MnO</b>	%	0,020	0,029	1,314	0,067	0,020	0,021
<b>Fe<sub>2</sub>O<sub>3</sub></b>	%	0,487	0,491	1,098	0,956	0,489	0,565
<b>LOI</b>	%	8,34	2,440	8,43	12,547	3,580	16,390
<b>Co</b>	ppm	16,4	10,4	23,6	179,4	8,5	13,2
<b>Ni</b>	ppm	4,2	5,3	20,7	58,2	5,6	5,9
<b>Cu</b>	ppm	13,3	6,7	75,8	1269,0	3,9	11,8
<b>Zn</b>	ppm	6,3	6,5	23,9	0,6	6,7	7,1
<b>Ga</b>	ppm	4,3	3,9	1,5	3,3	3,3	3,6
<b>Ge</b>	ppm	0,4	0,3	0,4	0,8	0,3	0,3
<b>As</b>	ppm	1,2	2,3	1,5	9,8	1,1	1,8
<b>Se</b>	ppm	0,3	0,2	0,3	0,9	0,2	0,2
<b>Br</b>	ppm	9,7	10,8	10,9	19,1	8,4	9,9
<b>Rb</b>	ppm	11,4	11,5	9,5	13,2	9,7	12,3
<b>Sr</b>	ppm	455,4	538,7	691,6	474,4	442,1	469,0
<b>Y</b>	ppm	5,6	6,3	5,7	1,9	6,9	6,3
<b>Zr</b>	ppm	52,5	76,1	83,3	101,6	44,5	58,8
<b>Nb</b>	ppm	2,3	2,6	3,5	3,5	2,6	2,9
<b>Mo</b>	ppm	2,6	2,9	6,7	4,0	2,1	3,0
<b>Cd</b>	ppm	0,8	0,8	0,8	1,5	0,7	1,0
<b>In</b>	ppm	0,7	0,8	0,8	1,3	0,8	0,9
<b>Sn</b>	ppm	2,4	0,9	10,7	113,7	0,8	3,3
<b>Sb</b>	ppm	0,8	1,0	143,9	4,7	0,8	1,1
<b>Te</b>	ppm	1,1	1,2	1,1	2,2	1,2	1,6
<b>I</b>	ppm	2,0	2,1	2,0	4,3	2,0	2,8
<b>Cs</b>	ppm	3,5	3,6	3,5	6,9	3,5	5,3
<b>Ba</b>	ppm	254,8	262,3	324,9	226,8	246,6	276,1
<b>La</b>	ppm	18,3	14,7	7,2	31,0	21,8	21,3
<b>Ce</b>	ppm	24,9	23,2	20,5	42,0	23,4	43,0
<b>Hf</b>	ppm	2,1	2,0	4,8	58,0	3,2	4,5
<b>Ta</b>	ppm	2,3	2,0	4,5	18,0	1,8	2,3
<b>W</b>	ppm	1,6	1,7	2,1	3,4	1,6	1,7
<b>Hg</b>	ppm	0,6	0,6	0,7	1,6	0,6	0,6
<b>Tl</b>	ppm	0,6	0,6	0,9	4,0	0,5	0,6
<b>Pb</b>	ppm	37,8	19,4	184,3	4511,0	8,7	39,0
<b>Bi</b>	ppm	0,5	0,5	0,8	3,5	0,4	0,6
<b>Th</b>	ppm	0,7	1,4	2,3	28,2	1,0	0,9
<b>U</b>	ppm	6,6	7,2	7,0	8,4	6,3	6,0

Table B.5. (continued)

Element	Dimension	ASK-G55a	ASK-G59d	ASK-G60d	ASK-G62c	ASK-G62d	ASK-G62e
Na <sub>2</sub> O	%	13,620	10,870	11,010	10,590	6,370	11,240
MgO	%	0,844	0,454	0,607	0,631	0,200	0,699
Al <sub>2</sub> O <sub>3</sub>	%	1,002	0,359	0,963	1,461	0,414	0,609
SiO <sub>2</sub>	%	69,530	63,590	69,120	73,030	62,460	50,290
P <sub>2</sub> O <sub>5</sub>	%	0,079	0,002	0,050	0,068	0,002	0,051
SO <sub>3</sub>	%	0,427	0,400	0,234	0,267	0,211	0,461
Cl	%	0,664	0,709	0,722	0,628	0,515	0,562
K <sub>2</sub> O	%	0,798	0,541	0,797	0,880	0,601	0,776
CaO	%	7,578	5,682	8,114	7,707	11,706	16,309
TiO <sub>2</sub>	%	0,170	0,105	0,108	0,121	0,051	0,139
V <sub>2</sub> O <sub>5</sub>	%	0,012	0,007	0,006	0,006	0,001	0,009
Cr <sub>2</sub> O <sub>3</sub>	%	0,002	0,002	0,002	0,002	0,002	0,002
MnO	%	1,346	0,031	0,374	0,468	1,003	1,273
Fe <sub>2</sub> O <sub>3</sub>	%	1,091	0,672	0,618	0,735	0,375	0,809
LOI	%	2,840	16,380	7,930	3,560	14,970	16,680
Co	ppm	30,0	39,8	15,9	31,9	22,5	5,7
Ni	ppm	24,9	15,5	9,7	12,0	15,6	18,2
Cu	ppm	91,7	81,8	56,1	65,4	9,3	65,0
Zn	ppm	20,4	8,7	23,3	19,6	18,8	19,0
Ga	ppm	2,3	0,9	3,3	2,4	4,0	1,5
Ge	ppm	0,5	0,7	0,7	1,6	0,4	0,3
As	ppm	4,2	1,8	1,4	3,3	1,8	2,2
Se	ppm	0,3	0,3	0,3	0,5	0,2	0,3
Br	ppm	10,5	17,4	9,6	9,0	6,7	12,0
Rb	ppm	9,4	8,1	11,1	13,3	8,4	7,7
Sr	ppm	695,8	505,2	529,8	521,6	575,0	661,2
Y	ppm	6,0	7,5	6,1	5,4	6,7	5,6
Zr	ppm	113,0	67,6	58,3	70,5	39,0	107,8
Nb	ppm	3,3	3,0	4,6	6,2	2,5	7,9
Mo	ppm	8,6	3,5	2,8	4,5	2,5	4,7
Cd	ppm	1,9	1,2	0,9	3,0	0,8	1,1
In	ppm	1,0	1,2	0,9	1,0	0,8	0,5
Sn	ppm	13,4	3,2	6,4	7,1	1,0	8,0
Sb	ppm	144,5	1,4	37,6	36,6	1,0	12,4
Te	ppm	1,3	1,8	1,3	1,3	1,3	1,5
I	ppm	2,2	3,5	2,4	2,3	2,3	2,6
Cs	ppm	3,7	8,6	4,2	3,8	4,0	4,7
Ba	ppm	343,9	181,0	286,7	278,6	227,5	282,5
La	ppm	13,0	14,0	9,0	9,1	20,1	9,9
Ce	ppm	32,7	31,0	12,0	24,8	17,9	32,8
Hf	ppm	6,4	10,9	8,4	7,2	1,6	7,7
Ta	ppm	4,8	4,7	3,7	8,1	2,2	4,0
W	ppm	1,9	2,2	1,8	4,1	1,9	1,9
Hg	ppm	0,6	0,7	0,6	1,3	0,6	0,6
Tl	ppm	0,7	1,8	0,7	1,6	0,6	0,4
Pb	ppm	188,3	291,7	72,5	170,4	16,0	304,4
Bi	ppm	0,8	1,0	0,6	1,6	0,5	1,4
Th	ppm	1,3	3,1	1,3	0,7	0,5	0,8
U	ppm	18,2	6,8	6,3	7,2	8,3	12,6

Table B.5. (continued)

Element	Dimension	ASK-G69a	ASK-G69b	ASK-G69c	ASK-G71a	ASK-G73	ASK-G75b
Na <sub>2</sub> O	%	9,720	3,030	12,910	8,190	13,570	12,030
MgO	%	0,487	0,209	0,791	0,528	0,913	0,019
Al <sub>2</sub> O <sub>3</sub>	%	0,659	0,602	0,851	0,624	0,938	0,064
SiO <sub>2</sub>	%	58,730	51,660	65,650	65,790	69,430	65,780
P <sub>2</sub> O <sub>5</sub>	%	0,024	0,003	0,042	0,038	0,110	0,002
SO <sub>3</sub>	%	0,347	0,088	0,350	0,340	0,461	0,338
Cl	%	0,529	0,265	0,735	0,441	0,678	0,798
K <sub>2</sub> O	%	0,723	0,672	0,603	0,870	0,876	0,404
CaO	%	6,577	15,858	6,954	6,351	7,231	5,307
TiO <sub>2</sub>	%	0,129	0,068	0,144	0,150	0,162	0,067
V <sub>2</sub> O <sub>5</sub>	%	0,009	0,005	0,009	0,009	0,010	0,005
Cr <sub>2</sub> O <sub>3</sub>	%	0,002	0,002	0,003	0,001	0,003	0,003
MnO	%	1,104	0,024	1,313	1,275	1,392	0,016
Fe <sub>2</sub> O <sub>3</sub>	%	1,273	0,469	0,902	0,990	0,946	0,331
LOI	%	19,840	26,770	8,930	14,740	3,550	14,470
Co	ppm	21,5	7,3	14,4	17,3	23,3	15,3
Ni	ppm	14,5	8,6	13,6	18,6	19,8	4,2
Cu	ppm	59,0	12,9	29,0	56,3	54,3	8,8
Zn	ppm	16,3	7,3	13,4	22,1	23,3	13,5
Ga	ppm	2,7	2,7	2,3	3,8	2,9	3,5
Ge	ppm	0,4	0,3	0,3	0,6	0,3	1,3
As	ppm	3,1	0,9	2,1	5,4	4,6	19,5
Se	ppm	0,3	0,2	0,3	0,3	0,2	0,2
Br	ppm	8,7	6,6	10,7	11,2	12,4	8,3
Rb	ppm	9,9	8,4	7,4	11,1	9,6	4,8
Sr	ppm	616,5	333,4	671,2	700,2	655,3	439,7
Y	ppm	5,8	4,6	6,5	6,4	5,5	5,0
Zr	ppm	86,4	37,7	89,1	113,9	101,6	37,6
Nb	ppm	9,1	2,1	2,5	3,0	2,7	2,6
Mo	ppm	7,7	1,9	10,0	3,4	3,0	2,8
Cd	ppm	2,9	0,6	1,0	1,1	0,9	3,2
In	ppm	1,2	0,6	1,1	1,2	0,8	2,8
Sn	ppm	15,2	1,2	4,0	9,4	6,5	21,7
Sb	ppm	136,3	0,6	139,0	80,0	71,0	3381,0
Te	ppm	1,7	0,8	1,5	1,8	1,3	2,0
I	ppm	3,1	1,5	2,7	3,1	2,2	3,1
Cs	ppm	5,3	2,7	4,7	5,6	3,8	5,2
Ba	ppm	336,8	102,3	357,4	341,8	364,7	109,0
La	ppm	12,0	5,6	10,0	12,0	15,6	10,0
Ce	ppm	16,0	7,8	24,3	35,0	20,7	23,1
Hf	ppm	6,4	4,2	6,5	3,8	6,3	4,1
Ta	ppm	3,9	1,9	3,1	3,9	3,8	1,9
W	ppm	2,0	1,4	1,9	2,1	2,0	1,7
Hg	ppm	0,6	0,4	0,6	0,6	0,6	0,6
Tl	ppm	0,7	0,5	1,2	0,7	0,7	0,6
Pb	ppm	139,6	41,3	56,4	92,2	94,7	24,4
Bi	ppm	0,7	0,4	0,6	0,7	0,7	0,6
Th	ppm	1,4	0,7	2,6	2,0	1,8	0,7
U	ppm	14,3	4,4	6,2	8,2	7,3	6,6

Table B.5. (continued)

Element	Dimension	ASK-G77	ASK-G79b	ASK-G79c	ASK-G80a	ASK-G81	ASK-G82b
Na <sub>2</sub> O	%	10,890	14,830	8,530	14,790	14,510	9,640
MgO	%	0,911	0,883	0,340	0,755	0,584	0,946
Al <sub>2</sub> O <sub>3</sub>	%	2,039	0,942	0,927	0,870	0,726	0,542
SiO <sub>2</sub>	%	63,670	61,660	64,020	71,990	71,610	71,030
P <sub>2</sub> O <sub>5</sub>	%	0,275	0,088	0,016	0,035	0,049	0,111
SO <sub>3</sub>	%	0,388	0,502	0,195	0,413	0,357	0,360
Cl	%	0,541	0,728	0,749	1,041	0,917	0,701
K <sub>2</sub> O	%	0,788	0,720	0,696	0,571	0,696	1,065
CaO	%	11,030	8,200	6,458	4,795	6,468	5,725
TiO <sub>2</sub>	%	0,194	0,158	0,050	0,149	0,110	0,117
V <sub>2</sub> O <sub>5</sub>	%	0,010	0,010	0,009	0,004	0,006	0,010
Cr <sub>2</sub> O <sub>3</sub>	%	0,010	0,003	0,001	0,006	0,003	0,001
MnO	%	1,199	1,455	2,921	0,024	0,040	1,401
Fe <sub>2</sub> O <sub>3</sub>	%	1,363	0,934	0,433	0,751	0,639	0,822
LOI	%	6,730	8,920	13,830	3,480	3,470	7,930
Co	ppm	18,7	19,8	33,2	9,9	19,0	11,0
Ni	ppm	29,9	17,9	15,6	7,2	4,8	23,3
Cu	ppm	92,6	51,6	7,9	15,1	24,8	570,8
Zn	ppm	30,1	17,0	13,5	21,3	20,7	28,4
Ga	ppm	0,9	2,1	4,7	2,2	1,2	1,5
Ge	ppm	0,4	0,7	0,4	0,5	0,7	0,5
As	ppm	3,0	4,8	2,5	266,5	30,6	83,1
Se	ppm	0,3	0,3	0,2	0,4	0,3	0,5
Br	ppm	13,8	11,9	8,0	7,8	8,4	9,2
Rb	ppm	13,3	7,8	9,4	6,3	8,2	7,8
Sr	ppm	630,1	755,1	551,1	379,7	608,8	589,7
Y	ppm	6,3	5,7	5,5	3,7	3,9	3,5
Zr	ppm	94,2	94,0	46,7	84,6	70,9	67,7
Nb	ppm	4,4	4,5	2,7	3,2	4,1	10,0
Mo	ppm	3,6	6,5	6,0	3,1	5,3	10,6
Cd	ppm	0,7	0,8	1,1	12,2	6,5	5,7
In	ppm	1,0	1,0	0,9	3,4	2,9	5,1
Sn	ppm	31,0	10,0	1,3	62,7	44,1	72,1
Sb	ppm	156,3	304,3	71,6	7395,0	4451,0	8918,0
Te	ppm	1,2	1,2	1,6	18,6	1,9	4,9
I	ppm	2,3	2,2	3,0	3,1	2,4	5,3
Cs	ppm	3,6	3,6	5,3	4,7	4,3	8,3
Ba	ppm	280,7	386,1	524,5	149,5	154,2	335,2
La	ppm	6,9	12,0	11,0	8,3	7,6	15,0
Ce	ppm	17,2	15,9	29,0	10,0	30,3	35,0
Hf	ppm	11,0	5,5	2,2	6,4	6,5	33,8
Ta	ppm	5,0	3,7	2,1	2,3	2,9	12,0
W	ppm	2,1	1,9	1,9	1,7	1,8	2,9
Hg	ppm	0,9	0,7	0,6	0,7	0,7	0,8
Tl	ppm	0,7	0,6	0,6	0,7	0,4	1,8
Pb	ppm	389,9	92,5	19,6	267,9	310,4	810,8
Bi	ppm	1,0	0,7	0,5	1,0	1,0	1,7
Th	ppm	5,3	2,0	0,9	1,9	3,2	3,3
U	ppm	8,3	11,1	6,3	16,2	8,3	9,8

Table B.5. (continued)

Element	Dimension	ASK-G83a	ASK-G84	Mean	Sdev
Na <sub>2</sub> O	%	13,780	11,600	<b>11,23</b>	<b>3,15</b>
MgO	%	0,653	0,531	<b>0,58</b>	<b>0,23</b>
Al <sub>2</sub> O <sub>3</sub>	%	0,845	0,938	<b>0,92</b>	<b>0,39</b>
SiO <sub>2</sub>	%	72,000	73,790	<b>64,48</b>	<b>6,42</b>
P <sub>2</sub> O <sub>5</sub>	%	0,063	0,095	<b>0,06</b>	<b>0,05</b>
SO <sub>3</sub>	%	0,297	0,243	<b>0,31</b>	<b>0,11</b>
Cl	%	0,768	0,801	<b>0,67</b>	<b>0,16</b>
K <sub>2</sub> O	%	0,772	0,556	<b>0,73</b>	<b>0,12</b>
CaO	%	6,857	7,592	<b>8,20</b>	<b>2,86</b>
TiO <sub>2</sub>	%	0,124	0,063	<b>0,13</b>	<b>0,04</b>
V <sub>2</sub> O <sub>5</sub>	%	0,009	0,008	<b>0,01</b>	<b>0,00</b>
Cr <sub>2</sub> O <sub>3</sub>	%	0,002	0,003	<b>0,00</b>	<b>0,00</b>
MnO	%	2,869	1,383	<b>0,88</b>	<b>0,79</b>
Fe <sub>2</sub> O <sub>3</sub>	%	0,772	0,552	<b>0,79</b>	<b>0,30</b>
LOI	%	0,730	2,430	<b>11,09</b>	<b>7,78</b>
Co	ppm	25,0	18,5	<b>23,88</b>	<b>29,47</b>
Ni	ppm	31,5	17,0	<b>15,85</b>	<b>10,48</b>
Cu	ppm	153,5	12,0	<b>105,68</b>	<b>235,03</b>
Zn	ppm	16,5	14,8	<b>17,33</b>	<b>9,37</b>
Ga	ppm	0,9	3,4	<b>2,63</b>	<b>1,14</b>
Ge	ppm	0,6	0,9	<b>0,58</b>	<b>0,31</b>
As	ppm	4,0	2,4	<b>15,08</b>	<b>48,30</b>
Se	ppm	0,3	0,2	<b>0,30</b>	<b>0,13</b>
Br	ppm	6,6	4,7	<b>9,80</b>	<b>2,93</b>
Rb	ppm	10,5	6,2	<b>9,52</b>	<b>2,13</b>
Sr	ppm	529,6	517,4	<b>554,04</b>	<b>101,22</b>
Y	ppm	5,7	5,4	<b>5,59</b>	<b>1,15</b>
Zr	ppm	89,5	55,4	<b>79,97</b>	<b>26,77</b>
Nb	ppm	2,9	5,3	<b>4,26</b>	<b>2,20</b>
Mo	ppm	8,5	8,4	<b>4,79</b>	<b>2,54</b>
Cd	ppm	0,8	1,2	<b>1,84</b>	<b>2,34</b>
In	ppm	0,9	0,8	<b>1,29</b>	<b>0,97</b>
Sn	ppm	17,3	1,0	<b>17,80</b>	<b>24,91</b>
Sb	ppm	143,0	4,2	<b>818,90</b>	<b>2157,77</b>
Te	ppm	1,2	1,2	<b>2,09</b>	<b>3,10</b>
I	ppm	2,3	2,1	<b>2,65</b>	<b>0,82</b>
Cs	ppm	3,7	3,6	<b>4,61</b>	<b>1,52</b>
Ba	ppm	672,1	415,6	<b>304,06</b>	<b>114,92</b>
La	ppm	7,6	10,7	<b>12,75</b>	<b>5,53</b>
Ce	ppm	22,8	16,8	<b>23,20</b>	<b>8,97</b>
Hf	ppm	10,9	3,3	<b>8,33</b>	<b>10,67</b>
Ta	ppm	6,1	2,4	<b>4,35</b>	<b>3,25</b>
W	ppm	2,1	1,7	<b>2,04</b>	<b>0,54</b>
Hg	ppm	0,7	0,6	<b>0,69</b>	<b>0,22</b>
Tl	ppm	1,0	0,6	<b>0,91</b>	<b>0,67</b>
Pb	ppm	337,7	65,3	<b>299,71</b>	<b>786,22</b>
Bi	ppm	1,0	0,6	<b>0,86</b>	<b>0,58</b>
Th	ppm	2,4	1,0	<b>2,61</b>	<b>4,81</b>
U	ppm	7,9	21,4	<b>8,94</b>	<b>3,81</b>

Table B.6. PED-XRF results for the window panes

Element	Dimension	ASK-G6	ASK-G22c	ASK-G23a	ASK-G23c	ASK-G30	ASK-G36a
Na <sub>2</sub> O	%	11,98	13,04	12,11	14,74	15,92	12,71
MgO	%	0,496	0,493	0,024	0,513	0,593	0,663
Al <sub>2</sub> O <sub>3</sub>	%	0,708	0,978	0,627	0,757	0,994	0,894
SiO <sub>2</sub>	%	60,36	64,73	60,60	65,80	70,00	62,63
P <sub>2</sub> O <sub>5</sub>	%	0,007	0,053	0,006	0,022	0,052	0,019
SO <sub>3</sub>	%	0,160	0,237	0,226	0,265	0,186	0,140
Cl	%	0,848	0,809	0,778	0,850	0,988	1,069
K <sub>2</sub> O	%	0,654	0,791	0,710	0,788	0,839	0,524
CaO	%	6,58	7,72	6,85	7,34	7,74	5,62
TiO <sub>2</sub>	%	0,203	0,065	0,163	0,192	0,096	0,134
V <sub>2</sub> O <sub>5</sub>	%	0,010	0,005	0,011	0,008	0,001	0,008
Cr <sub>2</sub> O <sub>3</sub>	%	0,005	0,005	0,005	0,005	0,006	0,002
MnO	%	1,450	1,313	0,883	0,971	0,543	1,141
Fe <sub>2</sub> O <sub>3</sub>	%	0,902	0,575	1,026	1,099	0,519	0,858
LOI	%	15,65	9,19	15,98	6,66	1,52	13,59
Co	ppm	19,6	14,7	23,1	22,8	4,6	19
Ni	ppm	13,2	10,3	11,1	12,1	9,3	14,6
Cu	ppm	83,6	95	60,8	87,1	65	31,6
Zn	ppm	14,8	14,3	15,4	19,8	12,5	10,2
Ga	ppm	1,5	2,8	0,6	0,7	1,7	3
Ge	ppm	0,3	0,5	0,4	0,4	0,3	0,3
As	ppm	1	2,9	2	3,7	1,6	2,4
Se	ppm	0,3	0,3	0,3	0,3	0,3	0,2
Br	ppm	6,4	6,9	8,8	8,7	8,1	7,4
Rb	ppm	7,8	9,9	8,9	9,6	11,8	6,4
Sr	ppm	465,3	514,4	453	486,2	480,4	408
Y	ppm	5,7	5,4	6	6,4	5	5,2
Zr	ppm	111,7	52,9	94	105,1	60,7	72,6
Nb	ppm	2,8	6,9	2,5	2,6	2,6	2,6
Mo	ppm	6,3	8,1	3,1	2,9	3,2	6,2
Cd	ppm	0,8	0,9	0,9	0,7	0,8	0,8
In	ppm	1	0,9	0,9	0,9	1,2	0,8
Sn	ppm	12,6	11,8	15,3	23,5	5,7	1,1
Sb	ppm	54,7	33,6	44,8	45,3	66,1	1,4
Te	ppm	1,4	1,3	1	1,4	1,2	1,5
I	ppm	2,6	2,4	2,6	2,7	2,1	1,8
Cs	ppm	4,6	4	4,7	4,6	3,6	4,7
Ba	ppm	415,2	501,3	331,1	416,8	306,5	220,8
La	ppm	9,9	8,4	10	15,8	12,3	15,9
Ce	ppm	14	12	19,4	35,8	10	14
Hf	ppm	9,8	7,3	7,5	10,7	7	3,7
Ta	ppm	4,4	4,7	3,9	4,6	4,1	2,8
W	ppm	1,8	1,1	1,7	1,1	1,8	1,8
Hg	ppm	0,6	0,6	0,6	0,6	0,6	0,6
Tl	ppm	0,8	0,8	0,9	1,1	0,8	0,6
Pb	ppm	195,5	127,2	274,4	375,3	174,7	42,3
Bi	ppm	0,8	0,7	0,8	1	0,8	0,5
Th	ppm	0,7	1,3	3,5	3,5	2	1,4
U	ppm	6,5	20,7	6,4	10,2	7,1	6,1

Table B.6. (continued)

Element	Dimension	ASK-G40a	ASK-G40b	ASK-G41a	ASK-G41b	ASK-G45	ASK-G47
Na <sub>2</sub> O	%	15,05	11,47	12,40	13,28	11,86	14,250
MgO	%	0,028	0,549	0,516	0,504	0,407	0,871
Al <sub>2</sub> O <sub>3</sub>	%	0,657	1,001	0,680	0,701	0,931	1,027
SiO <sub>2</sub>	%	66,54	62,24	62,49	62,98	64,40	61,63
P <sub>2</sub> O <sub>5</sub>	%	0,003	0,041	0,002	0,002	0,056	0,079
SO <sub>3</sub>	%	0,235	0,247	0,211	0,209	0,109	0,349
Cl	%	1,078	0,780	0,947	0,938	0,918	0,709
K <sub>2</sub> O	%	0,628	0,880	0,678	0,711	0,647	0,920
CaO	%	6,63	7,66	6,72	7,27	7,02	7,77
TiO <sub>2</sub>	%	0,127	0,222	0,129	0,111	0,065	0,166
V <sub>2</sub> O <sub>5</sub>	%	0,011	0,009	0,009	0,007	0,007	0,008
Cr <sub>2</sub> O <sub>3</sub>	%	0,005	0,006	0,002	0,002	0,002	0,002
MnO	%	1,273	1,016	1,195	0,945	0,266	1,330
Fe <sub>2</sub> O <sub>3</sub>	%	0,809	1,526	0,817	0,653	0,351	1,034
LOI	%	6,92	12,35	13,21	11,69	12,97	9,86
Co	ppm	23,7	19,1	19,4	17,2	17,4	19,3
Ni	ppm	16,4	15,9	13,1	12,4	7,3	17,9
Cu	ppm	129,4	224,5	144,5	89,8	7,4	69,5
Zn	ppm	15,1	16,1	11	14,5	8,6	20,9
Ga	ppm	2,2	1,3	2,5	1,5	2,4	2,7
Ge	ppm	0,4	0,4	0,7	0,4	0,5	1,2
As	ppm	3,7	3,6	5,8	1,8	0,5	5,1
Se	ppm	0,3	0,4	0,3	0,3	0,2	0,3
Br	ppm	9,3	9,3	7,8	7,6	5,6	10,3
Rb	ppm	7,8	10,9	7,4	8,5	6,6	12,3
Sr	ppm	535	487,4	501,9	487,4	409	685,8
Y	ppm	7,3	7,3	6	6,4	5	5,1
Zr	ppm	71,3	130,9	73	60	37,1	91
Nb	ppm	5,2	3	5,1	2,9	2,4	2,8
Mo	ppm	5,1	3,4	6,1	3,2	2,5	2,9
Cd	ppm	1,1	1	1,1	1	0,8	0,9
In	ppm	1,3	1,3	1,3	1,1	0,8	0,9
Sn	ppm	8	48,2	9,7	8,9	1	10,3
Sb	ppm	162,6	270,5	235,5	141,9	0,9	166,3
Te	ppm	1,8	1,5	1,7	1,6	1,3	1,2
I	ppm	3,3	2,9	3	2,8	2,2	2,1
Cs	ppm	6	4,8	5,5	5,2	4	3,7
Ba	ppm	326,2	441,8	319,6	354,7	244,9	327,3
La	ppm	31,8	19,3	12	11	10,4	7,7
Ce	ppm	21	23,7	22	16	12	22,5
Hf	ppm	7,2	19,7	9,8	3	1,8	9,4
Ta	ppm	6	7,2	6	4,5	1,9	4,4
W	ppm	2,3	2,2	2,1	1,9	1,5	1,8
Hg	ppm	0,8	0,7	0,7	0,9	0,6	0,6
Tl	ppm	0,6	1,5	0,8	0,8	0,5	1,3
Pb	ppm	118,8	847,5	94,6	121,5	5,7	146
Bi	ppm	0,8	1,4	0,7	0,7	0,4	0,8
Th	ppm	1,3	6,9	2,5	1,1	0,5	1,7
U	ppm	7,7	10,4	10,3	6,4	6,2	9,3

Table B.6. (continued)

Element	Dimension	ASK-G52b	ASK-G62a	ASK-G67a	ASK-G68	ASK-G74a	ASK-G74b
Na <sub>2</sub> O	%	7,72	12,65	15,91	12,22	13,50	12,16
MgO	%	0,277	0,544	0,907	0,607	0,875	0,747
Al <sub>2</sub> O <sub>3</sub>	%	0,933	1,193	1,098	1,337	1,883	1,708
SiO <sub>2</sub>	%	60,32	59,69	67,55	62,03	64,93	69,22
P <sub>2</sub> O <sub>5</sub>	%	0,003	0,047	0,093	0,057	0,102	0,100
SO <sub>3</sub>	%	0,152	0,249	0,377	0,197	0,406	0,132
Cl	%	0,622	0,729	0,819	0,749	1,129	0,730
K <sub>2</sub> O	%	1,028	0,816	0,954	0,854	1,904	1,056
CaO	%	8,62	7,02	8,35	7,70	7,66	9,24
TiO <sub>2</sub>	%	0,110	0,188	0,159	0,209	0,223	0,124
V <sub>2</sub> O <sub>5</sub>	%	0,009	0,006	0,008	0,010	0,010	0,006
Cr <sub>2</sub> O <sub>3</sub>	%	0,002	0,009	0,005	0,006	0,006	0,011
MnO	%	0,045	1,906	1,313	0,895	1,711	0,143
Fe <sub>2</sub> O <sub>3</sub>	%	0,681	0,973	0,956	1,205	1,157	0,718
LOI	%	19,48	13,98	1,5	11,93	4,51	3,91
Co	ppm	22,9	23,6	30,9	15,9	18,9	7,9
Ni	ppm	6,6	15,9	16,8	15,8	30,8	9,1
Cu	ppm	12,2	161	99,6	123	79,7	36,8
Zn	ppm	8,1	16,3	14,8	17,4	22,6	12,1
Ga	ppm	3,6	1	1,3	1,1	2,3	3,8
Ge	ppm	0,4	1,2	0,5	0,4	0,4	0,7
As	ppm	2	4,8	2,1	3	5,6	1,5
Se	ppm	0,2	0,3	0,3	0,3	0,3	0,2
Br	ppm	7,5	7	10,4	8,9	17,4	8,7
Rb	ppm	10,9	10,3	10,5	11,8	11	13,6
Sr	ppm	462,5	437,7	649,2	485,5	724,8	498,9
Y	ppm	6,6	4,9	5,3	6,8	6,1	6,2
Zr	ppm	52,5	111,1	77,6	109	108,2	69,2
Nb	ppm	6,8	2,7	5,2	2,8	3	3,9
Mo	ppm	3,1	5,9	3	3	9,3	3,5
Cd	ppm	1,2	0,8	0,8	0,8	0,8	0,7
In	ppm	1,2	1,2	0,9	0,8	0,8	0,8
Sn	ppm	2,4	20,4	10,5	23,1	9,3	3,4
Sb	ppm	1,7	81,6	114,9	76,2	138,3	12,6
Te	ppm	2	1,1	1,2	1	1,3	1,2
I	ppm	3,5	2,1	2,1	2,2	2	2,1
Cs	ppm	6,5	3,5	3,7	3,7	3,5	3,6
Ba	ppm	239,7	574,6	367,8	409,9	275,1	285,1
La	ppm	14	7	11	10,9	8,2	7,4
Ce	ppm	20	19,4	10	13,7	10	26,2
Hf	ppm	2,5	13,9	8,7	17,1	7,8	3,1
Ta	ppm	2,4	5,9	5	5,4	4,6	3,2
W	ppm	2	1,9	1,8	1,9	2,1	1,7
Hg	ppm	0,6	0,7	0,6	0,4	0,6	0,6
Tl	ppm	0,6	1,3	0,9	1,3	1	0,8
Pb	ppm	32	576,3	247,7	610,5	230,3	106
Bi	ppm	0,6	1,1	0,9	1,3	0,5	0,6
Th	ppm	1,2	5	3,9	3,2	2,6	1,6
U	ppm	6,5	6,2	6,6	6,6	7,3	7,5

Table B.6. (continued)

Element	Dimension	ASK-G75a	ASK-G93a	ASK-G93b	Mean	Sdev
Na <sub>2</sub> O	%	14,64	12,35	11,53	<b>12,93</b>	<b>1,82</b>
MgO	%	0,494	0,468	0,408	<b>0,52</b>	<b>0,23</b>
Al <sub>2</sub> O <sub>3</sub>	%	0,924	1,348	0,983	<b>1,02</b>	<b>0,33</b>
SiO <sub>2</sub>	%	68,47	67,93	64,33	<b>64,23</b>	<b>3,13</b>
P <sub>2</sub> O <sub>5</sub>	%	0,093	0,063	0,063	<b>0,05</b>	<b>0,03</b>
SO <sub>3</sub>	%	0,166	0,120	0,104	<b>0,21</b>	<b>0,08</b>
Cl	%	1,116	0,966	0,925	<b>0,88</b>	<b>0,14</b>
K <sub>2</sub> O	%	0,611	0,726	0,629	<b>0,83</b>	<b>0,28</b>
CaO	%	7,92	7,36	7,21	<b>7,43</b>	<b>0,78</b>
TiO <sub>2</sub>	%	0,070	0,069	0,062	<b>0,14</b>	<b>0,05</b>
V <sub>2</sub> O <sub>5</sub>	%	0,006	0,006	0,001	<b>0,01</b>	<b>0,00</b>
Cr <sub>2</sub> O <sub>3</sub>	%	0,005	0,008	0,002	<b>0,00</b>	<b>0,00</b>
MnO	%	0,645	0,286	0,289	<b>0,93</b>	<b>0,52</b>
Fe <sub>2</sub> O <sub>3</sub>	%	0,372	0,397	0,350	<b>0,81</b>	<b>0,32</b>
LOI	%	4,47	7,9	13,11	<b>10,02</b>	<b>4,97</b>
Co	ppm	14,5	15,5	19,1	<b>18,53</b>	<b>5,59</b>
Ni	ppm	10,9	7,7	6,7	<b>13,04</b>	<b>5,39</b>
Cu	ppm	7,5	7,5	8,1	<b>77,31</b>	<b>57,87</b>
Zn	ppm	14,5	9	7,9	<b>14,09</b>	<b>4,10</b>
Ga	ppm	3,8	2,9	3,1	<b>2,18</b>	<b>1,00</b>
Ge	ppm	0,5	0,3	0,3	<b>0,50</b>	<b>0,26</b>
As	ppm	1,1	0,6	0,3	<b>2,62</b>	<b>1,68</b>
Se	ppm	0,2	0,2	0,2	<b>0,27</b>	<b>0,06</b>
Br	ppm	4,7	5,9	5,9	<b>8,22</b>	<b>2,60</b>
Rb	ppm	6,2	7,9	6,6	<b>9,37</b>	<b>2,17</b>
Sr	ppm	475,2	437,1	411,2	<b>499,80</b>	<b>85,95</b>
Y	ppm	5,4	5,2	4,9	<b>5,82</b>	<b>0,77</b>
Zr	ppm	44,4	44,2	37,9	<b>76,88</b>	<b>27,99</b>
Nb	ppm	2,6	2,4	2,3	<b>3,48</b>	<b>1,45</b>
Mo	ppm	2,6	2,5	3,7	<b>4,27</b>	<b>1,97</b>
Cd	ppm	0,8	0,7	0,7	<b>0,86</b>	<b>0,14</b>
In	ppm	0,7	0,7	0,6	<b>0,96</b>	<b>0,22</b>
Sn	ppm	0,5	0,8	0,8	<b>10,82</b>	<b>11,16</b>
Sb	ppm	1,7	0,9	0,8	<b>78,68</b>	<b>80,74</b>
Te	ppm	1,2	1,2	1	<b>1,34</b>	<b>0,27</b>
I	ppm	2	2,2	1,9	<b>2,41</b>	<b>0,47</b>
Cs	ppm	3,6	3,9	5	<b>4,40</b>	<b>0,87</b>
Ba	ppm	289,1	257,8	240	<b>340,25</b>	<b>92,39</b>
La	ppm	14,5	8,3	14,6	<b>12,40</b>	<b>5,52</b>
Ce	ppm	20,4	19,5	20,1	<b>18,18</b>	<b>6,32</b>
Hf	ppm	1,4	2,9	1,8	<b>7,43</b>	<b>5,05</b>
Ta	ppm	2,1	2,1	1,9	<b>4,15</b>	<b>1,53</b>
W	ppm	1,8	1,8	1,6	<b>1,80</b>	<b>0,30</b>
Hg	ppm	0,5	0,6	0,5	<b>0,62</b>	<b>0,10</b>
Tl	ppm	0,6	0,6	0,5	<b>0,86</b>	<b>0,29</b>
Pb	ppm	19,7	5,2	4,3	<b>207,40</b>	<b>224,59</b>
Bi	ppm	0,5	0,5	0,4	<b>0,75</b>	<b>0,27</b>
Th	ppm	0,5	0,5	0,6	<b>2,17</b>	<b>1,67</b>
U	ppm	8	6,2	5,5	<b>7,99</b>	<b>3,27</b>

Table B.7 PED-XRF results for the droplets and threads

Element	Dimension	ASK-G51e	ASK-G55b	ASK-G57a	ASK-G57e	ASK-G58e	ASK-G59c
Na <sub>2</sub> O	%	9,23	11,75	12,08	10,80	14,04	11,11
MgO	%	0,716	0,634	0,687	0,506	0,854	0,769
Al <sub>2</sub> O <sub>3</sub>	%	1,173	1,343	1,901	1,111	0,924	0,759
SiO <sub>2</sub>	%	54,64	64,38	67,83	61,84	61,60	55,84
P <sub>2</sub> O <sub>5</sub>	%	0,020	0,069	0,073	0,038	0,090	0,093
SO <sub>3</sub>	%	0,320	0,132	0,159	0,212	0,375	0,363
Cl	%	0,652	0,792	0,821	0,694	0,700	0,722
K <sub>2</sub> O	%	1,185	0,832	0,786	0,846	0,906	0,874
CaO	%	7,42	9,41	10,12	8,68	7,65	7,04
TiO <sub>2</sub>	%	0,194	0,094	0,105	0,105	0,154	0,143
V <sub>2</sub> O <sub>5</sub>	%	0,012	0,005	0,007	0,001	0,005	0,001
Cr <sub>2</sub> O <sub>3</sub>	%	0,010	0,004	0,005	0,004	0,003	0,002
MnO	%	2,016	0,018	0,031	0,346	1,193	1,592
Fe <sub>2</sub> O <sub>3</sub>	%	1,326	0,510	0,578	0,642	0,898	1,026
LOI	%	21,09	10,02	4,82	14,18	10,61	19,66
Co	ppm	21,5	6,2	4,6	11,4	13,7	17,9
Ni	ppm	34,9	7,4	6,6	9,1	16,3	15,1
Cu	ppm	62,6	2,9	6,1	38,1	79,1	83,2
Zn	ppm	24,3	6	8,5	11,1	18,1	18,3
Ga	ppm	3,6	4,2	4,2	3,5	2	1,1
Ge	ppm	2,3	0,3	0,7	0,7	0,5	0,3
As	ppm	5,9	0,4	1,6	3	3,8	2,3
Se	ppm	0,3	0,2	0,2	0,2	0,3	0,3
Br	ppm	16,5	7,6	7,6	9	10,1	9,1
Rb	ppm	9,8	9,3	9,1	11,3	11	7,8
Sr	ppm	834,5	465,8	531,8	521,8	667,4	657,7
Y	ppm	8,5	6	6,5	6,2	5,8	5,1
Zr	ppm	103	47,8	52,4	64	98,4	83
Nb	ppm	6,2	2,8	4,5	2,4	4,3	3,7
Mo	ppm	8,2	2,5	2,7	2,8	3,2	4,2
Cd	ppm	1,4	0,8	0,8	0,9	0,9	0,7
In	ppm	1,4	0,8	0,6	0,9	0,9	0,8
Sn	ppm	1,9	0,8	1	5,3	13,6	22,8
Sb	ppm	64,9	0,8	0,9	22,1	143,7	61,9
Te	ppm	2,3	1,1	0,5	1,4	1,3	1,1
I	ppm	4,1	2	2,2	2,6	2,3	2
Cs	ppm	7,5	3,5	3,8	4,6	3,9	3,4
Ba	ppm	395,5	300,7	324,2	307,5	317,8	353,9
La	ppm	17	15,3	9,6	9,9	8,2	7
Ce	ppm	60	18,7	18,4	30,1	18,4	16,6
Hf	ppm	3,4	2,2	2,9	3,9	7,7	7,9
Ta	ppm	4,8	1,7	1,9	3,4	4,4	4,4
W	ppm	2,9	1,5	1,8	2,1	1,9	1,9
Hg	ppm	0,8	0,6	0,6	0,6	0,6	1,1
Tl	ppm	0,9	0,5	0,4	0,7	0,9	1
Pb	ppm	53,9	6,4	15,6	65,7	191,5	357,9
Bi	ppm	0,8	0,5	0,5	0,6	0,4	0,9
Th	ppm	1,2	0,5	1	1,3	2,2	2,6
U	ppm	7,6	6,6	7	8,8	7,2	6,1

Table B.7. (continued)

Element	Dimension	ASK-G60b	ASK-G60c	ASK-G72c	ASK-G72d	Mean	Sdev
Na <sub>2</sub> O	%	12,17	10,54	9,72	12,69	<b>11,41</b>	<b>1,44</b>
MgO	%	0,527	0,755	0,442	0,757	<b>0,66</b>	<b>0,13</b>
Al <sub>2</sub> O <sub>3</sub>	%	1,261	0,959	1,204	0,856	<b>1,15</b>	<b>0,32</b>
SiO <sub>2</sub>	%	65,76	60,15	56,81	60,27	<b>60,91</b>	<b>4,32</b>
P <sub>2</sub> O <sub>5</sub>	%	0,055	0,020	0,003	0,062	<b>0,05</b>	<b>0,03</b>
SO <sub>3</sub>	%	0,138	0,329	0,316	0,360	<b>0,27</b>	<b>0,10</b>
Cl	%	0,811	0,658	0,670	0,727	<b>0,72</b>	<b>0,06</b>
K <sub>2</sub> O	%	0,815	1,176	0,967	0,853	<b>0,92</b>	<b>0,14</b>
CaO	%	8,32	8,76	8,22	7,90	<b>8,35</b>	<b>0,93</b>
TiO <sub>2</sub>	%	0,097	0,196	0,194	0,161	<b>0,14</b>	<b>0,04</b>
V <sub>2</sub> O <sub>5</sub>	%	0,007	0,013	0,015	0,009	<b>0,01</b>	<b>0,00</b>
Cr <sub>2</sub> O <sub>3</sub>	%	0,002	0,003	0,003	0,005	<b>0,00</b>	<b>0,00</b>
MnO	%	0,056	1,168	1,490	1,439	<b>0,93</b>	<b>0,75</b>
Fe <sub>2</sub> O <sub>3</sub>	%	0,552	1,834	1,400	1,134	<b>0,99</b>	<b>0,44</b>
LOI	%	9,43	13,44	18,55	12,79	<b>13,46</b>	<b>5,10</b>
Co	ppm	7	19,7	18,8	40,9	<b>16,17</b>	<b>10,59</b>
Ni	ppm	8	21,3	21,6	25,6	<b>16,59</b>	<b>9,31</b>
Cu	ppm	10,6	70	102,1	144,7	<b>59,94</b>	<b>46,00</b>
Zn	ppm	7,7	24,2	19,3	17,5	<b>15,50</b>	<b>6,71</b>
Ga	ppm	3,7	3,8	2,2	1,1	<b>2,94</b>	<b>1,22</b>
Ge	ppm	0,4	0,5	1	1,3	<b>0,80</b>	<b>0,61</b>
As	ppm	1,8	6,3	7,2	2,9	<b>3,52</b>	<b>2,25</b>
Se	ppm	0,2	0,3	0,3	0,3	<b>0,26</b>	<b>0,05</b>
Br	ppm	8,9	13	10,4	10,6	<b>10,28</b>	<b>2,70</b>
Rb	ppm	10,9	16,4	10,3	9,4	<b>10,53</b>	<b>2,32</b>
Sr	ppm	456,8	768,5	721,1	657,1	<b>628,25</b>	<b>129,31</b>
Y	ppm	6,2	9,2	7,9	5,7	<b>6,71</b>	<b>1,35</b>
Zr	ppm	60,9	117,3	95,6	97,1	<b>81,95</b>	<b>24,00</b>
Nb	ppm	2,7	4	3,3	4	<b>3,79</b>	<b>1,11</b>
Mo	ppm	4,9	3,9	3,7	3,3	<b>3,94</b>	<b>1,67</b>
Cd	ppm	0,7	1,3	1	0,9	<b>0,94</b>	<b>0,24</b>
In	ppm	0,8	1,2	1,4	0,9	<b>0,97</b>	<b>0,27</b>
Sn	ppm	1,1	11,9	16,3	13,6	<b>8,83</b>	<b>7,83</b>
Sb	ppm	3,2	125,9	158,2	129	<b>71,06</b>	<b>63,44</b>
Te	ppm	1,6	2,1	1,9	1,3	<b>1,46</b>	<b>0,53</b>
I	ppm	2,2	3,9	3,4	2,3	<b>2,70</b>	<b>0,80</b>
Cs	ppm	3,9	7,1	6	4,1	<b>4,78</b>	<b>1,52</b>
Ba	ppm	265,5	387,1	406,4	324,8	<b>338,34</b>	<b>45,94</b>
La	ppm	8,3	26	23,9	13,2	<b>13,84</b>	<b>6,70</b>
Ce	ppm	32,6	22	28	12	<b>25,68</b>	<b>13,70</b>
Hf	ppm	1,9	7,2	10,3	10,2	<b>5,76</b>	<b>3,26</b>
Ta	ppm	2,1	4,7	5,3	5,8	<b>3,85</b>	<b>1,48</b>
W	ppm	1,6	2,5	2,5	2	<b>2,07</b>	<b>0,44</b>
Hg	ppm	0,6	0,8	0,7	0,7	<b>0,71</b>	<b>0,16</b>
Tl	ppm	0,6	0,8	0,9	1,3	<b>0,80</b>	<b>0,26</b>
Pb	ppm	29,4	109,1	210,9	558,7	<b>159,91</b>	<b>178,25</b>
Bi	ppm	0,5	0,8	1	1,2	<b>0,72</b>	<b>0,26</b>
Th	ppm	1,2	1,8	3	4,3	<b>1,91</b>	<b>1,14</b>
U	ppm	6,6	7	6,8	6,7	<b>7,04</b>	<b>0,74</b>

Table B.8. PED-XRF results for the glass samples adhered to crucible and soil fragments

Element	Dimension	ASK-G24	ASK-G29	ASK-G86a	ASK-G88b	ASK-G90	ASK-G92
Na <sub>2</sub> O	%	5,08	4,91	9,17	12,87	4,66	8,01
MgO	%	0,89	0,63	1,01	1,10	0,87	1,66
Al <sub>2</sub> O <sub>3</sub>	%	1,05	2,06	1,79	1,68	2,90	2,79
SiO <sub>2</sub>	%	38,44	48,43	54,20	68,37	55,96	51,76
P <sub>2</sub> O <sub>5</sub>	%	0,002	0,302	0,047	0,063	0,203	0,084
SO <sub>3</sub>	%	0,200	0,133	0,375	0,291	0,044	0,441
Cl	%	0,535	0,442	0,518	0,686	0,315	0,362
K <sub>2</sub> O	%	0,84	0,61	0,88	0,97	0,58	0,88
CaO	%	6,24	6,65	7,43	9,78	8,43	12,81
TiO <sub>2</sub>	%	0,092	0,114	0,173	0,130	0,220	0,258
V <sub>2</sub> O <sub>5</sub>	%	0,009	0,005	0,009	0,001	0,012	0,012
Cr <sub>2</sub> O <sub>3</sub>	%	0,007	0,005	0,003	0,004	0,004	0,013
MnO	%	1,022	1,954	1,389	0,333	1,813	0,984
Fe <sub>2</sub> O <sub>3</sub>	%	0,94	0,87	1,12	0,79	2,70	1,90
LOI	%	43,82	32,94	20,98	2,84	11,93	18,89
Co	ppm	19,9	23,4	14,1	24	63,5	26,8
Ni	ppm	21,5	51,5	28,3	13	66,9	58,9
Cu	ppm	92,5	139,5	93,7	29,4	547,9	53,9
Zn	ppm	15,8	29,1	54,9	26,4	16,2	33,2
Ga	ppm	3,7	0,5	0,7	5,3	3,5	4,7
Ge	ppm	0,4	0,3	0,4	0,8	0,8	0,5
As	ppm	5	4,3	2,7	1,5	11	3,2
Se	ppm	0,3	0,3	0,3	0,2	1	0,3
Br	ppm	6,1	4,7	9,7	7,2	10,6	7
Rb	ppm	20,4	10,7	21,2	14,8	14,3	24,1
Sr	ppm	506	543,4	654,9	614,1	540,7	687,8
Y	ppm	4,5	5,8	6,1	7,9	1,3	8,4
Zr	ppm	56,1	48,8	92,6	78,4	89	110,4
Nb	ppm	5,2	2,4	5,1	3,3	4	3
Mo	ppm	4,4	8,8	5,2	3,1	3,3	4,1
Cd	ppm	1,7	0,7	0,9	0,6	1,8	0,9
In	ppm	1,6	0,8	1	1,2	2	0,9
Sn	ppm	10,9	21,9	73,1	6	1416	6,7
Sb	ppm	38,2	36,3	89,1	32,5	76,7	80,8
Te	ppm	2,7	1,2	1,4	1,7	1,8	3,1
I	ppm	4,8	2,1	2,7	3,1	7,8	2,2
Cs	ppm	8,7	3,5	4,3	5,6	5,8	3,8
Ba	ppm	415	410,5	317,5	423,9	308,7	294,6
La	ppm	34	11,1	9,1	28	13	17,1
Ce	ppm	28	10	23,8	54	18	11
Hf	ppm	6,6	7,9	9,3	2,9	27,6	5,1
Ta	ppm	5,1	5,6	4,8	3,2	13	4,1
W	ppm	2,5	2,2	2,4	2,1	3,6	2,3
Hg	ppm	0,8	0,6	1	0,7	1,5	0,7
Tl	ppm	0,8	0,7	1,1	0,7	4,5	0,8
Pb	ppm	101,4	249,2	384,1	65,3	5093	96
Bi	ppm	0,8	0,6	1,1	0,7	3,9	0,7
Th	ppm	1,3	0,5	4,5	2,4	28,2	2,8
U	ppm	8,5	5,7	7	6,6	7,2	7,9

Table B.9. PED-XRF results for the clay samples, lumps, crucible and kiln fragments

Element	Dimension	ASK-G4	ASK-G24	ASK-G25b1	ASK-G25b2	ASK-G86a	ASK-G88b	ASK-G90	ASK-G92	ASK-B1
Na <sub>2</sub> O	%	0,600	1,43	0,057	0,059	0,066	0,057	0,059	0,054	0,056
MgO	%	2,52	2,25	0,70	1,40	3,08	2,51	2,64	3,34	0,75
Al <sub>2</sub> O <sub>3</sub>	%	9,87	4,83	13,47	8,94	6,95	7,01	7,58	7,94	10,79
SiO <sub>2</sub>	%	43,65	42,42	63,23	35,10	37,01	39,75	38,97	39,14	45,00
P <sub>2</sub> O <sub>5</sub>	%	0,976	0,503	0,164	1,115	0,155	0,083	0,153	0,131	0,536
SO <sub>3</sub>	%	0,113	0,235	0,151	0,174	0,375	0,540	0,381	0,480	0,117
Cl	%	0,007	0,113	0,019	0,009	0,028	0,062	0,023	0,026	0,006
K <sub>2</sub> O	%	1,35	0,60	0,97	0,94	0,43	1,00	0,58	0,63	0,79
CaO	%	21,49	20,68	1,75	16,04	28,73	29,94	26,39	30,30	5,08
TiO <sub>2</sub>	%	0,661	0,424	0,880	0,656	0,487	0,475	0,487	0,529	0,805
V <sub>2</sub> O <sub>5</sub>	%	0,028	0,019	0,032	0,012	0,019	0,019	0,011	0,019	0,035
Cr <sub>2</sub> O <sub>3</sub>	%	0,047	0,033	0,120	0,046	0,044	0,032	0,033	0,044	0,088
MnO	%	0,114	0,236	0,038	0,175	0,129	0,081	0,460	0,074	0,075
Fe <sub>2</sub> O <sub>3</sub>	%	6,65	4,80	9,24	6,43	4,80	4,35	4,78	4,84	8,18
LOI	%	11,94	21,37	9,83	28,83	17,76	14,93	17,63	12,65	27,81
Co	ppm	58,4	43	77	45,1	47,2	28,4	39,1	42,9	65,1
Ni	ppm	225,5	177,6	133,2	165,8	166,7	181,2	170,8	167,9	129,4
Cu	ppm	195	108,2	91,4	1794	28,7	27,2	71,3	32,1	261,5
Zn	ppm	304,3	59	46340	8799	57,6	47,5	67,3	52,1	48850
Ga	ppm	13,8	11,3	3,9	1,8	11,8	12,2	10,5	11,6	4,2
Ge	ppm	0,5	0,4	2,8	1	0,5	0,4	0,5	1,3	3
As	ppm	6,9	15,4	65,7	24,4	7,1	9,9	7,7	9,7	72,2
Se	ppm	0,3	0,3	0,5	0,4	0,3	0,3	0,4	0,3	0,5
Br	ppm	3,6	4,1	0,5	9,1	3,6	2,8	7,7	4,4	1,7
Rb	ppm	101,9	27,3	91,9	58,7	22,4	21,2	30,7	22,9	57
Sr	ppm	383,6	553,7	74,6	349,2	624,2	419,4	591,1	657,2	95,6
Y	ppm	26	16,7	34,2	25,1	16,3	17,5	16,6	19,6	34,1
Zr	ppm	178,3	118,3	313,4	166,1	110,5	123,7	126,1	138,4	342,5
Nb	ppm	15,4	11,4	27,9	13,2	6,7	10,5	12,1	10,9	20,8
Mo	ppm	5,9	8,3	4,2	8,9	3,8	5,1	3,5	4	4,6
Cd	ppm	0,7	1	1	0,7	1,1	0,8	1,1	1	0,9
In	ppm	0,9	1	0,9	1	1,1	0,9	1,1	0,9	0,8
Sn	ppm	2,9	32,8	2,1	48,5	1,4	1,7	46,4	2,7	2,3
Sb	ppm	1	11,2	1,7	0,9	5,2	1,2	12,7	5,7	0,9
Te	ppm	1,3	1,5	1,3	1,4	1,8	1,2	1,5	1,2	1,2
I	ppm	2,2	2,9	2,2	2,9	2,8	2,1	2,9	1,5	2,1
Cs	ppm	3,8	5	47	7,5	5,8	3,6	4,8	3,6	30,4
Ba	ppm	327,1	332,4	193,3	613,8	285,2	243,1	417	217,5	236,1
La	ppm	39,3	27,3	62,4	28,7	38,5	38,7	25,6	23,2	63,1
Ce	ppm	34,5	40,1	125,1	81,6	72	24,7	41,4	39,7	136,4
Hf	ppm	6,4	6,6	8,6	19	5	2,9	4,7	3,7	11
Ta	ppm	8,3	6,3	9,1	23	4,4	4,2	5,8	4,5	80,4
W	ppm	4,9	3,7	45	18	3,7	3,6	3,9	3,8	47
Hg	ppm	0,9	0,8	4,6	2,9	1	0,9	1	0,9	10,1
Tl	ppm	1	1	1,7	1,6	0,6	1	1,5	1	1,7
Pb	ppm	28,6	49,6	19,8	377,3	30,8	36,2	333	23,4	58
Bi	ppm	0,5	0,7	1,1	1,4	0,8	0,9	1,3	0,7	1,3
Th	ppm	5,9	3,4	0,7	0,9	4,3	5,3	6,3	5,8	0,9
U	ppm	18,2	7,5	10	7,8	8,5	8,5	6,8	10	7,8